

PARAMETRIC ANALYSIS OF MFBI MEASUREMENTS ON HUMAN FOREARM

Kartik Kalra

A thesis submitted to
Auckland University of Technology
in partial fulfilment of the requirements for the degree of
Master of Engineering (M.E.)



Institute of Biomedical Technologies
School of Engineering, Computer and Mathematical Sciences
Faculty of Design and Creative Technologies

Supervisor: Dr. Gautam Anand

© **Kartik Kalra**

2020

Abstract

Bioelectrical impedance analysis or bioimpedance analysis (BIA) is a non-invasive procedure originating in the early 1930s and 1940s that involves the measurement of the electrical impedance of a region of tissue. Bioimpedance measurements provide information about the physical and electrochemical processes in the tissue region and hence can be used for monitoring physiological properties and variations. For example, BIA is commonly employed to estimate body fat or water composition as a measure of general health. BIA has been implemented in diagnostic techniques such as electrical impedance cardiography (ICG) for estimating cardiac output, electrical impedance tomography (EIT) for imaging modality and electrical impedance spectroscopy (EIS) for multi-frequency analysis of materials with different electrical domains such as cellular membranes and tissues. Single frequency BIA (SFBIA) applications like ICG are more commonly used and provide an approximate response of the volume changes of blood within the thorax. However, the results are unreliable due to several assumptions related to tissue geometry and disregard the contribution of the surrounding tissues to the overall measurements. Herein, multi-frequency BIA (MFBIA) applications like EIS can be useful to provide an impedance spectrum containing information about the relaxation phenomenon of all the tissues. The aim of this research is to investigate the potential of MFBIA in determining the impedance response of each tissue through parametric electrical modelling, thereby helping to isolate the effects of one tissue from others.

This thesis discusses a simulation perspective to determine the dielectric response of a human forearm section modelled with four layers – bone, fat, muscle and blood. The model, although assuming isotropic dielectric properties for each tissue, aims at simulating the dielectric response of the tissue layers within the major portion of β dispersion frequency range – 1 kHz to 1 MHz. The results established a Cole type behavior of the model within a frequency range of 10 kHz to 1 MHz. The simulation was followed by a pilot experimental investigation on a human forearm in two subjects. The results indicated a Cole type behavior for both the subjects within the measured frequency range of 1 kHz – 349 kHz. Both the simulation and the experimental measurements were modelled electrically to a single and multi-dispersion Cole equation to determine the Cole parameters for each tissue domain. The resultant model fit showed excellent correlation with the corresponding measured data and establishes this methodology to determine individual tissue response from overall MFBIA measurements.

Acknowledgements

I am using this opportunity to express my gratitude to my supervisor Dr. Gautam Anand. He taught me a great deal on how to deal with roadblocks and find a solution to all the problems not only professionally but also personally. I am thankful to him for his unconditional support and guidance throughout my Masters study. Besides that, I would also like to thank my sister Dr. Anubha Kalra who guided and motivated me throughout my study. Both these people inspired and taught me a great deal about scientific research and life in general.

I am also grateful to my parents who taught me to be fearless and dedicated to my goal. This research would not have been possible without their love and affection.

Lastly, I want to dedicate this thesis to my deceased grandmother who meant everything to me.

Table of Contents

Abstract.....	i
Acknowledgements	ii
Table of Contents	iii
List of Figures.....	vii
List of Tables	xi
Attestation of Authorship.....	xii
List of Units, Symbols and Abbreviations	xiii
Chapter 1: Introduction	1
1.1 Measurement Principle.....	1
1.2 Theoretical basis for Bioimpedance analysis	2
1.3 Dielectric Relaxation Theories.....	4
1.3.1 Debye dielectric relaxation theory	4
1.3.2 Maxwell Wagner effects	5
1.3.3 Cole theory.....	5
1.4 Applications of Bioimpedance analysis	6
1.4.1 Impedance Cardiography	6
1.4.2 Impedance plethysmography	7
1.4.3 Impedance Spectroscopy/ Electrical Impedance Tomography	8
Chapter 2: Literature Review.....	9

2.1	Electrical Properties of Tissues	9
2.2	Electrode Configurations for Bioimpedance analysis	18
2.2.1	Types of electrodes	19
2.3	Bioimpedance analysis for Hemodynamic monitoring.....	20
2.3.1	Blood flow induced impedance variations	21
2.4	Instrumentation for Bioimpedance analysis.....	23
2.4.1	Operational frequency and safety standards	23
2.4.2	Driving circuits	24
2.4.3	Proposed bioimpedance measurement systems	25
2.5	Electrical modelling for Bioimpedance measurements.....	27
2.6	Research Gaps	32
2.7	Research Question and Objectives.....	33
Chapter 3:	Simulation of a human forearm model	35
3.1	Ansyz High Frequency structure simulator (HFSS).....	35
3.1.1	Ansyz Solver	36
3.2	Model of a human forearm.....	36
3.3	Simulation Setup	37
3.3.1	Material properties of tissue domains	39
3.3.2	Finite Element Modelling	40
3.4	Simulation Results.....	41
3.5	Discussion	44

Chapter 4:	Pilot experimentation on human forearm.....	46
4.1	Experimental setup and methodology	46
4.2	Impedance Measurement Results.....	49
4.3	Discussion	51
4.3.1	Comparison with the simulation results.....	52
Chapter 5:	Electrical modelling.....	54
5.1	Modelling methodology	54
5.2	Simulation modelling.....	55
5.2.1	Single dispersion Cole modelling	56
5.2.2	Multi-dispersion Cole modelling	58
5.3	Experimental modelling	61
5.3.1	Single dispersion Cole modelling	61
5.3.2	Multi-dispersion Cole modelling	65
5.4	Discussion	69
5.4.1	Simulation modelling.....	70
5.4.2	Experimental modelling.....	70
Chapter 6:	Conclusion and Future Work	71
6.1	Simulation study.....	71
6.2	Experimentation on human forearm.....	72
6.3	Electrical modelling	72
6.4	Future Work	73

References 74

List of Figures

<i>Figure 1.1: BIA measurement principle using 4 electrodes</i>	<i>1</i>
<i>Figure 1.2: Cole-Cole plot with different parameters</i>	<i>6</i>
<i>Figure 1.3: a. Band electrode placement and b. Output Signals from ICG measurement</i>	<i>7</i>
<i>Figure 2.1: High and Low frequency current distributions in cell suspensions</i>	<i>10</i>
<i>Figure 2.2: Permittivity and conductivity of tissues: prediction of the model (black filled and dotted curves), experimental data at 37°C (grey filled and dotted curves) and data from the literature (triangles and circles). (a) Bone. (b) Blood, (c) Fat, and, (d)Muscle</i>	<i>15</i>
<i>Figure 2.3: Cole plots for transverse and longitudinal impedances of skeletal muscle</i>	<i>16</i>
<i>Figure 2.4: Debye model using three frequency-independent components.....</i>	<i>17</i>
<i>Figure 2.5: An equivalent circuit showing the replacement of capacitor, C, by CPE.....</i>	<i>17</i>
<i>Figure 2.6: [A]. Kubicek’s method-based impedance change curves and [B]. Use of impedance change to correspond to Stroke volume</i>	<i>18</i>
<i>Figure 2.7: The circuit diagrams for (A). Bipolar and (B). Tetra polar electrode configurations.....</i>	<i>19</i>
<i>Figure 2.8: Resistivity increase with haematocrit being graphically illustrated by the two equations.....</i>	<i>21</i>
<i>Figure 2.9: (a). Specific resistance variation with velocity for three samples of beef blood, and, (b). Comparison of the varying specific resistance with haematocrit at rest (upper curve) and at a linear velocity of 15cm/sec (middle curve). The lower curve states the difference between the two curves</i>	<i>22</i>
<i>Figure 2.10: Block Diagram of a transfer (bio)impedance measuring system.....</i>	<i>24</i>
<i>Figure 2.11: (a). A basic current mirror circuit, and (b). An improved Howland current generator circuit used in EIT.....</i>	<i>25</i>
<i>Figure 2.12: Various capacitances and impedances encountered in a BIA setup.....</i>	<i>25</i>
<i>Figure 2.13: Block diagram of the forearm impedance measurement stated by Wang et al., 2011</i>	<i>26</i>

<i>Figure 2.14: The block diagram of the real time monitoring ICG system as proposed by Shyu et.al.</i>	27
<i>Figure 2.15: Electrical circuit analogous to Cole model</i>	28
<i>Figure 2.16: A. Tetra polar BIS configuration with measurement circuit, B. Equivalent circuits for standard and textile electrodes using passive elements, C. Equivalent circuits for standard and textile electrodes using CPE (Q)</i>	30
<i>Figure 2.17: A model and the corresponding electrical circuit for a limb segment</i>	31
<i>Figure 2.18: Electrical analogue for oscillatory blood flow impedance with all suitable corrections (R_o is the correction for anomalous viscosity, C is the capacitance and R_i, L_i are the longitudinal impedance parameters where the extent of i defines the accuracy of the system)</i>	31
<i>Figure 3.1: Longitudinal view of the designed 3-D model in Ansys HFSS</i>	38
<i>Figure 3.2: Top view of the 3-D model</i>	38
<i>Figure 3.3: Conductivity (S/m) for bone, blood, fat and muscle tissues as compiled by Gabriel</i>	39
<i>Figure 3.4: Relative Permittivity for bone, blood, fat and muscle tissues as compiled by Gabriel</i>	39
<i>Figure 3.5: Mesh distribution in overall human forearm section, including the electrodes.</i>	41
<i>Figure 3.6: Electric field distribution at 1 kHz (a). front view, (b). top view</i>	42
<i>Figure 3.7: Electric field distribution at 1 MHz (a). front view, (b). top view</i>	42
<i>Figure 3.8: $Re[Z]$ vs frequency plot obtained from simulation results</i>	43
<i>Figure 3.9: $-Im[Z]$ vs frequency plot obtained from simulation results</i>	43
<i>Figure 3.10: $-Im[Z]$ vs $Re[Z]$ (Cole) plot obtained from simulation results</i>	44
<i>Figure 4.1: Schematic of the single shunt front end used in this experimentation</i>	47
<i>Figure 4.2: Single shunt front end configuration of the Quadra impedance spectroscopy measurement device</i>	48
<i>Figure 4.3: Electrode setup on the forearm section</i>	48

<i>Figure 4.4: Re[Z] vs frequency plot for subjects 1 and 2</i>	<i>49</i>
<i>Figure 4.5: Im[Z] vs frequency plot for subjects 1 and 2</i>	<i>50</i>
<i>Figure 4.6: Re[Z] vs Im[Z] (Cole plot) for subjects 1 and 2</i>	<i>50</i>
<i>Figure 4.7: Difference in the impedance magnitudes between the two subjects</i>	<i>51</i>
<i>Figure 4.8: Comparison of the simulation results with the experimental results of subjects 1 and 2</i>	<i>52</i>
<i>Figure 5.1: Comparison of the simulation measured data with single dispersion model fit for (a): Re[Z], (b): Im[Z], and (c) Re[Z] vs Im[Z] (Cole plot).....</i>	<i>56</i>
<i>Figure 5.2: Correlation and Bland Altman plots for single dispersion fit (a). Re[Z] and (b). Im[Z]</i>	<i>57</i>
<i>Figure 5.3: Comparison of measured data with multi-dispersion model fit data for simulation (a): Re[Z], (b): Im[Z], and (c) Re[Z] vs Im[Z] (Cole plot).....</i>	<i>59</i>
<i>Figure 5.4: Correlation and Bland Altman plots for multi-dispersion fit (a). Re[Z] and (b). Im[Z]</i>	<i>60</i>
<i>Figure 5.5: Complete response within 1 kHz – 1 MHz obtained from multi-dispersion model fit for simulation data (a): Re[Z], (b): Im[Z], and (c) Re[Z] vs Im[Z] (Cole plot)</i>	<i>61</i>
<i>Figure 5.6: Comparison of the experimental measured data with single-dispersion model fit for Subject 1 and 2, (a): Re[Z], (b): Im[Z], and (c) Re[Z] vs Im[Z] (Cole plot)</i>	<i>62</i>
<i>Figure 5.7: Correlation and Bland Altman plots for (a). Re[Z] and (b). Im[Z] for subject 1</i>	<i>63</i>
<i>Figure 5.8: Correlation and Bland Altman plots for (a). Re[Z] and (b). Im[Z] for subject 2</i>	<i>64</i>
<i>Figure 5.9: Complete response within 1 kHz – 1 MHz obtained from single dispersion model fit for subjects 1 and 2 (a): Re[Z], (b): Im[Z], and (c) Re[Z] vs Im[Z] (Cole plot)</i>	<i>65</i>
<i>Figure 5.10: Comparison of the experimental measured data with multi-dispersion model fit for Subject 1 and 2, (a): Re[Z], (b): Im[Z], and (c) Re[Z] vs Im[Z] (Cole plot)</i>	<i>66</i>
<i>Figure 5.11: Correlation and Bland Altman plots for multi-dispersion fit (a). Re[Z] and (b). Im[Z] for subject 1</i>	<i>67</i>

Figure 5.12: Correlation and Bland Altman plots for multi-dispersion fit (a). $Re[Z]$ and (b). $Im[Z]$ for subject 2 68

Figure 5.13: Complete response within 1kHz – 1MHz obtained from multi-dispersion model fit for subjects 1 and 2 (a): $Re[Z]$, (b): $Im[Z]$, and (c) $Re[Z]$ vs $Im[Z]$ (Cole plot) 69

List of Tables

<i>Table 2.1: Resistivity of different tissues [24]</i>	<i>11</i>
<i>Table 2.2: Different dielectric relaxation models.....</i>	<i>29</i>
<i>Table 3.1: Summary of tetrahedrons for each tissue layer</i>	<i>40</i>
<i>Table 4.1: Comparison between simulation and forearm measurements.....</i>	<i>53</i>
<i>Table 5.1: Cole parameters as estimated from the fit for simulation data</i>	<i>56</i>
<i>Table 5.2: Cole parameters as estimated from the multi-dispersion model fit for simulation.....</i>	<i>59</i>
<i>Table 5.3: Cole parameters as estimated from the fit for experimental data for Subject 1 and 2</i>	<i>62</i>
<i>Table 5.4: Cole parameters as estimated from the multi-dispersion model fit for subject 1 and 2</i>	<i>66</i>

Attestation of Authorship

“I hereby declare that this submission is my own work and that, to the best of my knowledge and belief, it contains no material previously published or written by another person (except where explicitly defined in the acknowledgements), nor material which to a substantial extent has been submitted for the award of any other degree or diploma of a university or other institution of higher learning.”

..... (signed)

.....26/10/2019..... (date)

List of Units, Symbols and Abbreviations

Units

Symbol	Unit
F	Farad
Hz	Hertz
mA	milli-Ampere
mV	milli-Volt
S	Siemens
s ⁻¹	per-second
Ω	Ohm

Symbols

Symbol	Quantity	Unit
C	Capacitance	F
D	Electric Flux Density	C m ⁻²
E	Electric Field Strength	V m ⁻¹
G	Conductance	S
H	Magnetic Field Intensity	A/m
I	Current	A or mA
J	Electric Current Density	A m ⁻²

V	Voltage	V
Z	Impedance	Ω
ϵ	Permittivity	F/m
ϵ_0	Permittivity of free space (8.85 x 10 ⁻¹²)	F/m
ϵ_r	Relative Permittivity	
ρ	Resistivity	$\Omega\text{-m}$
σ	Conductivity	S/m
τ	Time constant	seconds
ω	Angular Frequency	rad s ⁻¹

Abbreviations

BIA	Bioimpedance Analysis
BAA	Bland Altman Analysis
CI	Confidence Intervals
DVT	Deep Vein Thrombosis
ECF	Extra-cellular Fluid
ECG	Electrocardiogram
EEG	Electroencephalogram
EIS	Electrical Impedance Spectroscopy
EIT	Electrical Impedance Tomography
EMG	Electromyogram

HFSS	High Frequency Structure Simulator
ICF	Intra-cellular Fluid
ICG	Impedance Cardiography
IPG	Impedance Plethysmography
MF-BIA	Multi-Frequency – Bioimpedance Analysis
PWV	Pulse Wave Velocity
RMSE	Root Mean Squared Error
SF-BIA	Single Frequency – Bioimpedance Analysis
SSE	Sum of Squared Errors

Chapter 1: Introduction

Bioimpedance is referred to as the electrical impedance offered by biological materials to the flow of current [1]. Bioimpedance analysis (BIA) has been a topic of interest in clinical research since the last two-three decades as it has helped in decoding various complex anatomical functions of biological organisms. BIA is a medical technology that originated in the 1930-40s ([2], [3]). It stems from the exogenic branch of bioelectricity measurement. It got popularity in its application as pectoral method of impedance measurement for the estimation of cardiac output [4]. Procedurally, BIA is a non-invasive impedance measurement method which is used to estimate physiological indices like body fat and water composition as well as pulse wave velocity and arterial stiffness ([5]–[9]). Determination of biophysical parameters from measured bio-electrical quantities also constitute the application of BIA.

1.1 Measurement Principle

Generally, the principle of BIA measurement involves the calculation of electrical impedance of the test biological material or living tissue. A small amount of current, within safety limits, is applied through a pair of electrodes and the resulting voltage due to the stimulation is measured through the same or a different pair of electrodes. The ratio of the measured output voltage to the supplied input current is quantified as transfer impedance of the tissue or bioimpedance, which is reflects the overall dielectric response. The BIA measurement principle is shown in Figure 1.1.

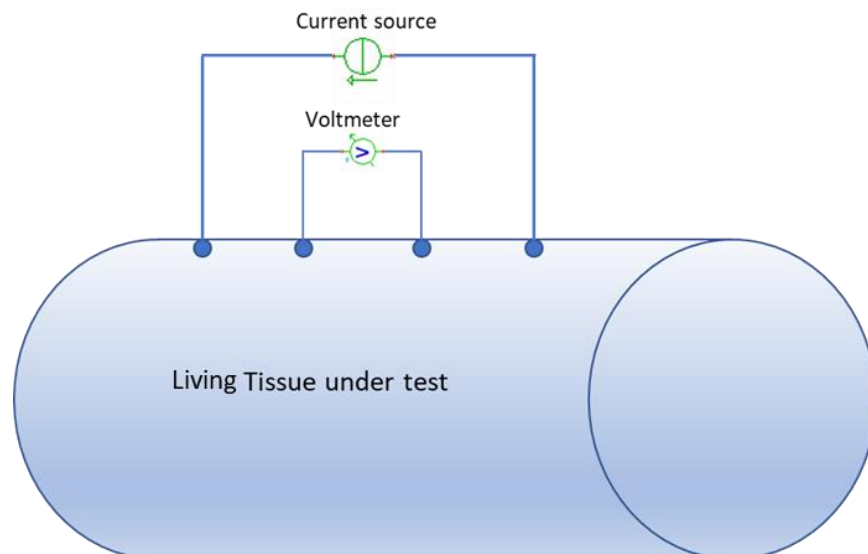


Figure 1.1: BIA measurement principle using 4 electrodes

The measured voltage is dependent on the electrodes – their geometry, placement and configuration. In Figure 1.1 shows an arrangement of 4 electrodes– the outer electrodes to provide the input current stimulus and the inner electrodes to measure the resulting voltage response. The inter-electrode spacing contributes to the output voltage and depends on the application requirements. However, a two-electrode system can also be used. The input excitation is a small magnitude AC current, applied at a certain frequency to obtain an electrical response of the tissues. This type of BIA is referred to as Single frequency BIA or SFBIA. Some applications of BIA require the input to be applied at multiple frequencies, which is referred to as Multi-frequency BIA or MFBIA. These will be discussed later with reference to BIA applications.

1.2 Theoretical basis for Bioimpedance analysis

The analysis of electric fields distribution within the human tissue volumes is important to understand in aiding the investigation of bioelectrical signal acquisition. Lead Field theory provides the basis for this understanding [10]. This theory can be used to understand and optimize the measurement methodologies for any bioelectric measurements – endogenous electric fields like Electrocardiogram (ECG) and exogenous electric fields as in BIA. Lead field can be described as the electric field generated due to a pair of input excitation sources (called a lead) throughout the tissue volume. It assumes that several point current sources and sinks (dipoles) exist within the tissue volume, which orient and configure in a direction resulting in an electrical double layer. This layer acts a Gaussian surface which follows the concept of lead vector wherein the electrical field at any point within or at the surface can be calculated through Gauss theorem. The electrodes form a lead dipole which can be considered to be placed inside a Gaussian surface. As the current through a region changes, there is change in the conductivity and due to this the impedance of the region varies.

Lead field theory helps in understanding the defining the sensitivity distribution of electric fields, following the theorem of reciprocity [11]. This means that sensitivity distribution in case of electrical impedance measurement, detection of bioelectric signals and electrical distribution are similar ([12], [13]). Einthoven, Frank and Burger triangles can also be accurately described by the lead triangles ([14], [15]). Impedance variations can be calculated mathematically (as was illustrated by Geselowitz (1971) [10]) through the development of a mathematical formula that verifies the lead field theoretical approach and is employed as a reference in a BIA application - Impedance Plethysmography. Moreover, using different electrodes for voltage and current measurements yield more accurate results as compared to the mathematically similar results that were obtained when same electrodes were considered [13].

In addition to the Lead Field theory, it is important to understand the dielectric characteristics of tissues and their response under an applied external electric field. A biomaterial exhibits the properties of a conductor as well as a dielectric. The flux density (\vec{D}) linked with an electric field (\vec{E}) is given by the following equation:

$$\vec{D} = \epsilon \vec{E} \quad \text{Equation 1-1}$$

In this case, ϵ is the permittivity of the medium.

The application of an external electric field modifies the above expression and is given by:

$$\vec{D} = \epsilon_0 \vec{E} + \epsilon_0 \chi \vec{E} = \epsilon_0 (1 + \chi) \vec{E} = \epsilon_0 \epsilon_r \vec{E} \quad \text{Equation 1-2}$$

Wherein ϵ_0 is the permittivity exhibited by free space or vacuum (8.85×10^{-12} F/m), and χ denotes electric susceptibility which is a measure of the polarizability of the medium. $1 + \chi$ collectively defines the relative permittivity of the medium or material, denoted by ϵ_r .

The variation in polarization is a gradual process and this might explain the complex permittivity. With increment in frequency, a difference in phase is introduced between the flux density and electric field which is expressed in the equation below:

$$\epsilon = \frac{|D|}{|E|} e^{-j\varphi} \quad \text{Equation 1-3}$$

$|D|$ is the flux density, $|E|$ is the electric field and φ is the phase angle.

The exponential relation in Equation 1-3 can be expressed as:

$$\epsilon(\omega) = \frac{|D|}{|E|} (\cos \varphi - j \sin \varphi) = \epsilon'(\omega) - j\epsilon''(\omega) \quad \text{Equation 1-4}$$

Equation 1-4 describes the permittivity of a biomaterial as a frequency dependent complex quantity. This forms the characteristic of most of the biological tissues and helps analyze their dielectric response.

Additionally, a manifestation of Ohm's law derived from the time-varying electric fields identifies the complex conductivity as:

$$\sigma(\omega) = \sigma'(\omega) + j\sigma''(\omega) \quad \text{Equation 1-5}$$

Maxwell's equation for the time-varying electric fields, assuming a harmonic time dependence, state:

$$\nabla \times \vec{H} = \vec{J} + j\omega \vec{D} = \vec{J} + j\omega \epsilon \vec{E} \quad \text{Equation 1-6}$$

In this case, \vec{H} is the magnetizing field whereas \vec{J} is the vector defining the current density.

The expression for complex permittivity from Equation 1-4 can be substituted in Equation 1-6:

$$\nabla \times \vec{H} = \vec{J} + j\omega(\epsilon' - j\epsilon'')\vec{E} \quad \text{Equation 1-7}$$

$$\nabla \times \vec{H} = \vec{J} + (\omega\epsilon'' + j\omega\epsilon')\vec{E} \quad \text{Equation 1-8}$$

Equation 1-8 assists in relating the complex conductivity to complex permittivity as:

$$\sigma(\omega) = \sigma'(\omega) + j\sigma''(\omega) = \omega\epsilon''(\omega) + j\omega\epsilon'(\omega) = j\omega(\epsilon'(\omega) - j\epsilon''(\omega)) \quad \text{Equation 1-9}$$

Equation 1-9 shows the relationship between complex permittivity and conductivity as complex conjugates. In practical terms, $\sigma'(\omega)$ indicates the power loss in the material and hence $\epsilon''(\omega)$ indicates the power loss per cycle.

The combined relation involving these complex quantities is given in Equation 1-10:

$$\epsilon(\omega) = \epsilon_0\epsilon_r(\omega) - j\frac{\sigma(\omega)}{\omega} \quad \text{Equation 1-10}$$

1.3 Dielectric Relaxation Theories

Electric current is composed of conduction and displacement current. Conduction current is the current that flows due to conduction ions, electrons and holes. Thus, it is unaffected by frequency variations. Displacement current is the electric current of time varying electric fields and hence it will vary with increment of frequency [16]. If permittivity and conductivity of the material are constant, the displacement current will increase with frequency whereas the conduction current remains unchanged. The material behaves like a conductor for low frequencies, but the capacitive effects become more pronounced at higher frequencies. These material properties are not constant for most materials and they are dependent on frequency of the source. This type of variation in distribution of tissue properties into resistive and capacitive, exhibited by materials is known as dispersion. The lag between the conduction and the displacement electric fields is identified through a relaxation time or time constant (τ). Based on the effect of the relaxation time constant, several theories exist which define the behavior of different types of dielectrics. The theories relevant to understanding biological tissues have been mentioned here.

1.3.1 Debye dielectric relaxation theory

Debye in 1913 [17] devised a theory that the delay or lag experienced by all the dipoles is the same and hence characterized the system with a single time constant. The system was accurately modelled electrically

using a parallel representation of Resistance and Capacitance. The formula for complex relative permittivity is given in Equation 1-11.

$$\varepsilon(\omega) = \varepsilon_{\infty} + \frac{\varepsilon_0 - \varepsilon_{\infty}}{1 + j\omega\tau} \quad \text{Equation 1-11}$$

Here the electrical permittivity at frequencies much above the dispersion is given by ε_{∞} whereas ε_0 describes the DC permittivity. This theory explained the electric behavior of polar compounds effectively but was inefficient when human tissues were involved.

1.3.2 Maxwell Wagner effects

The Maxwell Wagner Sillars effect ([18]–[20]) explained the phenomenon that took place at lower frequencies, wherein a charged layer was formed inside the dielectrics (especially biological dielectrics). The reason for this was the variations in permittivity and conductivity of the different layers and dielectrics. Thus, this difference in properties led to the formation of interfacial layer playing a key role in beta (β) dispersion spectrum described by the capacitive effect of the cellular membrane. This capacitive effect is caused due to polarization at the inner surface of the dielectric [21].

1.3.3 Cole theory

The Debye theory could not describe the broadness of the dispersion spectrum obtained. As a result, complex response of the human tissues was represented by distributed time constant system. Cole and Cole suggested the empirical model to explain the dielectric behavior of tissues in 1941 ([22], [23]). The characteristic Cole-Cole relation can be formulated as:

$$\varepsilon(\omega) = \varepsilon_{\infty} + \frac{\varepsilon_0 - \varepsilon_{\infty}}{1 + (j\omega\tau)^{1-\alpha}} \quad \text{Equation 1-12}$$

The parameter α , termed as the coefficient of relaxation, is dependent on the nature of the material. It lies between 0 and 1 and is 0 for Debye-type dispersions. The parameter becomes smaller as the width of the dispersion increases.

Another way of representing Cole-Cole equation is in the form of impedance expressed in terms of complex permittivity and complex conductance (Equation 1-13).

$$Z(\omega) = R_{\infty} + \frac{R_0 - R_{\infty}}{1 + (j\omega\tau)^{1-\alpha}} \quad \text{Equation 1-13}$$

Here $Z(\omega)$ is the total impedance while R_{∞} is the resistance offered after the dispersion has taken place or the resistance at infinite (very high) frequency, whereas the resistance at zero (very low) frequency is R_0 .

The Cole-Cole equation can be expressed graphically by plotting the imaginary part on the y-axis and the real part on the x-axis. This type of plot is known as Nyquist plot where the imaginary part is negative while the maxima is obtained at $\omega\tau = 1$ as the frequency increases from right part of the graph to the left side or in an anti-clockwise direction. Figure 1.2 display the Cole-Cole plot with different parameters.

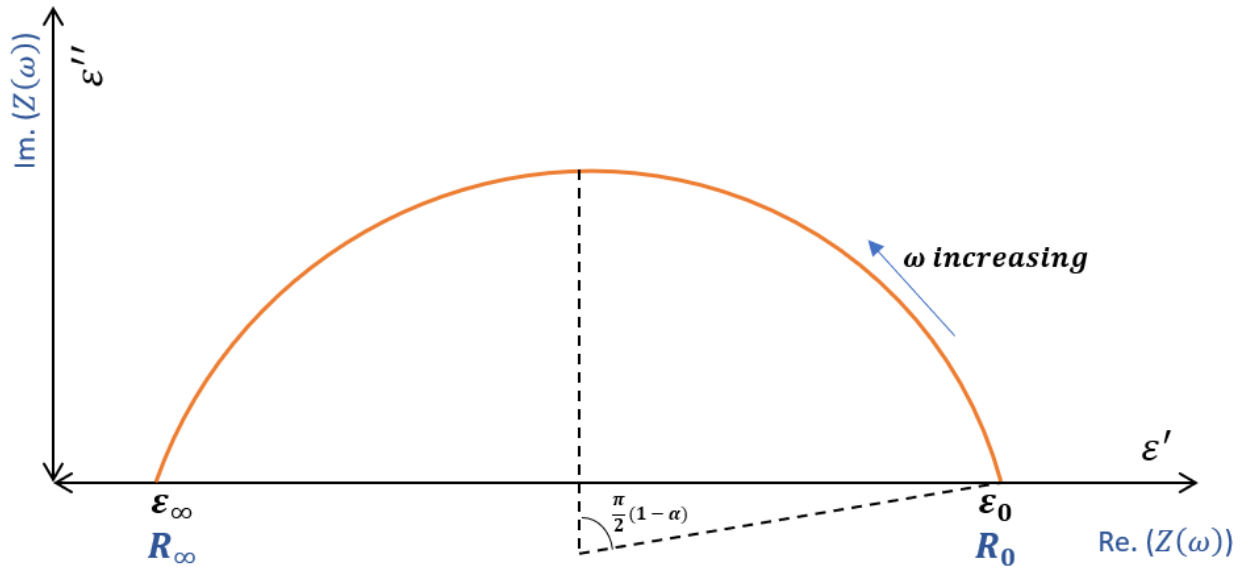


Figure 1.2: Cole-Cole plot with different parameters

From Figure 1.2, it can be seen that the x-axis intercepts denote the resistances (R_0 and R_∞) or the real parts of permittivity (ϵ_0 and ϵ_∞) at DC or low frequency and at very high frequency, respectively. The frequency at which maximum impedance is obtained is known as the characteristic frequency.

1.4 Applications of Bioimpedance analysis

This section presents some of the real time application areas of BIA. The principle of BIA can be applied in several forms to understand and provide a diagnostic measure of living tissues in several conditions. Some of the major applications of BIA have been discussed here forth.

1.4.1 Impedance Cardiography

Impedance cardiography is a non-invasive technique employed for measurement of real time impedance variations in the chest region. The impedance changes in thorax region are measured at a single frequency. The set up involves 2 or 4 electrodes originating from the diaphragm and terminating at the aorta of the heart. The current applied is a low frequency alternating current. The impedance variations occurring in the

aorta are due to its haemodynamics. The blood flow influences the impedance which changes periodically as current travels through the aorta and vena cava to find the path of least resistance.

The dynamics of blood flow assist in calculation of impedance related physiological parameters like ECG, ventricular ejection time (VET), stroke volume as well as for investigating heart failures, hypertension and dyspnea. Figure 1.3 a explains the placement of electrodes for measurement of impedance cardiography along with Figure 1.3 b which shows the corresponding output signals.

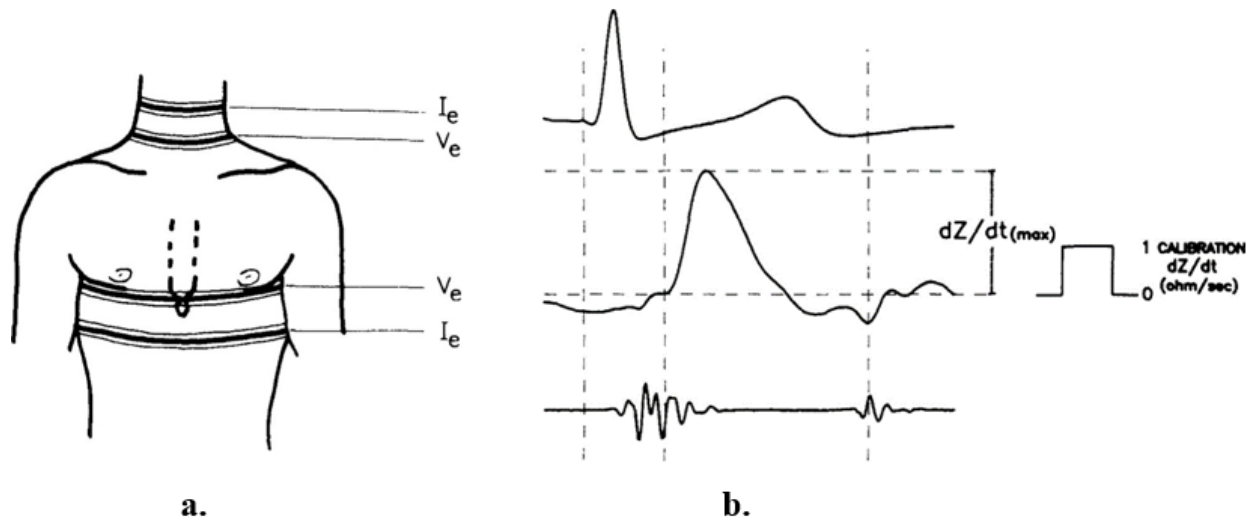


Figure 1.3: a. Band electrode placement and b. Output Signals from ICG measurement [24]

1.4.2 Impedance plethysmography

It is a technique that is aimed at calculating tissue volumetric changes occurring inside the human body ([25]–[29]). The procedure involved is a non-invasive one and the target area can be human chest or any other body part. In the chest region, however, ICG yields similar results by calculating the lung volume variations as well as the peripheral impedance. It finds application in detection of deep vein thrombosis ([30]–[32]) or the obstruction offered by the veins to the volumetric flow of current. In this application too, the current considered has a single frequency within the range of 50 kHz-100 kHz and a 2 or 4 electrode system is considered ([33]–[36]). It assists in determination of body fat/water composition.

1.4.3 Impedance Spectroscopy/ Electrical Impedance Tomography

Some of the applications utilizing Electrical impedance tomography are determination of a tumour ([37]–[39]) and monitoring organs ([40]–[44]) by observation of any irregularities in the conductivity and permittivity of tissues. It is carried out at low current over a range of frequencies. This multi frequency non-invasive medical technique employs a set of surface electrodes that acquire equal potential on application of current. Image reconstruction algorithms can be collaborated with this technique to obtain clear static images of the conductivity pattern. The main concept behind this technique is the difference in properties of the electric tissues.

BIA finds extensive potential in hemodynamic monitoring and determination of cardiovascular parameters associated with blood flow. Blood consisting of red blood cells (RBCs), white blood cells (WBCs) and plasma has a specific response to the application of current. This causes changes in the flow of blood as well as changes in its volume. The influence of blood flow and its volumetric variations on the BIA needs to be independently analysed. One of the techniques employed for similar purpose is doppler ultrasonography. However, the instrumentation for the ultrasound system is bulky and does require training and skills to operate. The motivation behind this research is to be able to use BIA (specifically, MFBIA) to model the overall electrical response of major human tissues, calculating their individual response and isolating the response due to blood flow. This approach seeks to standardize BIA in terms of determining the blood flow profile in a simpler, non-invasive and portable system. The following chapter will present a literature review of the BIA techniques and their implications and the several factors that influence the modelling of BIA measurements

Chapter 2: Literature Review

This chapter aims to review the existing literature and works which are of significance in BIA analysis and hemodynamic monitoring. This chapter is divided into the following sections:

1. **Electrical properties of tissues:** This section highlights the various studies conducted to quantify the dielectric response of tissues.
2. **Electrode configurations for BIA:** This section discusses the structure, geometry and configurations of electrodes and their corresponding effect on the bioimpedance measurements.
3. **BIA for Hemodynamic monitoring:** This section contains information about the flow of blood, volumetric characteristics and the effects of blood composition on bioimpedance measurements.
4. **Instrumentation for BIA:** This ventures into the type of circuits and electrode configurations designed to accurately measure the impedance.
5. **Electrical modelling for BIA measurements:** This section features the electrical modelling of the bioimpedance data in accordance with the Cole-Cole equation.

2.1 Electrical Properties of Tissues

The tissues are a fundamental part of biological organisms and an in-depth knowledge of functioning and characteristics of tissues when subjected to electric current is of utmost importance. Tissues are made up of cellular suspensions. The dielectric properties of tissues and cell suspensions are quite unique at various frequency levels and steps. Tissues are ultimately made up of cells which are mainly resistive in nature. The cells are surrounded by membranes which offer high capacitance, but the resistance offered is quite low. This explains the frequency dependence of the tissues. Tissues when subjected to electric current for a spectrum of frequencies are categorized into 3 dispersion regions α , β and γ as demonstrated by Schwan [45]. Alpha (α) dispersion occurs in the muscles due to the dispersion effect inside the endoplasmic reticulum (structure that store Calcium ions). The frequency at which it takes place is less than 1 kHz. However, this effect is more pronounced for permittivity than conductivity. Beta (β) dispersion takes place in the frequency range of 10 kHz -10 MHz. The main causes of these types of dispersions are the cellular structure of the tissues separating cytoplasm and extra cellular membrane. The cellular membranes of tissues exhibit capacitive nature that play a part in these dispersions. Gamma(γ) dispersions occur above 1 GHz. They are mainly caused by the relaxation effects of water molecules at microwave frequencies.

Tissues or cells in general have both an intracellular as well as extracellular fluid. The tissue structures can also be assumed as cell suspensions. The theory of tissues exhibiting both resistance and impedance can be consequent of the tissues exhibiting heterogeneous and anisotropic properties. This means that the properties are irregular throughout their volume and they are unique along different directions. The tissues can be considered as having an insulating membrane that serves as a capacitive membrane. The current flows through the extra-cellular fluid at zero or DC frequency. With an increment in the frequency, the current also flows through the intra-cellular fluid due to the capacitive effect of the cellular membrane. The operating frequency range is between 0.01-100 MHz. When frequency above this range is applied, both extra-cellular and the intra-cellular fluid offer a combined resistance, and their capacitive effect is negligible [46].

At a characteristic frequency F_c , the maximum reactance is recorded and the capacitance offered by the cellular membrane (C_M) can be evaluated. Figure 2.1 depicts the structure of cells and passage of currents through the cellular suspensions at lower and higher frequencies.

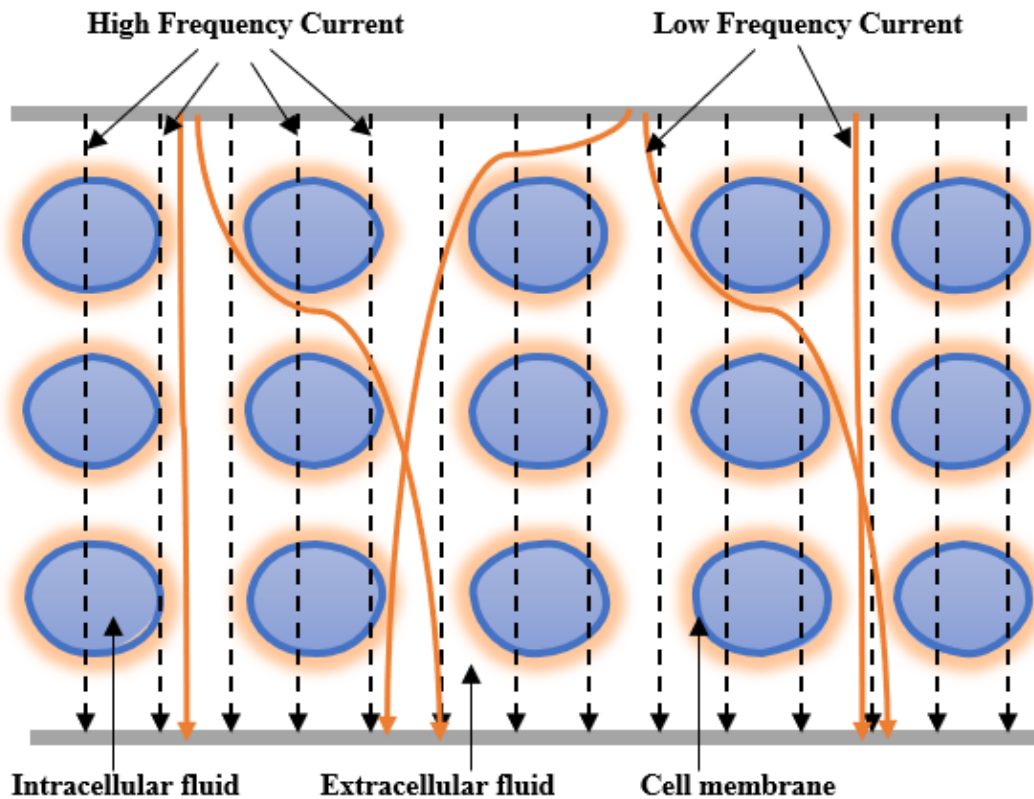


Figure 2.1: High and Low frequency current distributions in cell suspensions [47 (redrawn)]

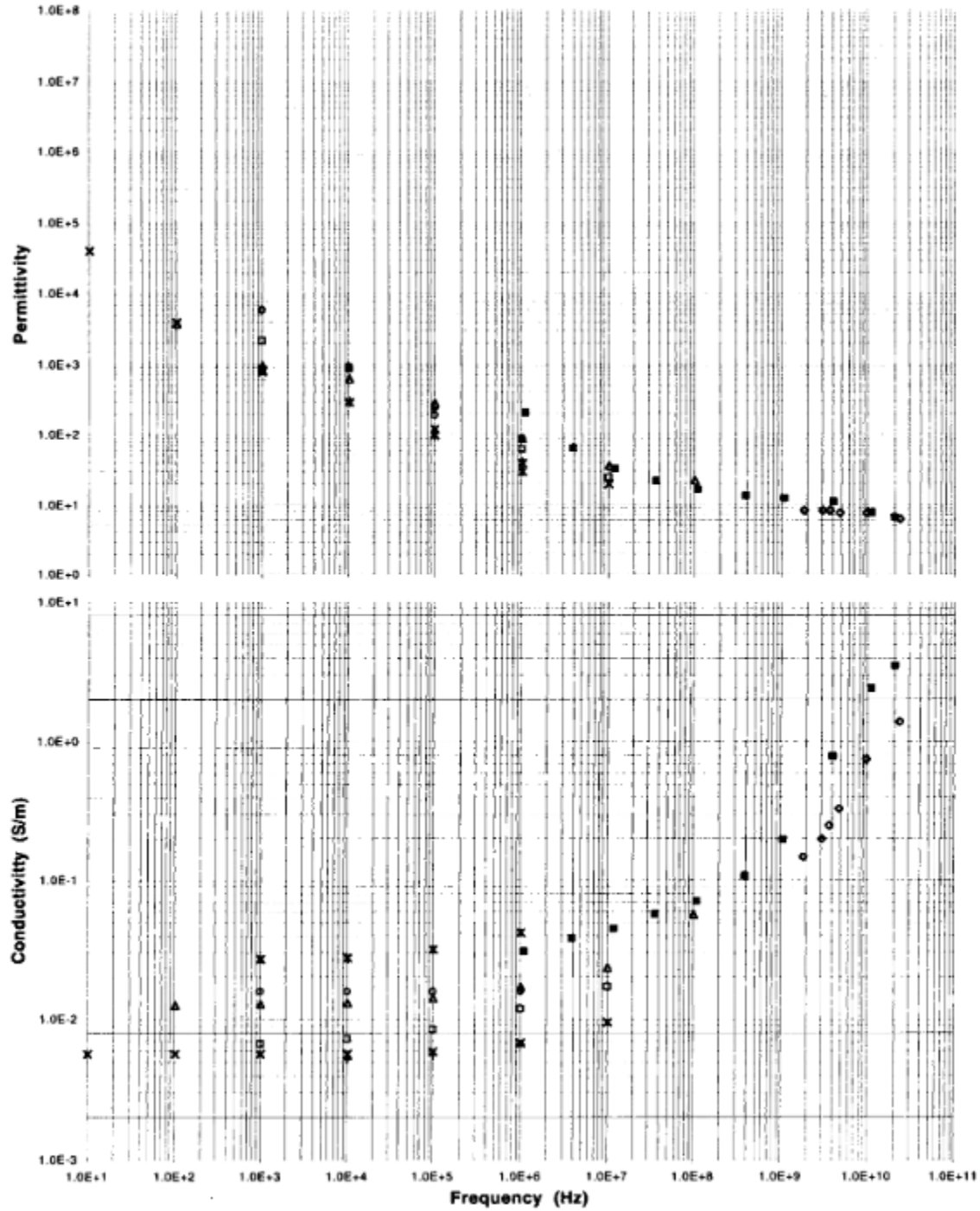
Table 2.1 demonstrates the resistivity values for some of the tissues in the human body, as documented in the literature.

Table 2.1: Resistivity of different tissues [24]

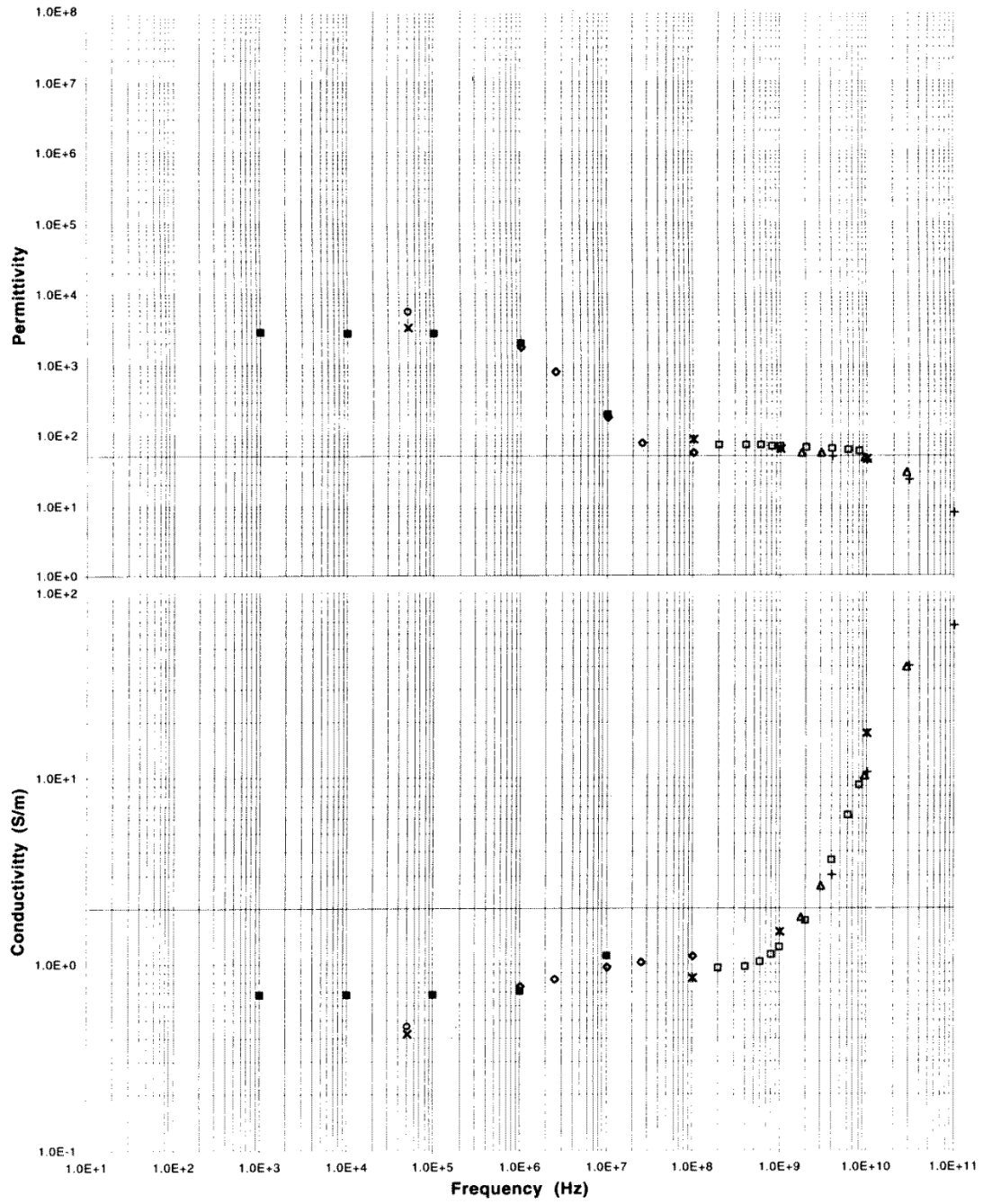
Tissue	Resistivity ($\Omega\text{-m}$)	Work/Experimental Reference
Brain		
• Gray Matter	2.2	Rush and Driscoll (1969) [48]
• White Matter	6.8	Barber et.al. (1984) [49]
• Average	5.8	Barber et.al. (1984) [49]
Cerebrospinal fluid	0.7	Barber et.al. (1984) [49]
Blood (Ht. 45)	1.6	Geddes and Sadler (1973) [50]
Plasma	0.7	Barber et.al. (1984) [49]
Heart Muscle		
• Longitudinal	2.5	Rush et.al. (1963) [51]
• Transverse	5.6	
Skeletal Muscle		
• Longitudinal	1.9	Epstein and Foster (1983) [52]
• Transverse	13.2	
Liver	7	Rush et.al. (1963) [51]
Lungs	11.2	Schwan and Kay (1954) [53]
Fat	25	Geddes and Baker (1967) [54]
Bone		
• Longitudinal	177	Saha and Williams (1992) [55]
• Circumferential	15	
• Radial	158	

In the electrical context, some of the major tissues that contribute to the BIA measurements can be skin, bone, fat, muscle and blood. Out of these, blood is the most conductive and is perfused within different other tissues in the human body. Blood, Fat and muscle comprise of approximately 70 – 80% of the body weight. The other major contributor is the bone tissue. For BIA measurements, bone, fat, muscle and blood tissue domains become important as most of the electrical and mechanical dynamics occur within these domains whereas the response of skin can be neglected by using gel (wet) electrodes. Gabriel and Gabriel

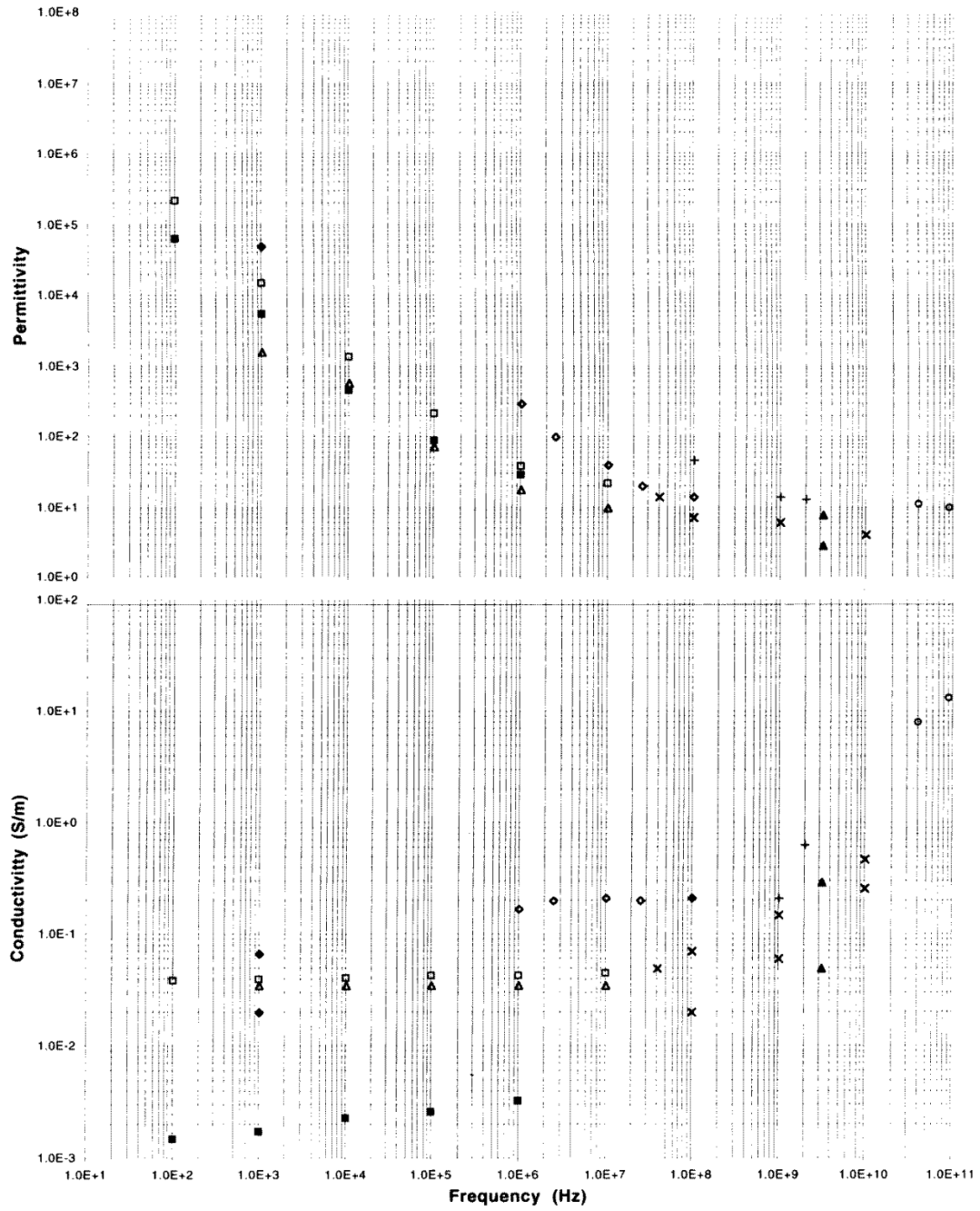
([56]–[59]) compiled a database of tissue dielectric properties through parametrically modelling those available from the literature, which serves as a useful resource in our study. The dielectric properties for bone, blood, fat and muscle, as modelled by Gabriel, have been shown in Figure 2.2 (a)–(d), respectively.



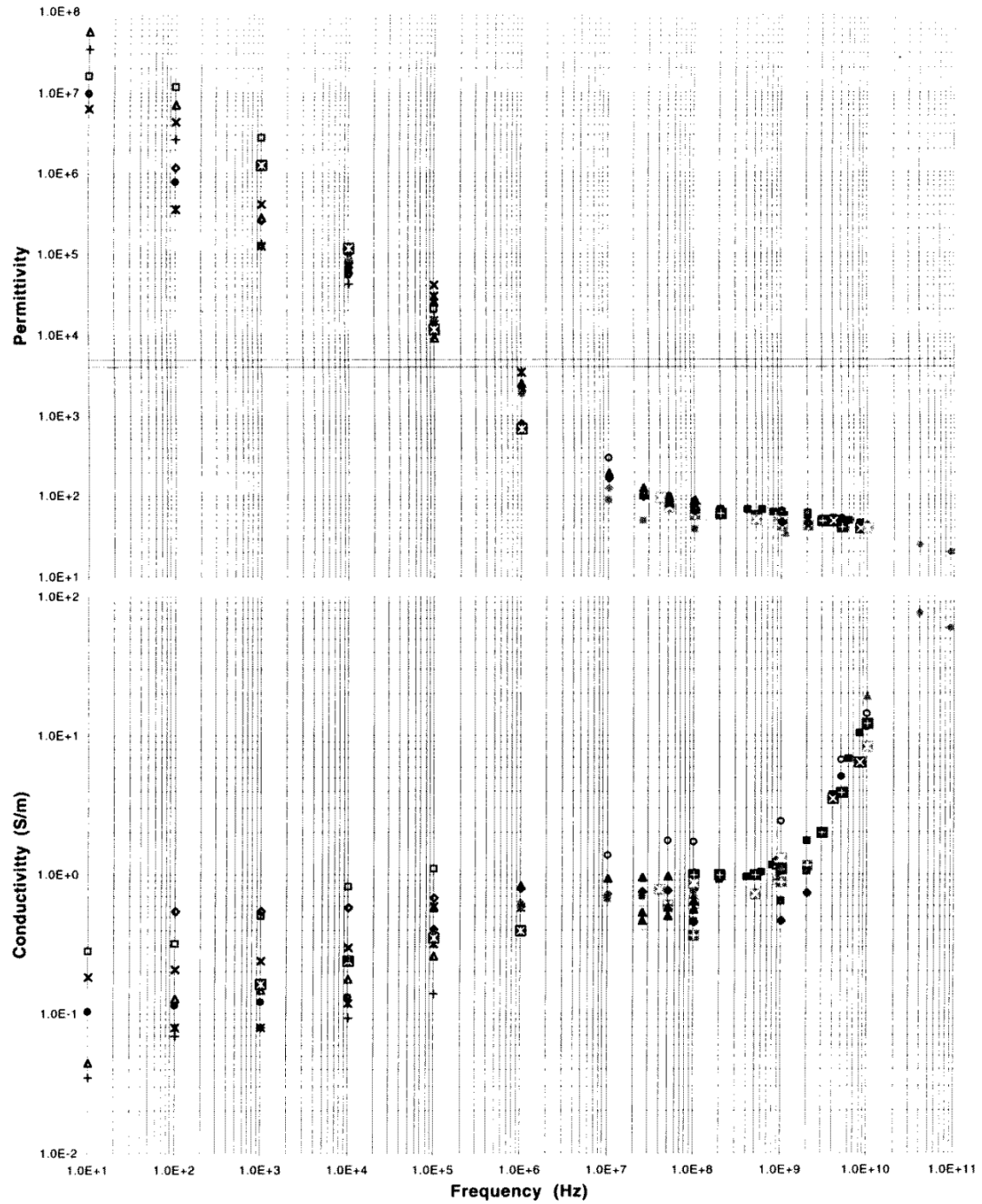
(a)



(b).



(c).



(d).

Figure 2.2: Permittivity and conductivity of tissues: prediction of the model (black filled and dotted curves), experimental data at 37°C (grey filled and dotted curves) and data from the literature (triangles and circles). (a) Bone. (b) Blood, (c) Fat, and, (d) Muscle [56]

The frequency dependence of the tissues is of high importance, especially in the fields of Impedance Plethysmography and Impedance Spectroscopy (Tomography). The reactance varies with frequency and

hence the tissues show different electrical behavior at different frequencies. Their behavior can be classified on the basis of the amount of resistance and capacitance offered by them. Cole and Cole (1941) [23], stated a graphical method of representing the impedance variation of the tissues with the frequencies. Named as the ‘Cole-Cole plot’, it represented the graphical plot of the real component, R, versus the imaginary component, X, for the impedance Z over a range of frequencies. It correlates with the Wessel diagram or the Nyquist plot, giving information about the frequency variations of the impedance components in the form of a semicircle which follows the Cole equation. An example can be seen in Figure 2.3

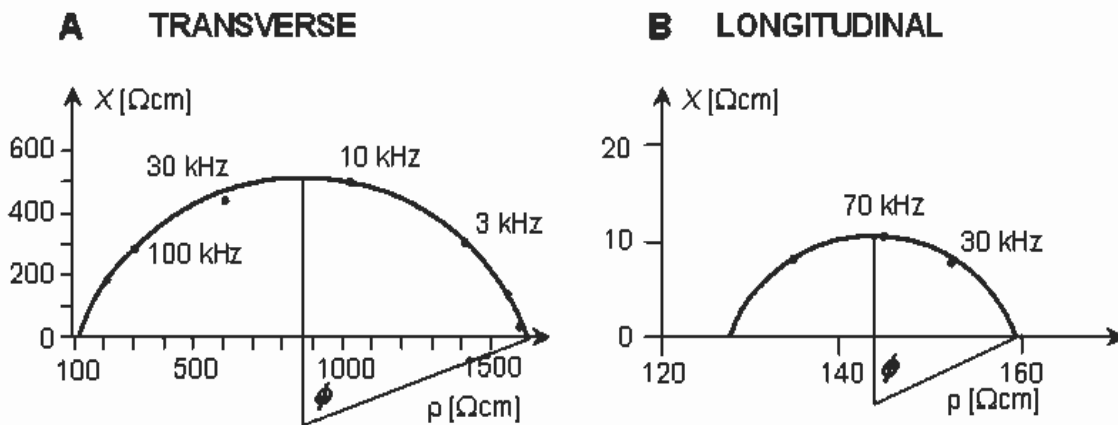


Figure 2.3: Cole plots for transverse and longitudinal impedances of skeletal muscle [52]

With the extremities of the Cole plot referring to the resistances at those frequencies, the reactance of the medium is maximum at the characteristic frequency, as mentioned earlier in Section 1.3.3. Hence, this representation gives the entire frequency response and can be used as an effective tool for electrical modelling of the tissues. The Cole plot along with the differentiated frequency behavior defined by Schwan led to the fact that the tissue response cannot be modelled by considering a simple conductive and dielectric passive behavior, but as a *bidomain* with the impeding elements being frequency sensitive.

Considering all the variability and physiological inhomogeneity of the tissues, they can be electrically modelled using a combination of a conductive element and capacitor in parallel -Debye model. The representation using a resistor and a capacitor provides a single frequency measurement but cannot express the immittance over a band of frequencies [60]. At the most, it can be modelled to mimic the response at the extreme frequency values (HF and LF) through the circuit presented in Figure 2.4.

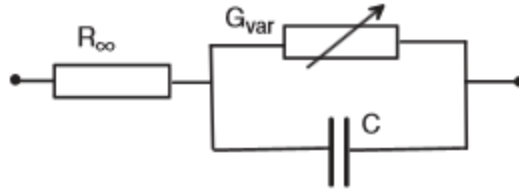


Figure 2.4: Debye model using three frequency-independent components [60]

The requirement of multiple frequency modelling was met by the proposition of a Constant Phase Element (CPE). It is a form of mathematical realization of a constant phase using a resistor and a capacitor, both of which are frequency dependent. This leads to an equivalent circuit (Figure 2.5), the time constant of which is the same, but exponentially scaled by a factor, α . This factor α directly contributes to a constant phase, being in accordance with Fricke's Law [61].

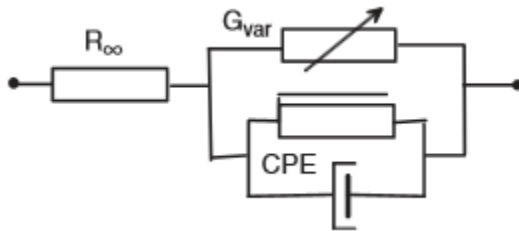


Figure 2.5: An equivalent circuit showing the replacement of capacitor, C , by CPE [60]

The first clinical trial came into effect in 1968 when Kubicek [62], based on his studies, developed a method deriving the stroke volume from Impedance Cardiography of the thorax. However, it was based on certain assumptions which made it unreliable. The method intended to obtain the curves for changes in impedance over time so as to compute the increase or decrease in the impedance value. The work was based on the cylindrical thorax modelling to investigate the origination of the bioimpedance signal which was rather a highly simplified approximation. The results can be seen in Figure 2.6.

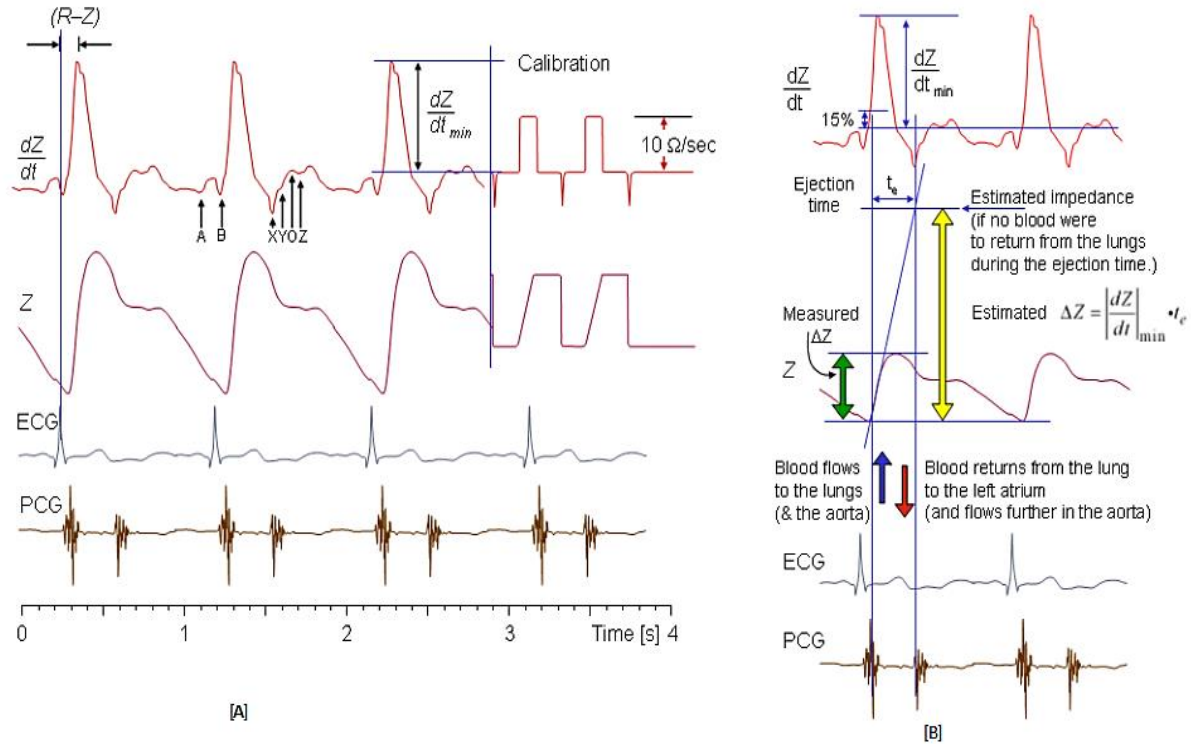


Figure 2.6: [A]. Kubicek's method-based impedance change curves and [B]. Use of impedance change to correspond to Stroke volume [13]

Also, the model remained unclear regarding the source of the bioimpedance signal as well as neglecting the contributions of the blood conductivity and the changes in the velocity. Mohapatra (1981) [63], analysed the non-invasive cardiac impedance monitoring and stated that the cardiac haemodynamic have an important role to play. The impedance change signal reflects a change in the blood volume along with the blood velocity.

In his studies, Pethig (1984) [64], stated the conductivity value and the capacitive measure of the cell membranes to be around 10^{-7} S/m and 10^{-2} F/m² respectively. This shows the high resistivity of the cell membranes along with the capacitance offered which is in significant amount.

2.2 Electrode Configurations for Bioimpedance analysis

In most of the instances involving non-invasive measurements like ECG, silver/silver chloride (Ag/AgCl) electrodes have been employed traditionally. Accurate measurement of bioimpedance involves measurement of voltage as well as feeding of current. To account for voltage due to the electrodes, the input impedance is considered as $100\text{k}\Omega$ as was demonstrated in the instrument developed by Kubicek [62].

Moreover, the electrode configurations exist as bipolar or tetrapolar. These configurations can be expressed in terms of electrical circuit, as in Figure 2.7. Z_{e1} , Z_{e2} , Z_{e3} and Z_{e4} represent the electrode impedances.

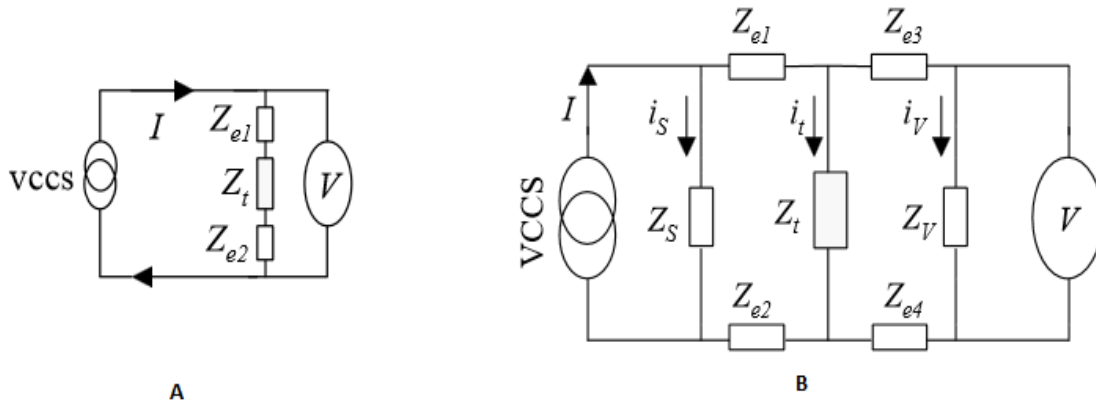


Figure 2.7: The circuit diagrams for (A). Bipolar and (B). Tetra polar electrode configurations [65]

The variations in tissue impedances can't be determined by the single measurement in the case of bipolar electrodes. In case of tetra polar electrodes, the input impedance of the amplifier for measuring the voltage Z_v and the output impedance of current source Z_s can be made quite high to minimize the current flowing through them. This assists in making the sensed voltage to a level that is comparable to that of the impedance of the tissue, Z_v . This led to the introduction of multi-polar electrodes that performed the function of picking of voltage and carrying of current resulting in transfer impedance [60].

Polarization of electrodes introduces error in impedance of tissues. Alignment as well as configuration of electrodes play an important role in the sensitivity of BIA measurements. It can be concluded that nature of electrodes and applied field strength dictate the electric field distribution of a tissue. Maxwell's and Geselowitz equation assist in describing the sensitivity of electrodes regarding the application.

2.2.1 Types of electrodes

Various types of electrodes can be employed for dielectric properties of tissues. It has been a convention to use surface electrodes since they cover larger area of the asymmetrical body tissue. Types of electrode include parallel plate electrode, needle electrode, needle array electrode as well as caliper electrodes. All of them offer specific advantages and disadvantages. The use of the type of electrode is dependent on the type of application [66]. For example, distance variation is one of the benefits of parallel plate electrodes. Uniform electric field produced due to these electrodes make them desirable for conduction of clinical trials. The most basic type of electrodes is needle electrodes, but due to their non-uniformity, they can be used in parallel bundles like arrays. The gap between the electrodes can be effectively managed by employing the caliper electrodes. The tetra-polar configuration derived from Kubicek's arrangement for measurement of thoracic impedance measurement is a standard reference for proposed configuration of

electrodes. Spot electrodes might be given preference over the band electrodes as they perform similar function while providing more comfort [67]. An eight electrode system has also been employed at various instances for measuring of bioimpedances [68]. The electrode alignment and configuration play an integral role along with number and material of electrodes. The movement of limb have been described in a really detailed way by studying the variations in impedance occurring in muscle tissue to obtain as accurate results as possible [69]. The distance between the electrodes can be effectively determined by testing various configurations wherein everything from the joint angle between the electrodes to unwanted noise signal is considered to calculate impedance changes [70]. All in all, tetrapolar electrodes offer the least of electrode impedance effect, and hence the contribution of electrode polarization is significantly reduced while some errors might creep in due to the volume of the surface conductor. Conclusively, tetrapolar configuration is preferred as it reduces the electrode polarization impedance, although, some contribution from the interface may still have an effect at low frequencies.

2.3 Bioimpedance analysis for Hemodynamic monitoring

The use of bioimpedance techniques to determine the physiological parameters has resulted in the development of bio-physical models that have led to applications like the estimation of pulsatile blood flow. Blood is a fluidic tissue which is composed of the blood cells (Red blood cells and White blood cells) and plasma. The consideration of blood contribution is necessary as every tissue is perfused with blood and the effect of the compositional characteristics and the dynamics of blood cannot be neglected. The resistivity of blood has been found to depend on the haematocrit value [71]–[73]. Mohapatra and Hill (1975), [74] verified the dependence of the blood resistivity on the haematocrit concentration and temperature. They devised a mathematical model and showed the increase of blood resistivity with haematocrit value. A single equation was developed relating the specific resistance of the blood with the temperature and the haematocrit, with the temperature rise resulting in the decrease of resistivity. The consideration of a constant haematocrit value can be presumed to analyse the effects of other parameters contributing to the blood resistivity but cannot be a basis for the entire modelling.

Additionally, conductivity and velocity of blood flow need to be considered for accurate calculation of stoke volume from impedance cardiography. The variation in blood flow affects the changes in impedance (ΔZ) especially in the diastole region as was depicted by the works of Mohapatra in 1981 and 1988 [63], [76]. Thus, significant errors might creep in calculation of impedance plethysmography by the simple consideration of cross-sectional cylindrical geometry changes due to blood flow variations.

The resistivity of blood is dependent on a variety of factors. The major ones are haematocrit ([71]–[73]) as well as the temperature. The resistivity of blood is proportional to hematocrit and inversely proportional to temperature, as was devised by Mohapatra and Hill (1975) [74]. The blood is composed of red blood cells, white blood cells and plasmas and the effect of haematocrit factor is quite significant on the blood flow. Thus, it cannot be ignored and considered as a constant. The haematocrit effect was expressed in terms of Maxwell-Fricke [75] equation through the study of spheroidal suspensions. Geddes and Sadler in 1973 [50] expressed the hematocrit effect on blood flow through an exponential relationship. The comparison is expressed graphically, as seen in Figure 2.8.

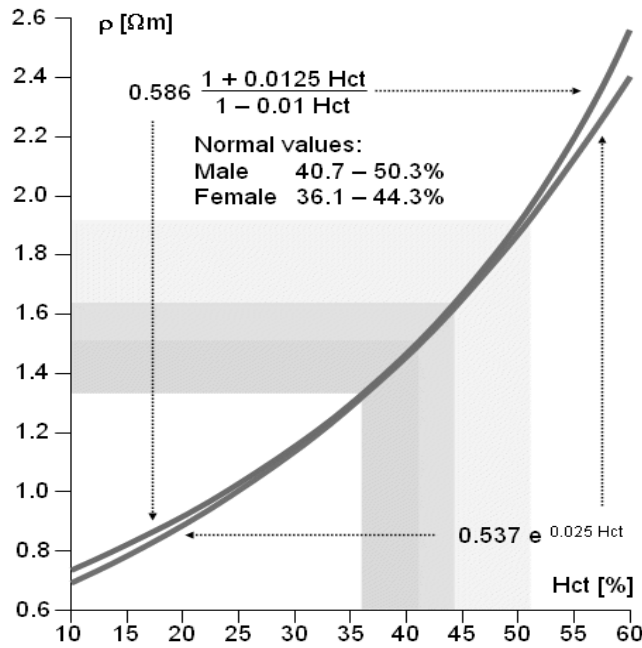


Figure 2.8: Resistivity increase with haematocrit being graphically illustrated by the two equations[13]

2.3.1 Blood flow induced impedance variations

The electrical impedance offered by the blood tissue is quite less than what is offered by other tissues due to its relatively higher conductivity. It is also rather unique in the way that the variability of the impedance characterizes the electrical response of the blood tissue. The properties and the velocity of the flow of blood have an impact on the specific resistance of the blood. During blood flow, the impedance of the blood undergoes a variation, called ‘flow effect’, which has an impact on applications such as impedance cardiography and impedance plethysmography.

The variation in the conductivity of blood during its continuous flow is caused because of a variety of reasons and one of the major ones is the amount or concentration of red blood cells or erythrocytes in the

volume of blood. The concept of haematocrit by Hause et al., 1989 [77] is basically the ratio of erythrocytes to the total blood volume and its corresponding impact on the impedance of blood flow. Sigman et. al. (1937) [78] postulated that the conductivity of blood undergoes a variation when it begins to flow. According to him, the variation is in a way that the specific resistance undergoes an increment initially as the blood's position is at rest but starts decreasing as the velocity of the blood increases. This decrease is significantly more when the concentration of RBC's is high. An explanation about the initial increment can be due to the interaction between the electrodes and the blood, whereas the velocity and characteristics of the blood impact the subsequent decrease in the resistance. Figure 2.9 (a) shows the specific resistance variation of beef blood in relation to velocity while Figure 2.9 (b) demonstrates the comparison of specific resistance with haematocrit at rest and at motion.

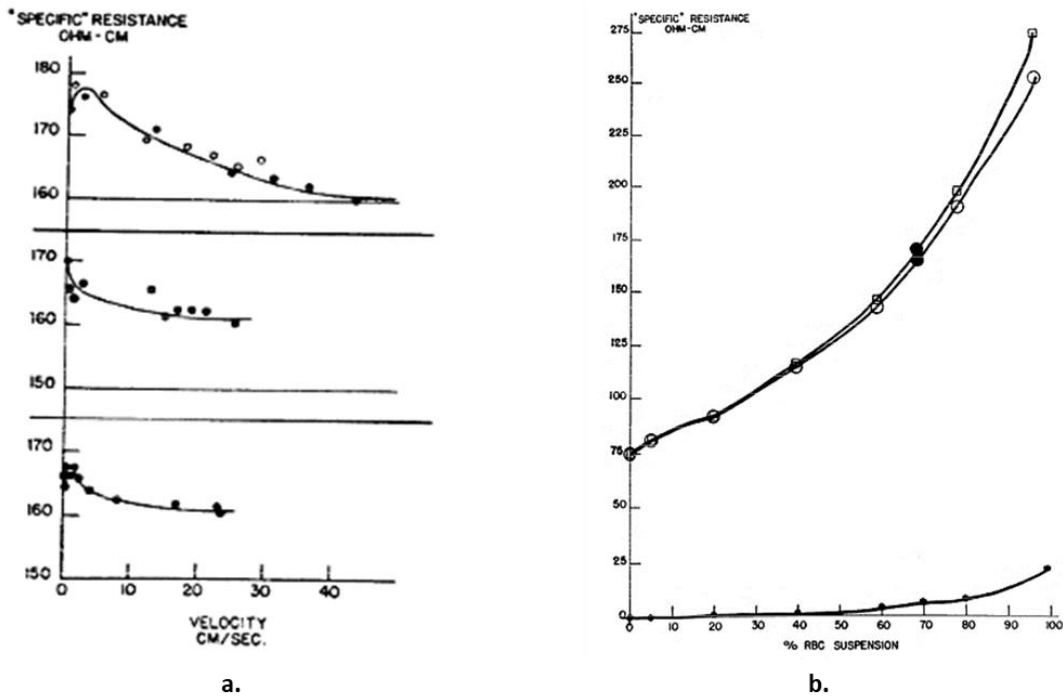


Figure 2.9: (a). Specific resistance variation with velocity for three samples of beef blood, and, (b). Comparison of the varying specific resistance with haematocrit at rest (upper curve) and at a linear velocity of 15cm/sec (middle curve). The lower curve states the difference between the two curves [78]

Since, the decrease in resistance was of the same order along the transverse and the longitudinal axis, therefore, the assumption of orientation having an influence on variation of impedance was neglected.

Higher velocity of the blood at the center than the edges accounted for more variation of resistance along the longitudinal axis than the transverse one. It was concluded that the erythrocytes were created during blood flow while during the time the blood was static, they were clumped together, and dynamic blood flow separated them.

The blood flow variations due to its dynamic nature and compositional characteristics, offer significant challenges in determination of their accurate contribution towards BIA measurements. Blood flow volume variations and concentration of erythrocytes are the major factors. A variety of other factors are also taken into consideration such as the quality of blood as well as the arterial compliance. Some other factors like the blood velocity which influence blood viscosity, and the acceleration which has an effect on impedance variations in the pulsatile flow can be taken into regard as well. A model depicting the variation of impedance alongside transfer of pressure pulse can be effective wherein pulse wave velocity and ventricular ejection have a significant impact in the process of calculation of stroke volume from the limb.

2.4 Instrumentation for Bioimpedance analysis

BIA is essentially a non-invasive measurement procedure and the instrumentation comprises of two parts: excitation system and the measurement system (electrodes). Kubicek et al., 1970 [79] conducted the Thoracic Impedance Cardiography for the calculating specific impedance using the Minnesota Impedance cardiograph (Model 303) [62]. Four-electrode configuration with conductive strip made of aluminum was employed in this experiment. The first and the fourth electrodes were used for supplying sinusoidal current of 4 mA while the frequency was set to 100 kHz. The second and third electrodes were employed for measuring the voltage after being fed through an amplifier that offered a resistance of 100 k Ω s [79]. The signal conditioner was employed that assisted in removing noise and yielding significant parameters such as impedance Z , variation in impedance ΔZ and the rate of change of impedance with time dZ/dt which is basically the ECG.

2.4.1 Operational frequency and safety standards

A spectrum of large range of frequencies is considered so that accurate results of electrical impedance of tissues are obtained. The two circuits considered are the excitation (driving) circuit and the measurement (sensing) circuit. The electrical impedance can be measured in different ways depending upon the consideration of driving and sensing circuits [65]. One of the methods employed is changing the frequency of the excitation current and measuring the consequent voltage [80]. Another method is employing the multiplexer to apply current with multiple frequency components to account for all layers of dispersion spectrum. (Lozano et al., 1990 [81]) A similar effect can be achieved by application of a pulse of broad spectral energy (Record et.al., 1992 [82] and Waterworth et al., 2000 [83]). The measurement process can be expressed in terms of a block diagram as seen in Figure 2.10.

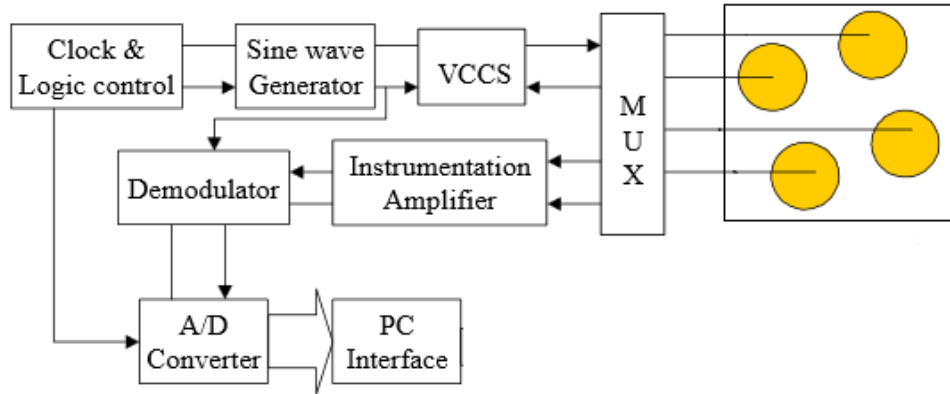


Figure 2.10: Block Diagram of a transfer (bio)impedance measuring system [65]

There is a maximum value of current that is considered as a safe limit above which the tissues and the skin might be damaged as postulated by Valentinuzzi, 1995 [84]. The value of this safe current is 1mA at 100 kHz frequency. The minimum level at which the sensitivity was experienced or the threshold value of the current is directly proportional to the frequency as demonstrated by Brown et al. 1999 [85]. According to the IEC 60601-1 (Section 8.7.3) safety standards [86], the maximum current stimulation to human tissues can be 10 μ A at DC and 100 μ A (rms) at 100 kHz.

2.4.2 Driving circuits

The excitation or driving circuit for BIA measurements is effectively a voltage controlled current source (VCCS). Electrical Impedance Tomography requires that the current source design is accurate [87]–[93]. The negative feedback current source accentuates the performance of VCCS at higher frequencies above 1 MHz. The transformers are not employed in the circuit as they may offer complications by slowing the performance of the circuit. Some of the common implementations of a VCCS include Howland circuit [94], [95] and the current mirror architecture. ([96]–[98]). There is no positive feedback with the VCSS in case of current mirror while Howland circuit has both positive and negative feedback loop along with an amplifier and is, thus, preferred for EIT and EIS applications. The current mirror circuit and the Howland current driver circuit have been shown in Figure 2.11 (a) and (b), respectively.

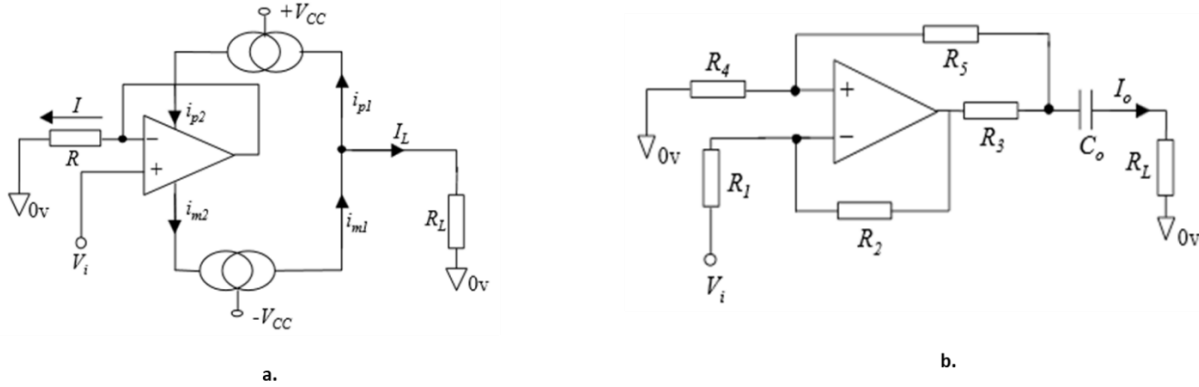


Figure 2.11: (a). A basic current mirror circuit, and (b). An improved Howland current generator circuit used in EIT

2.4.3 Proposed bioimpedance measurement systems

Electrodes might contribute to the impedance of the circuit and thus, they must be chosen accordingly while other parameters including stray capacitances may also influence the circuit by interacting with the impedances. The various capacitances as well as impedances in a bioimpedance set up can be demonstrated below in Figure 2.12.

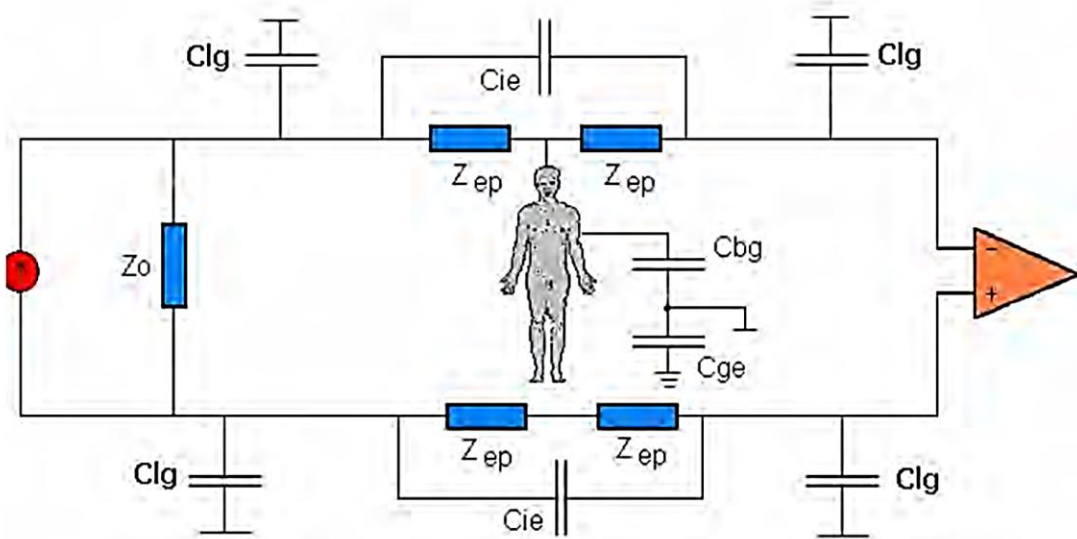


Figure 2.12: Various capacitances and impedances encountered in a BIA setup [99]

The value of the capacitance that exists between the two neighboring electrodes is C_{ie} while C_{lg} describes the capacitance between the signal leads and ground. The capacitance between the signal ground and earth C_{ge} and C_{bg} denotes the residual capacitance between body and ground. The value of Z_{ep} should be kept as

low as possible so that the interference offered by these parasitic capacitances is minimum, thereby, maintaining signal accuracy.

Wang et al., 2011 [100] conducted plethysmography on forearm by supplying a single frequency sinusoidal current of magnitude 1 mA at a frequency of 100 kHz by means of Wein bridge oscillator. The output voltage is fed towards instrumentation amplifier while after that it is subjected to a notch filter to reduce the noise. The circuit consisted of full wave rectifying modulator, a low-pass filter (30Hz) of the fourth order and a high-pass filter (0.5 Hz) of first order. The circuit for the impedance measurement according to Wang et. al. [100] is given in Figure 2.13.

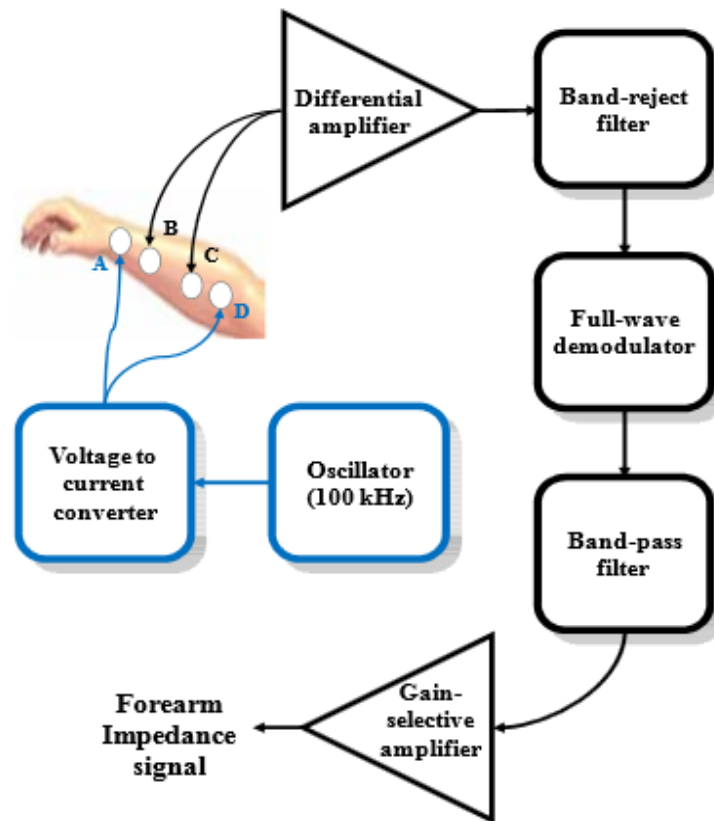


Figure 2.13: Block diagram of the forearm impedance measurement stated by Wang et al., 2011 [100]

A real time monitoring system for measurement of impedance cardiography was proposed by Shyu et al., 2000 [67]. 50 Hz was set as the upper band limit, based on the assessment by Hurwitz et al., 1993 [101] for measurement of ECG or the dZ/dt component. The circuit model postulated by Shyu is given in Figure 2.14.

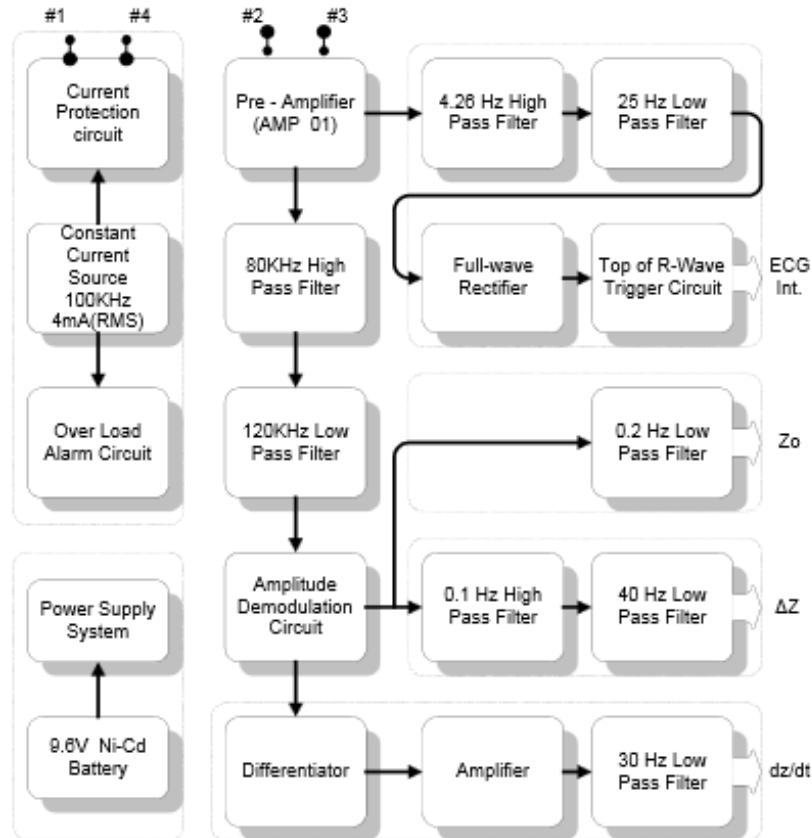


Figure 2.14: The block diagram of the real time monitoring ICG system as proposed by Shyu et.al.[67]

A general choice for the instrument setup can be obvious from the above discussion to account for the application. An appropriate choice for the current source must be made in correlation with the frequency operation. Normally, it is difficult to obtain a current source for operation at a frequency nearing the megahertz range. In that case, the design of the VCCS using a wide frequency voltage source can be a good choice, however, additional elements' compatibility and specifications must be taken into account. Appropriate signal conditioning can be achieved, depending upon the requirements in a particular application.

2.5 Electrical modelling for Bioimpedance measurements

Electrical modelling is the prerequisite for any type of bio-electrical signal analysis of the living body. Since the measurement of bioimpedance is a non-invasive procedure, various artefacts can influence the efficiency of the measurement and hence promote a greater need of accurate modelling. The modelling depends on factors like the types of electrodes- contact gel based or textile, frequency of operation- single or multiple frequency and the considerations based on the ultimate objective.

Cole-Cole model forms the theoretical basis for electrical modelling as was demonstrated by Schwan and Kubicek's model for ICG. The circuit given below describes intracellular and extracellular fluid responses separately in Figure 2.15. R_E is a single component value in ohms, R_I is the aggregated component resistance in ohms and C_M is the membrane capacitance in farads.

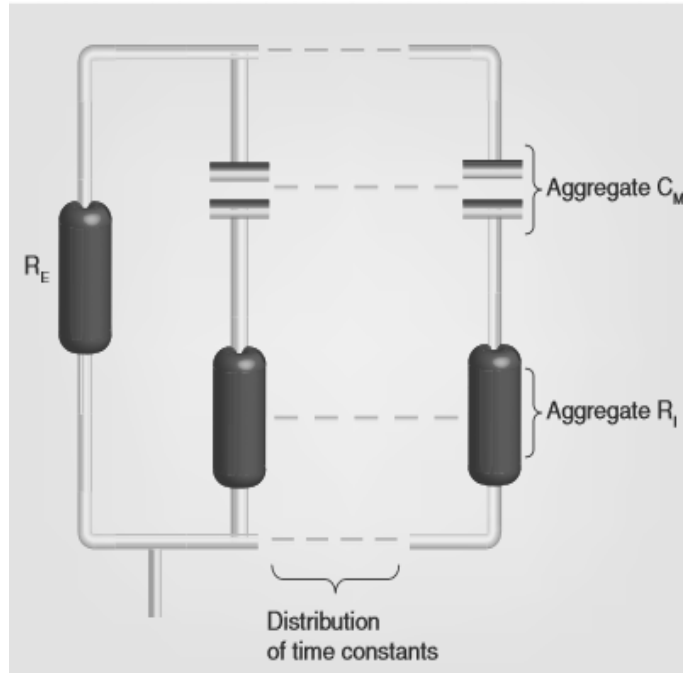


Figure 2.15: Electrical circuit analogous to Cole model [47]

The overall BIA measurements are a result of contributions from different tissues and measurement setup and hence isolating a single factor and its effect can be challenging. One of the ways to approximate the effects of tissues and predict their response is through the determination of their electrical behavior by modelling their physical structures. This can be observed in the thorax region wherein stroke volume needs to be estimated and the Kubicek model and equations associated with it are employed through ICG. The assumptions made for the thorax region are unreliable, but the same assumptions can fit for a more uniform geometry, like a section of human limb.

Multi-frequency electrical bioimpedance measurements (MF BIA) are generally analysed through a Cole-Cole model. As has been mentioned before, Cole equation is not definitive, but an empirical derivation of the dielectric response of biological materials that exhibit distributed or overlapping relaxation dispersion regions. However, it has been widely accepted to model the impedance data and define the dielectric behavior of inhomogeneous materials like biological tissues. The Cole-Cole model is one of the several models that theorize the phenomenon of distributed time constants for complex dielectric materials. The important general dielectric relaxation models are mentioned in Table 2.2.

Table 2.2: Different dielectric relaxation models

Dielectric Relaxation Model	Model Equation
Debye dielectric model [17]	$Z(\omega) = R_{\infty} + \frac{R_o - R_{\infty}}{1 + j\omega\tau_D}$
Havriliak – Negami model [102]	$Z(\omega) = R_{\infty} + \frac{R_o - R_{\infty}}{(1 + (j\omega\tau_{HN})^{\alpha})^{\beta}}$
Cole-Davidson model [103]	$Z(\omega) = R_{\infty} + \frac{R_o - R_{\infty}}{(1 + j\omega\tau_{CD})^{\beta}}$
Cole-Cole model [23]	$Z(\omega) = R_{\infty} + \frac{R_o - R_{\infty}}{1 + (j\omega\tau_{CC})^{1-\alpha}}$

For each model as mentioned above, the dielectric phenomenon exhibits its own relaxation time constant: τ_D as time constant for Debye relaxation, τ_{HN} for Havriliak – Negami relaxation, τ_{CD} for Cole-Davidson model and τ_{CC} for Cole – Cole model (all other terms have their usual meaning). It is worthwhile to note that all the models and relations are empirical and essentially modified relations of Debye type relaxation to account for different types of asymmetries occurring in the measured dielectric behavior. The Cole – Davidson and Cole model combine to form the Havriliak – Negami relaxation model, which generalises the overall dielectric relaxation in tissues. The characteristic frequency (ω_c) can be defined as the reciprocal of the time constant. In symmetric relationships it is also the frequency of maximal loss, although that does not hold true in cases of asymmetrical relaxations [104].

Conventionally, all the coefficients in all the above mentioned models, i.e. α and β , lie within 0 and 1 and the systems are often referred to as stretched exponential systems [105]. However, the value of either of α or β greater than 1 defines a state of a compressed exponential system which has been reported in various studies [106], [107] and reflects disorder in the material properties due to heterogeneity or random atomic re-arrangements.

The frequency dependent response of the tissues can be aided by modelling a part of the electrical circuit as a CPE, which can be mathematically defined through Equation 2-1.

$$Z_{CPE}(\omega) = \frac{A}{(j\omega)^k} \quad \text{Equation 2-1}$$

where k is the coefficient of relaxation in the Cole-Cole equation and A is the magnitude constant. One of the important considerations is defining the skin-electrode interface that is dependent on type of electrodes. CPE and other passive elements were employed for modelling the skin electrode interface along with consideration of tetra polar configuration for bioimpedance spectroscopy in the study conducted by Medrano et al., 2007 [108]. The circuit is expressed diagrammatically in Figure 2.16 considering the standard and the textile electrode.

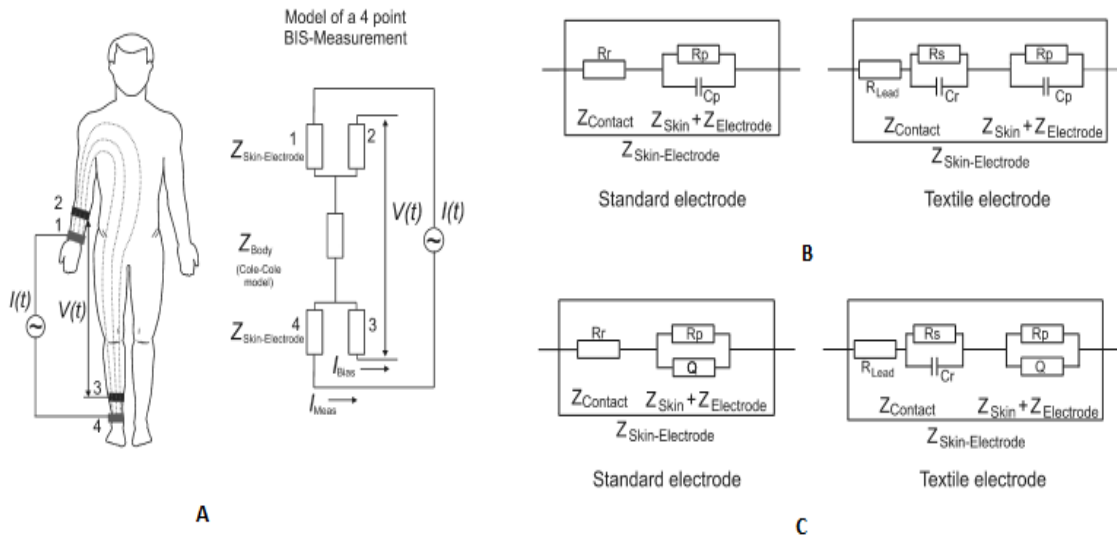


Figure 2.16: A. Tetra polar BIS configuration with measurement circuit, B. Equivalent circuits for standard and textile electrodes using passive elements, C. Equivalent circuits for standard and textile electrodes using CPE (Q)[108]

Among the very few electrical models of tissues present in the literature, the resistivity model of a tissue within a limb was postulated by Zhu and Levin, 2003 [109] and the model is depicted in Figure 2.17 simultaneously with the circuit representation.

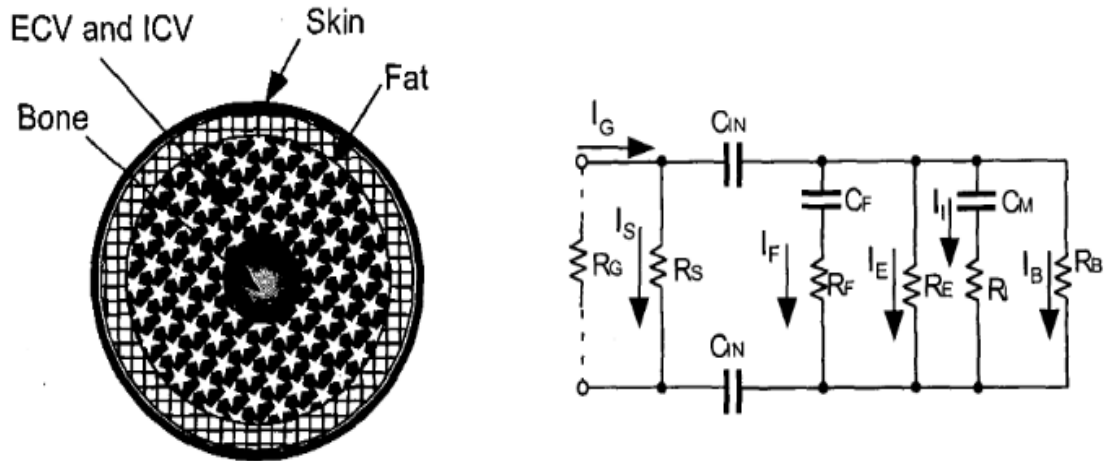


Figure 2.17: A model and the corresponding electrical circuit for a limb segment [109]

The Newtonian and the sleeve effect of blood on the mathematical modelling of tissues was studied in great depth by Jager et al., 1965 [110]. Laminar flow of blood was assumed to yield electrical analogue for oscillatory blood flow impedance which is depicted in form of a circuit in Figure 2.18.

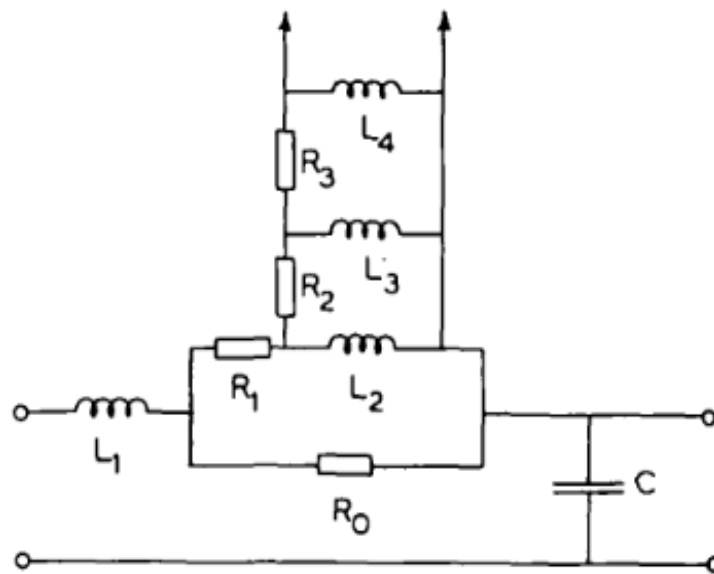


Figure 2.18: Electrical analogue for oscillatory blood flow impedance with all suitable corrections (R_0 is the correction for anomalous viscosity, C is the capacitance and R_i, L_i are the longitudinal impedance parameters where the extent of i defines the accuracy of the system [110])

The consideration of the frequency of operation depends on the type of application. With the exception of impedance cardiography, almost every application from BIS to impedance plethysmography makes use of

multiple frequency operation. Different electrical responses can be observed not only for different tissues like the muscle and bone but also for intracellular as well as extracellular fluid [111]. The characteristic frequency undergoes variation with changes in body fluid due to change in the phase and the reactance (X).

Bioreactance ([112]–[114]) is a newer concept that is aimed at calculating the cardiac output. It uses the concept of relative phase shifts that take place in the oscillating current flow that passes through the thorax region. The blood flow volume variations influence blood resistivity changes as well as reactance variation. The impedance cardiography measurement obtained doesn't have to be dependent on spacing between the electrodes as the relative phase shift is considered. However, the disadvantage with this method is that the haematocrit changes for different subjects and conditions are not considered.

Overall, it can be observed that the design of the system is dependent on the application. For calculating stroke volume, impedance plethysmography needs to be performed on a limb and electrical model needs to be correctly predicted for the limb section. Various parameters such as volume variations, changes in resistivity, geometry of the region, compliance of the brachial artery and most importantly interdependence between the parameters need to be considered and included in the prediction. The concept of electrical impedance velocimetry was touched upon in the estimation of stroke volume from brachial artery [115]. Some region-specific variations are applied in the Kubicek's equation for ICG along with the concept of supply of constant magnitude, high frequency current from upper arm to elbow pit or antecubital fossa.

2.6 Research Gaps

The literature review provides a substantial insight into various BIA techniques and simultaneously throws light on the various applications as well. Based on the existing literature, the following research gaps have been identified:

- Each tissue layer is quite complex and requires knowledge of the electric field distribution inside it. The electrical properties of each layer are quite complex and varies from each other tissue layer. The contribution from each layer needs to be studied in detail.
- Single frequency operation (SF BIA) cannot explain the influence of multiple factors involved in impedance measurements. In applications like plethysmography and hemodynamic monitoring, SF BIA is prone to several assumptions which might affect the accuracy of the estimated parameters.

- Geometry of the electrode along with the electrode configuration affect the electric field distribution. It has been established that the distribution of electric field is along both longitudinal and transverse direction thereby being influenced by the geometry of electrodes.
- The effect of the clumping and de-clumping of erythrocytes contribute towards the conductivity of flowing blood, however this variation of conductivity with flow is not well understood.
- No prior studies address an electrical simulation approach to model the distribution of electric field within the tissues.
- No previous studies have discussed the influence of the properties of other tissue layers on the overall BIA measurements. This is important, particularly in hemodynamic monitoring where it is essential to isolate the response of flowing blood from the overall BIA measurement.

2.7 Research Question and Objectives

Based on the above identified research gaps, the following research question was identified:

Can we isolate the response of individual tissues from an overall BIA measurement?

Following on this, the main objective of this research is to understand the independent contribution of each tissue layer on an overall BIA measurement. Existing literature has mentioned an established use of SFBIA through techniques like ICG for blood flow monitoring. Additionally, the associated drawbacks and assumptions have also been well addressed, hence this research seeks to investigate MFBIA and its potential in modelling the dielectric response of each tissue. The following objectives outline the scope of this work:

1. **Understanding the electric field distribution within different tissue layers through a simulation perspective in a human forearm structure.** This will help in the better understanding of the electrical properties of tissues through an externally applied electric field.
2. **Modelling the simulation results to determine the response of each tissue layer.** This aims to fit the simulated BIA measurements to a Cole model and isolate the response of individual tissues.
3. **Modelling the actual response of human forearm tissue layers – bone, fat, muscle and blood – to determine the individual tissue response.** This will aim at BIA measurement from actual human forearm to identify the response of each tissue domain and comparison with the simulated results. The effect of skin will not be considered as the use of gel electrodes is expected to bypass skin's impedance in real applications.

Overall, this study seeks to contribute a new simulation perspective along with new models that can form the basis for clinical implementation of accurate tissue response, the most likely to be hemodynamic monitoring.

To address these objectives, the remainder of the thesis has been structured as:

- Chapter 3 discusses a simulation analysis of human forearm model to investigate the electric field distribution within the modelled tissue layers.
- Chapter 4 will focus on a pilot experimentation of MFBIA on actual human forearm to determine the impedance response of real tissues.
- Chapter 5 will focus on electrically modelling the results obtained in Chapters 3 and 4 and estimate the response of individual tissue domains in the form of Cole parameters.

Chapter 3: Simulation of a human forearm model

This chapter focusses on the initial objective of understanding the distribution of electric field within the different tissue domains through BIA analysis. The investigation will be carried out through a multi-physics simulation of the major tissue layers – bone, fat, muscle and blood. The simulation will seek to obtain the overall model response as impedance measurements, which will be analyzed and modelled to estimate the response of each tissue layer.

The first part of the chapter introduces Ansys® HFSS, which has been used as the simulation platform. Subsequently, the model design and properties will be discussed followed by the measurements performed between the frequencies of 1 kHz and 1 MHz.

3.1 Ansys High Frequency structure simulator (HFSS)

Ansys HFSS (High Frequency Structure Simulator) is an electromagnetic simulation software. It is based on Maxwell's electromagnetic equations and employs the principle of finite element modelling through its advanced solvers for an effective analysis of various electronic devices and sensors [116]. A plethora of complex problems at high range of frequencies can be solved using the principles of 3-D electromagnetic equations. It is a simulation software used for testing, simulating and designing high frequency electronic devices such as antennas, high speed interconnectors, RF components, IC's etc.

An understanding of the HFSS simulation platform can be gathered through the following sequence of steps that are followed to perform the simulation:

1. Construction of a structure and defining its geometry.
2. Defining the solution type as terminal, modal or transient.
3. Initiation of excitation and setting up of the desired boundaries.
4. Assigning the materials to be used and defining the properties of the material.
5. Addition of type of meshing of the network.
6. Addition of solution setup by stating the desired frequency and the number of iterations to be performed.
7. Use of HFSS inbuilt calculator to define and express the complex electromagnetic equation and obtain the result in the form of real and imaginary impedances.
8. Validation of the final design and including all the definitions.
9. Running the simulation and subsequent analysis of the HFSS design.

The HFSS features the options of obtaining the results in the form of plots of simulated electric field(E), current density (J), magnetic field (H) etc. Another feature of the post analysis process is obtaining the result by employing an inbuilt calculator that has manifestations of Maxwell's complex electromagnetic equations as the input. It helps in determining any output that cannot be calculated using plots or graphs.

3.1.1 Ansys Solver

The fundamentals of the HFSS solver are based on the Maxwell's electromagnetic equations and their corresponding solutions. The differential form of Maxwell's equations is employed in the HFSS solver. Equation 3-1, Equation 3-2, Equation 3-3 and Equation 3-4 demonstrate the interdependence between the electric and magnetic fields while defining the properties of the materials employed. This is done by considering their permittivity (ϵ), electrical conductivity (σ) and magnetic permeability (μ).

$$\nabla \times \vec{E} = -j\omega\mu\vec{H} \quad \text{Equation 3-1}$$

$$\nabla \times \vec{H} = (\sigma + j\omega\epsilon)\vec{E} \quad \text{Equation 3-2}$$

$$\nabla \cdot \epsilon\vec{E} = \rho \quad \text{Equation 3-3}$$

$$\nabla \cdot \mu\vec{H} = 0 \quad \text{Equation 3-4}$$

These equations are expressed and stated in the inbuilt calculator in Ansys HFSS solver. Herein, the angular frequency is ω ($\omega=2\pi f$), while the resistivity is given by σ . There are some assumptions considered to get accurate results. First one is that the wavelength at the maximum frequency which yields a solution is more than the size of the geometric model. Second one is that the model is considered to have isotropic properties. This means that the properties of materials along different directions is uniform. The boundary needs to be properly set and defined. The excitation parameters need to be defined along with assigning their magnitude and direction. In this case, the current at 1mA is specified as the excitation parameter. This is because the safe limit for current is 1mA and it gets even lesser at very high frequencies. This value is suitable for practical BIA measurements. The potential difference is expressed in terms of line integral of electric field between the two inner electrodes. Its output is obtained in complex form with the real part as resistance and imaginary part as reactance.

3.2 Model of a human forearm

The 3-D model of human limb was designed in Ansys HFSS by means of a finite modelling process to perform the electrical simulation. The simulations were performed in a preferred frequency range of 1 kHz-1MHz. The emphasis of our investigation was to target a part of the β dispersion frequency range to reflect most of the tissue impedance (resistance and reactance). The tissue layers that were taken into consideration

at the outset were fat, muscle, blood and bone. Skin layer is a prominent contributor in the overall impedance measurements, so much so, that its high impedance was expected to make it behave like an insulator in the path of the small excitation for this work. It was not included in this analysis as this high impedance effect will be reduced to negligible through wet electrodes – which are conventionally used for BIA measurements.

The fat and the muscle layers were modelled as concentric layers along the same axis. The artery section was modelled to mimic the radial artery perfused through both the fat and the muscle domains. The artery wall enveloped the artery along its surface and was assigned the properties of muscle while forming the interface between muscle and blood. The bone was subdivided into two main regions - radius which was at the center and thicker, and, ulna which was relatively at the periphery and smaller in cross-section.

However, not all layers were concentric, and were distributed with different degrees of thickness. The longitudinal cross section of human forearm model was taken as 70 mm. The dimension in terms of thickness of the fat is 3-6 mm while for muscle it is 10-15 mm. The artery dimensions were taken as 2.35 mm ([117], [118]).

3.3 Simulation Setup

The simulation set up consisted of the structure of a section of human forearm in Ansys HFSS. The forearm section was designed as a trapezoid with the BIA measurements being carried out using 2 pair of cylindrical surface electrodes. The outer set of electrodes were used as current source while the inner set of electrodes were used for measuring the resultant potential difference. The amplitude of current for the simulation was considered to be 1mA to be in accordance with the electrical safety limits identified by IEC 60601 standards [86]. The main aim of designing the 3-D model in Ansys and performing the simulation was to evaluate the dielectric response and the electric field distribution within individual layers of the tissues. The entire structure was surrounded by a radiation boundary and a vacuum region to isolate it from external electromagnetic interferences. The electrodes were chosen to be conductive through defining their material properties as those of copper. The diameter of the electrodes was chosen to be 2 mm, with a separation between each of the electrodes being 20 mm. Figure 3.1 and Figure 3.2 depict the longitudinal and the top view of the 3-D model displaying the various tissue layers.

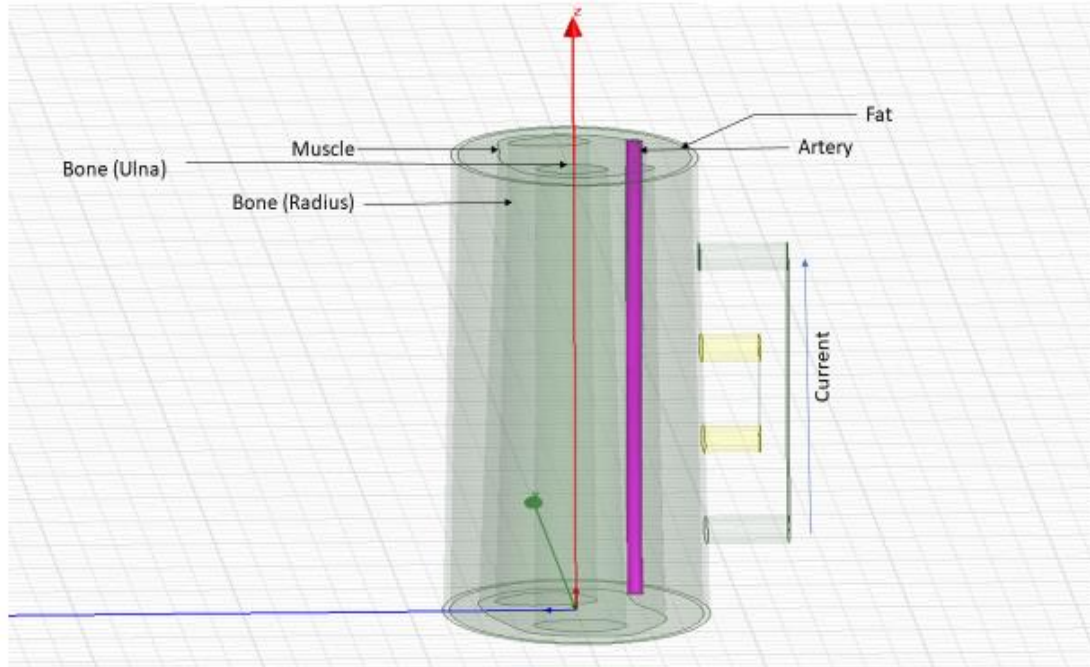


Figure 3.1: Longitudinal view of the designed 3-D model in Ansys HFSS

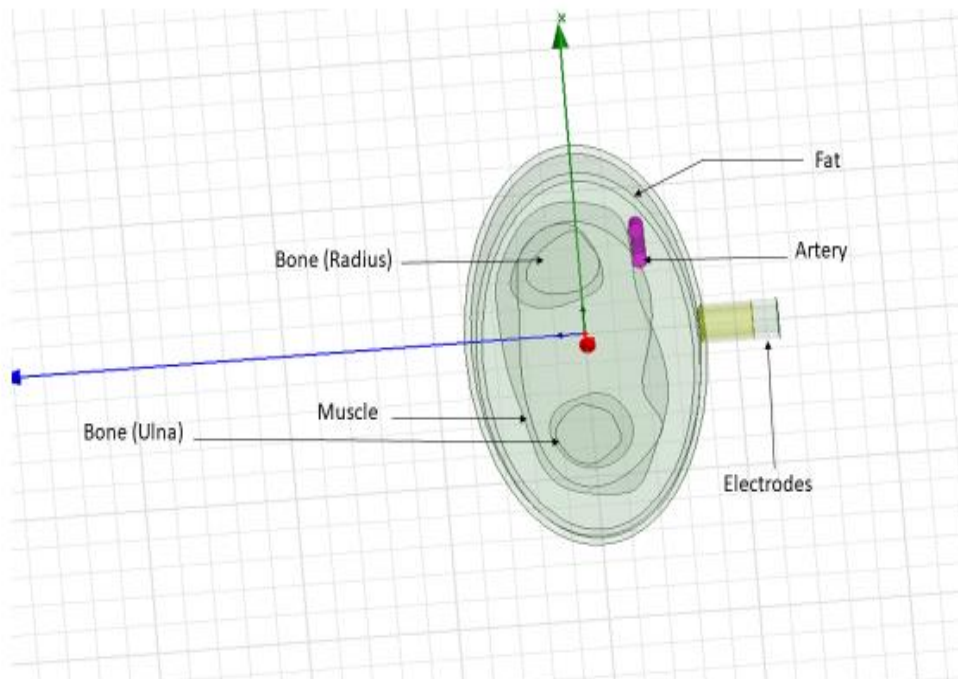


Figure 3.2: Top view of the 3-D model

3.3.1 Material properties of tissue domains

The human tissue layers were assigned frequency dependent material properties in the form of complex bulk conductivity and relative permittivity from the database developed by Gabriel and Gabriel ([56]–[59]).

Figure 3.3 and Figure 3.4 show the frequency dependence of bulk conductivity and relative permittivity, respectively, as documented in Gabriel’s database.

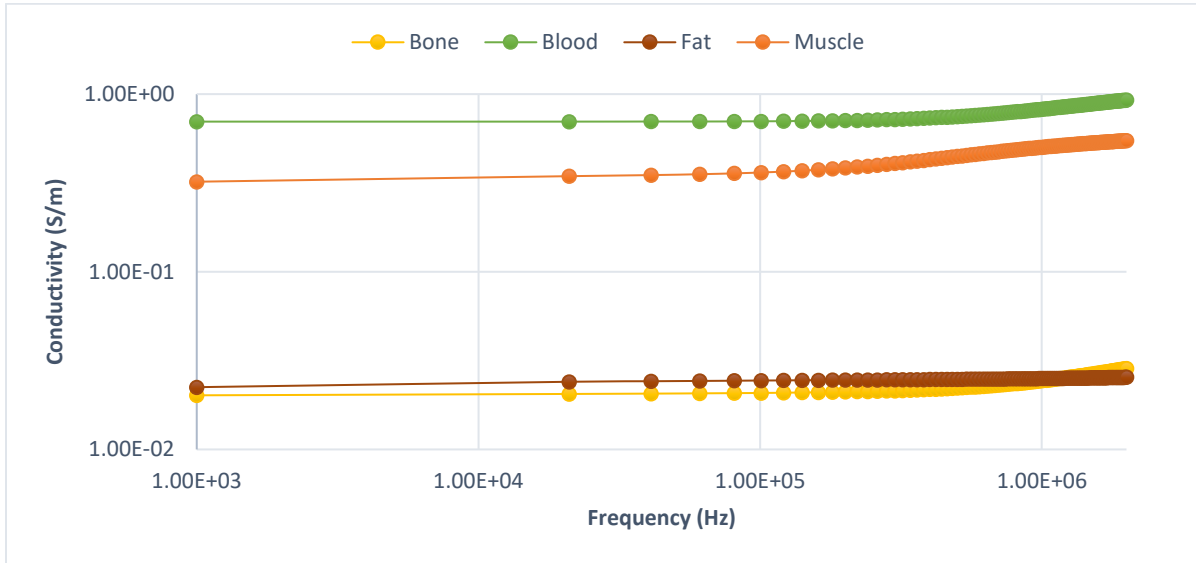


Figure 3.3: Conductivity (S/m) for bone, blood, fat and muscle tissues as compiled by Gabriel

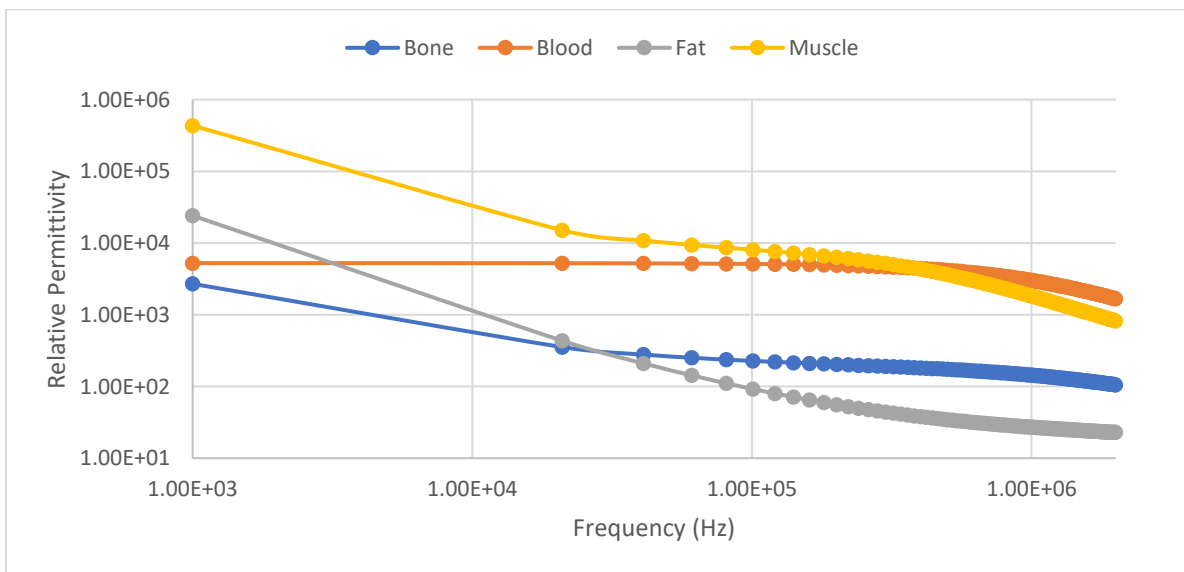


Figure 3.4: Relative Permittivity for bone, blood, fat and muscle tissues as compiled by Gabriel

3.3.2 Finite Element Modelling

Ansys® HFSS solves the electromagnetic equations for a given structure using finite element modelling (FEM). FEM is the basis of most common simulation platforms for multiphysics analysis and helps to determine solutions within a non-uniform geometry as well as interactions at the boundaries between multiple tissue domains. In this study, tetrahedral meshing with a patch independent algorithm was used. The optimization of the computing complexity and model efficiency was obtained by selecting the maximum mesh element sizes of 5 mm. Table 3.1 lists the number of tetrahedrons generated during the simulation process.

Table 3.1: Summary of tetrahedrons for each tissue layer

Tissue layer	Number of tetrahedron elements
Blood	9224
Bone	15671
Muscle	21768
Fat	31690

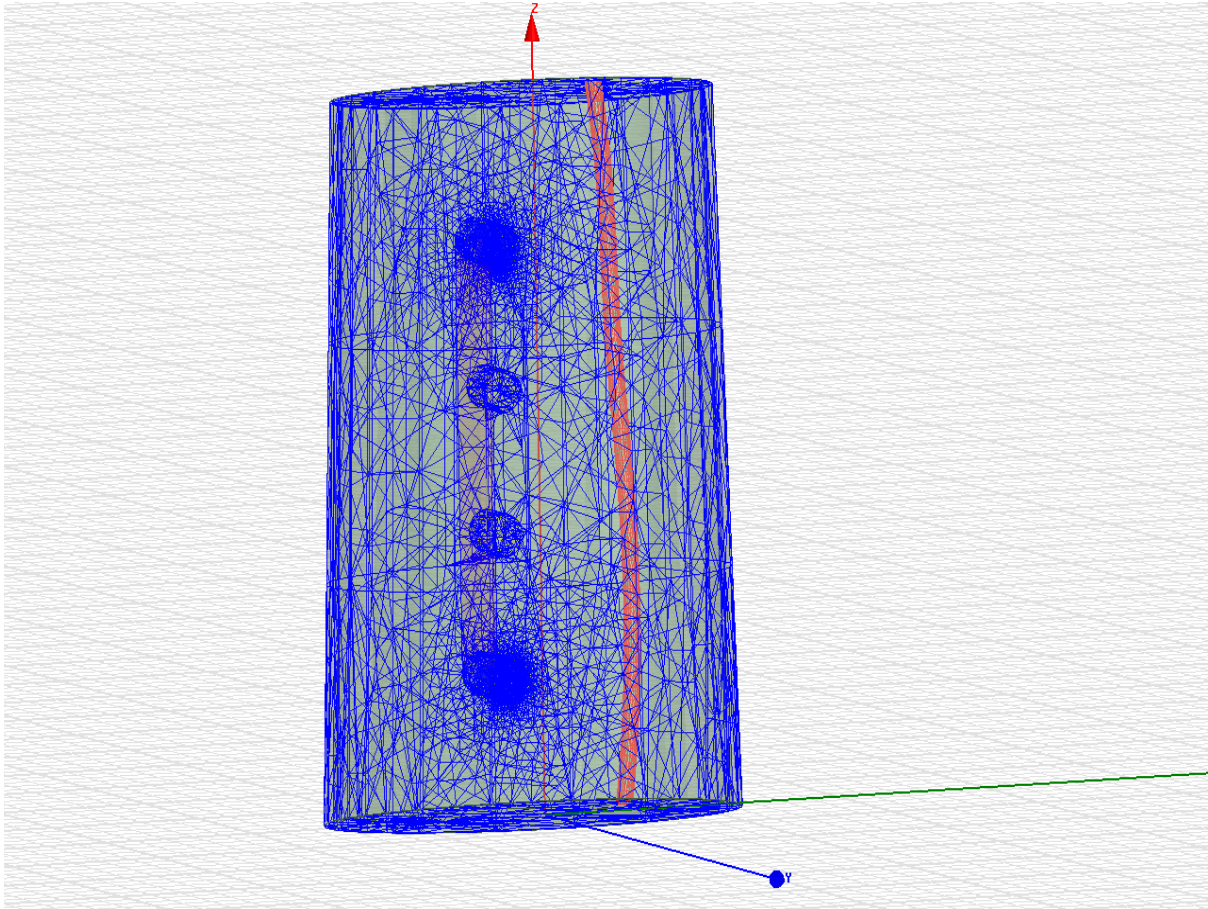


Figure 3.5: Mesh distribution in overall human forearm section, including the electrodes.

3.4 Simulation Results

Figure 3.6 and Figure 3.7 show the obtained distribution of electric field within the modelled tissue layers at 1 kHz and 1 MHz, respectively. The simulation results were obtained for a range of frequencies from 1 kHz - 1 MHz. The electric field distributed throughout its volume determines the direction of flow of current. The line integral of electric field along the inner electrodes was used to determine the corresponding voltage drop, which was used to calculate the impedance of the section. Due to the complex conductivity and permittivity defining the properties of the tissue layers, real and the imaginary parts of the impedances were evaluated.

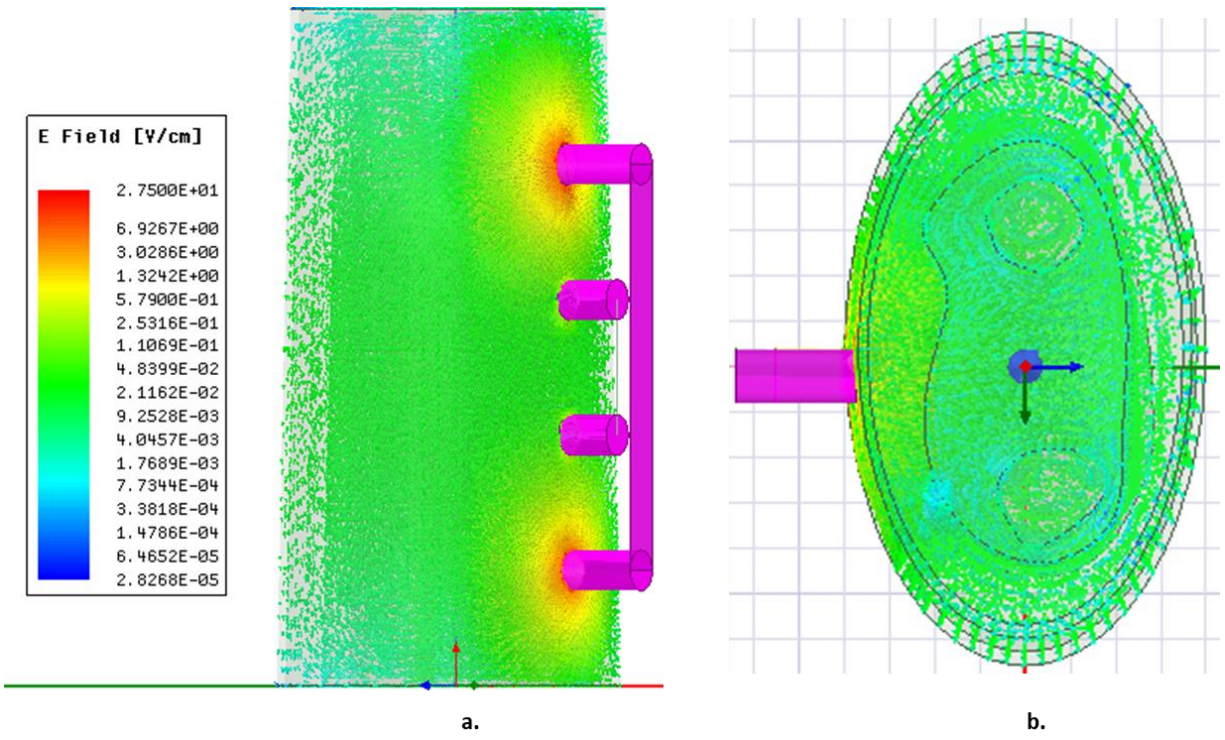


Figure 3.6: Electric field distribution at 1 kHz (a). front view, (b). top view

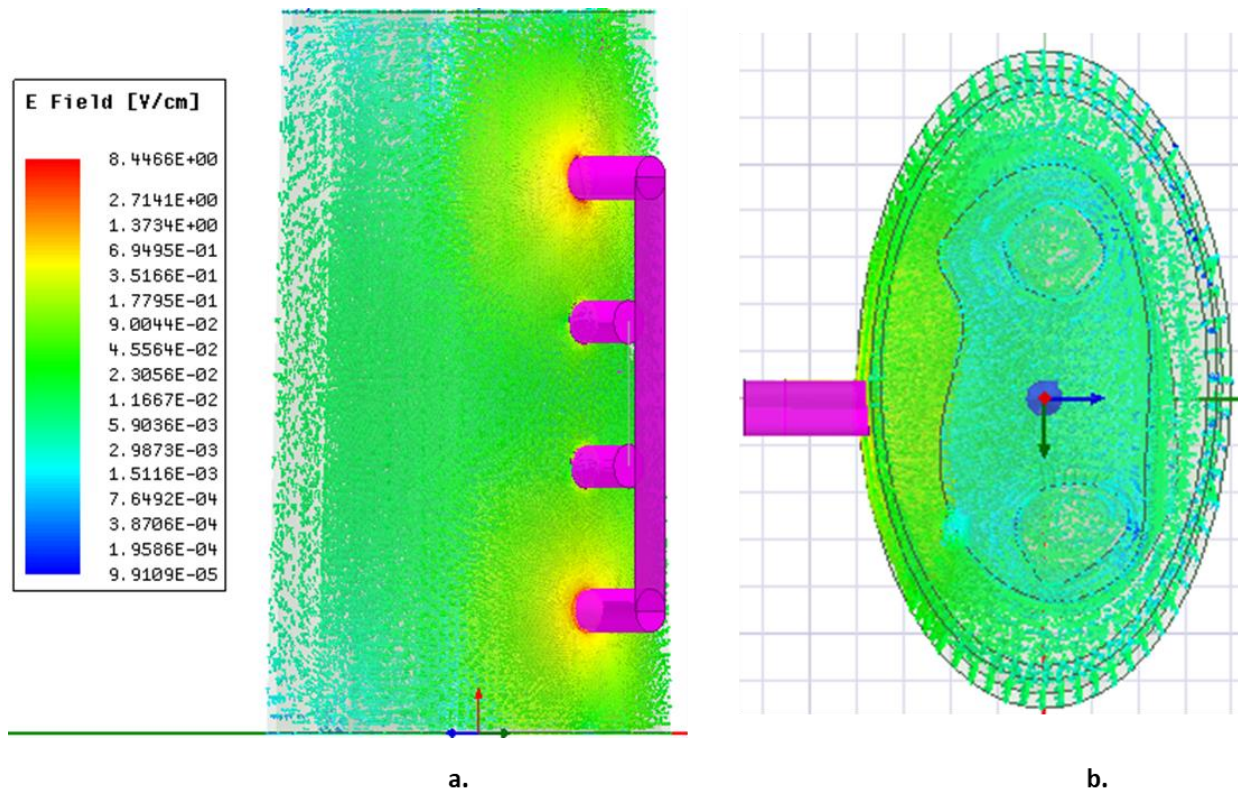


Figure 3.7: Electric field distribution at 1 MHz (a). front view, (b). top view

The simulation results were obtained as 2-D plots of real and imaginary parts of the impedance. Figure 3.8, Figure 3.9 and Figure 3.10 show the impedance spectra of real part of impedance, imaginary part of impedance and real vs imaginary parts, respectively.

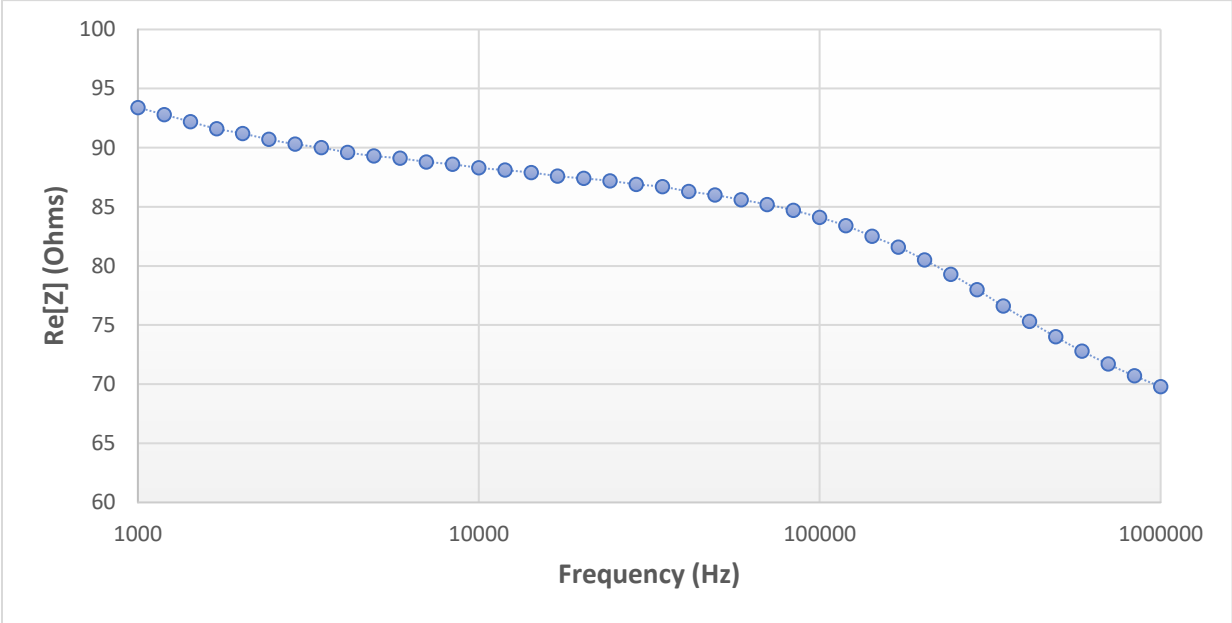


Figure 3.8: $Re[Z]$ vs frequency plot obtained from simulation results

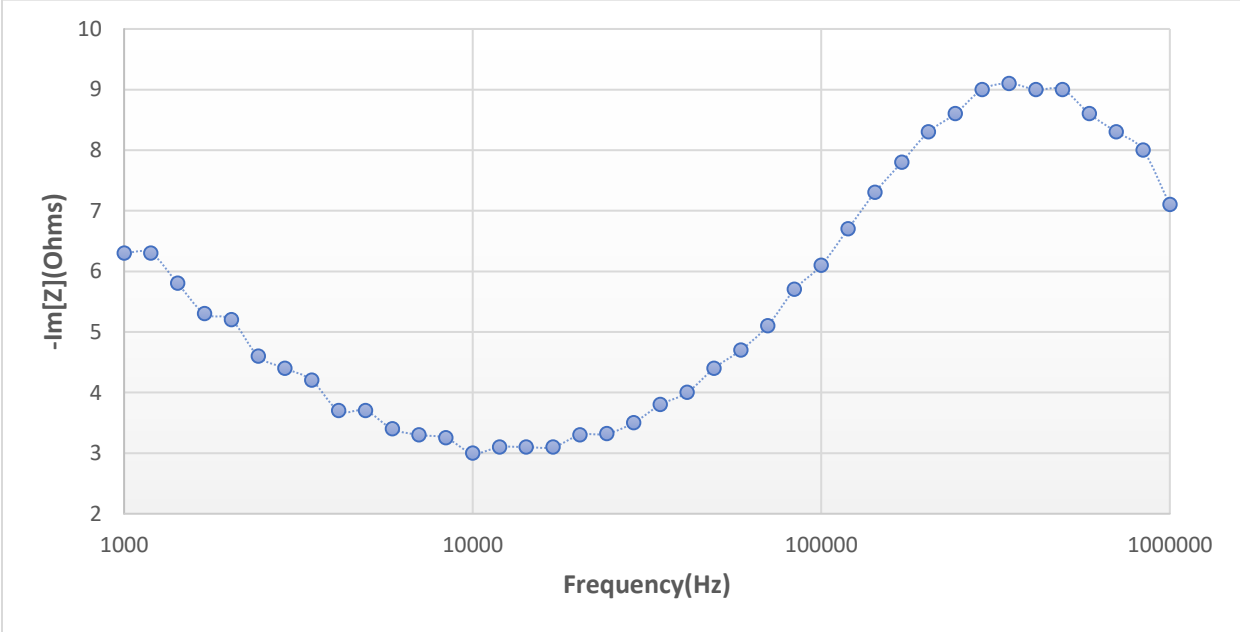


Figure 3.9: $-Im[Z]$ vs frequency plot obtained from simulation results

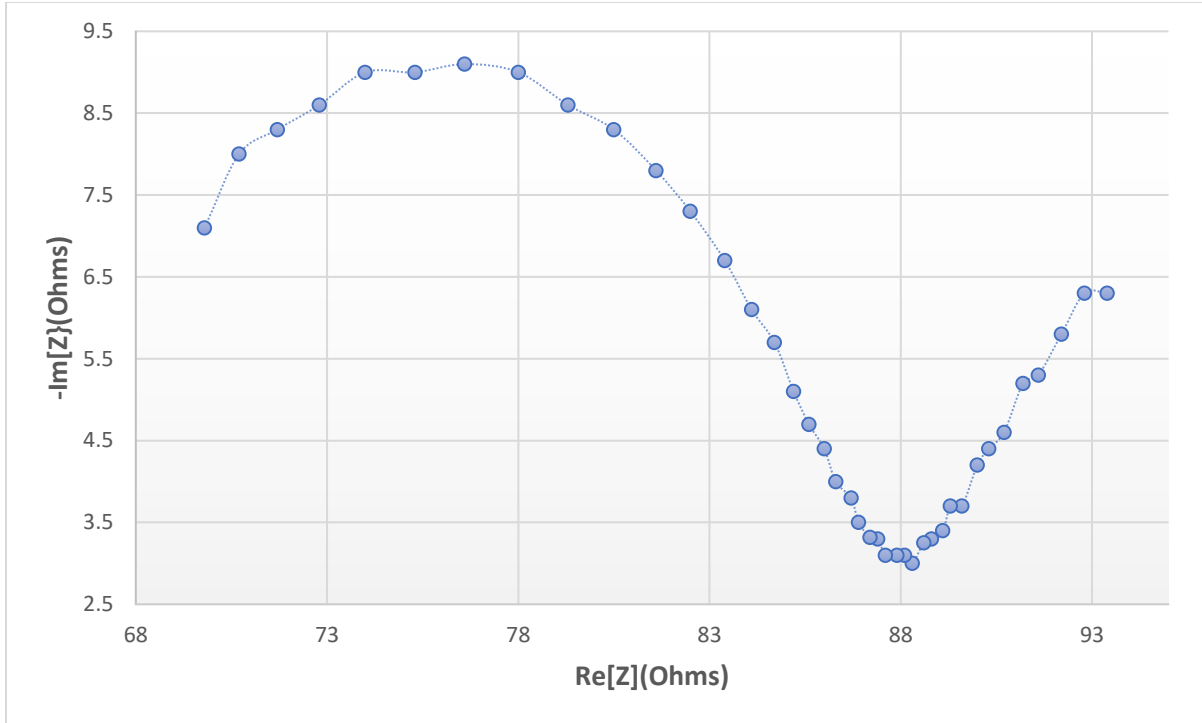


Figure 3.10: $-Im[Z]$ vs $Re[Z]$ (Cole) plot obtained from simulation results

Figure 3.10 shows the Cole type behavior of the simulation response. The behavior is existent beyond the frequency of 10 kHz ($Re[Z] = 88 \Omega$). The Cole parameters can be approximated by extrapolating the trend above 10 kHz to the real axis. The values at frequencies lower than 10 kHz did not follow a Cole-type behavior which can be explained through the overlap of α and β frequency dispersion regions as well as the dominantly resistive behavior of blood.

3.5 Discussion

The main objectives of the simulation study were:

- Simulating a 4 electrode BIA (Impedance spectroscopy) over a section of human forearm.
- Investigating the distribution of the electric field within the tissue layers.
- Determining the impedance spectra of the forearm section and verify its behavior as Cole type.

The simulation used material properties such as permittivity and bulk conductivity of various tissues to calculate the real and imaginary impedances. The blood domain considered in this study mimics the radial artery. Although blood has a pulsatile flow profile in real-life, this study investigates the compositional contribution of one of those diameter instances (2.35 mm). This also includes neglecting the longitudinal changes in the artery.

The values of real and imaginary impedance at 1 kHz were calculated to be 93.4 Ω and 6.3 Ω , respectively. Moreover, it was observed that the resistive effects are quite dominant at lower range of frequencies. This shows an overlap of the dispersion regions where for the set of properties considered in the simulation, the model does not exhibit β dispersion below 10 kHz. Thus, this causes the simulation model to deviate from the semi-circular Cole-Cole plot initially. However, after 10 kHz, the real and imaginary impedances values are 88.3 Ω and 3 Ω , respectively, where the plot begins to mimic the Cole behavior and can be used to estimate Cole parameters.

The blood flow or arterial hemodynamics does play a part in influencing the dielectric response of the overall human forearm. This study, however, is focused at calculating the individual compositional response of muscle, fat, bone and artery layers and isolating the blood contribution to the overall measurements.

The simulation has been performed while considering all the basic requirements for mimicking the collective layered human tissues at the forearm. However, some of the limitations can be identified as:

- Skin layer is not considered. This was done to reduce model complexity and under the assumption of employment of wet electrodes which bypass the effects of skin significantly.
- The dynamic factors like blood flow have not been taken into regard.

Chapter 4: Pilot experimentation on human forearm

This chapter aims to investigate the MFBIA procedure, experimentally, on a section of an actual human forearm. The results obtained from the simulation study in the previous chapter served as the motivation for actual experimentation. This study is intended to verify the Cole behavior observed in the simulation of the forearm model and compare the results. The experimentation was performed on the human forearm for verification of results from the simulation setup. Since this is not a complete validation, the testing was limited to the research team (2 subjects – the student and the supervisor) as a feasibility approach to identifying tissue response.

4.1 Experimental setup and methodology

The experimentation was setup to mimic the simulation conditions as closely as possible. To begin with, the ventral side of the forearm section, near the wrist, was chosen for electrode placement. This was done as the radial artery is located towards the ventral forearm surface, which has been modelled in the simulation. The electrodes were placed using the same separation distance as that in the simulation. The BIA measurements were carried out through a commercially available Quadra® Electrical Impedance Spectroscopy (EIS) device (Eliko® technologies, Estonia)[119] at Institute of Biomedical Technologies (IBTech), AUT University.

Quadra® EIS is a portable device that provides a state-of-the-art platform for impedance spectroscopy. The device offers a sampling rate of 1000 samples/sec while yielding impedance spectra at 15 different frequencies within 1 kHz and 349 kHz. It provides the ability of measuring 4 channels at a time. The device comes with 4, application specific front ends:

- **Single shunt front end:** This configuration uses a potential divider with the voltage excitation subjected to a fixed shunt resistance with a test impedance in series. It has the option of unipolar or differential excitation along with two or four mode wire of measurement.
- **Transimpedance front end:** This arrangement has a transimpedance amplifier attached with it that converts the measured current to voltage thereby yielding a fixed current to voltage ratio. Thus, the compensation against a leakage current is offered in this case.

- **Current source front end:** The current to voltage ratio at which the subject is excited in this case is 1V to 1mA and suffers leakage at high frequencies.
- **Breakout front end:** In this front end, the excitation and the sensing configuration can be manually defined. It provides an easy access to the pins of the device.

Since the device offers a maximum frequency limit of 349 kHz, extrapolation (in Matlab) was employed to generate the response within 1 kHz – 1 MHz. A single shunt front-end with a 4-wire differential mode was employed with the Quadra® device for this study. The circuit diagram of the configuration is given in Figure 4.1.

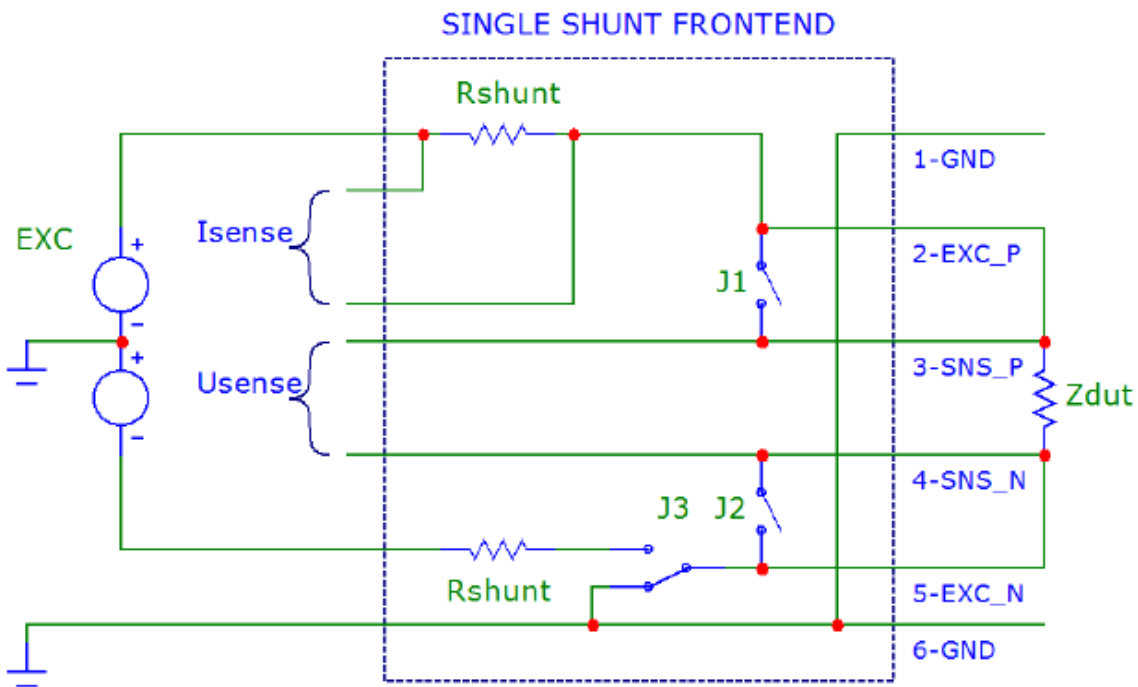


Figure 4.1: Schematic of the single shunt front end used in this experimentation

The jumpers J1, J2 and J3 are selected to opt for unipolar or differential excitation or two or four mode of measurement respectively. Pins 1-6 are the input ports that could be used for connection. The 1st and 6th are the ground ports and the pins 2,3,4 and 5 are used for connection of electrodes in case of four mode operation. The inner two electrodes (3rd and 4th) are used for sensing or measuring the voltage while the outer two electrodes (2nd and 5th) are used for current excitation. The device along with the front-end connection is shown in Figure 4.2.



Figure 4.2: Single shunt front end configuration of the Quadra impedance spectroscopy measurement device

The length of the human forearm section considered in both simulation and experimentation was small to ensure that the cross-sectional area remains uniform. The commercially available gel electrodes were trimmed down to be used in this study, with a diameter of 10 mm at the contact site. The distance between the four electrodes was taken as 20 mm in experimentation. No skin preparation was performed prior to any measurements. The measurement setup with the electrodes in the experiment can be seen in Figure 4.3.



Figure 4.3: Electrode setup on the forearm section

4.2 Impedance Measurement Results

The impedance measurements were taken on 2 subjects. For each subject, measurement was taken for a period of 10 seconds to allow for the consistency of the obtained spectra. For each frequency, a period of 10 seconds resulted in 10000 measurements, which were averaged to yield an average spectrum for both subjects. The Quadra® device interfaces via its software, which logs the impedance in terms of magnitude and phase. The magnitude and phase were used to calculate the real and the imaginary parts of impedance. The spectra for real parts of impedance, imaginary parts of impedance and the Cole plots for both the subjects have been shown in Figure 4.4, Figure 4.5 and Figure 4.6, respectively.

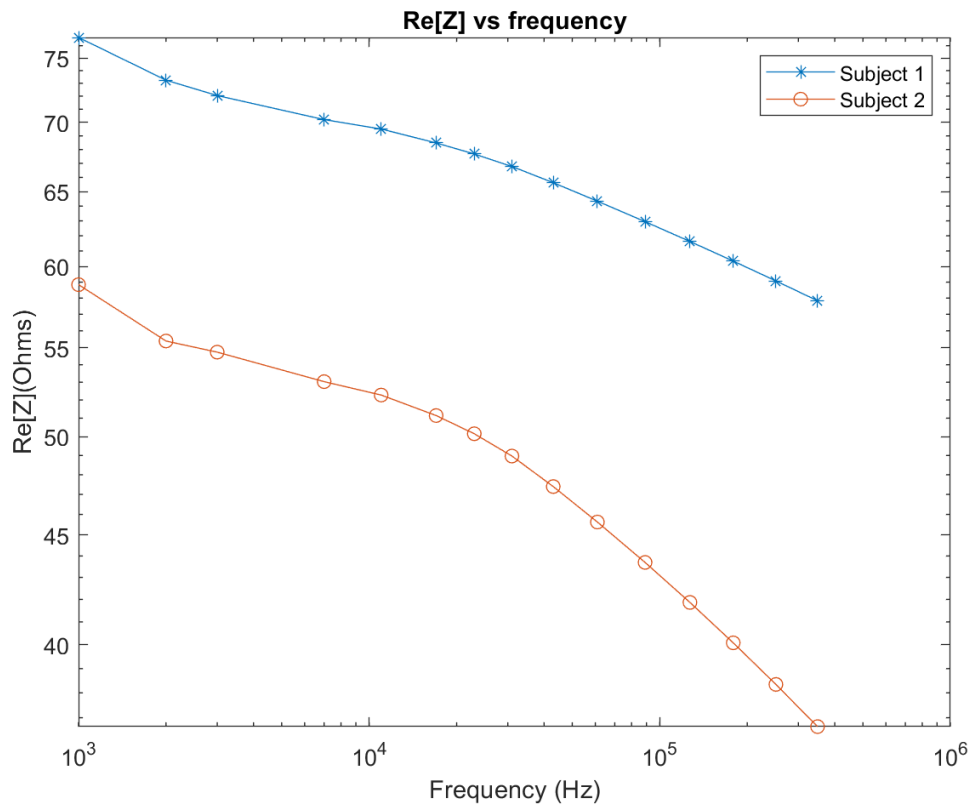


Figure 4.4: $Re[Z]$ vs frequency plot for subjects 1 and 2

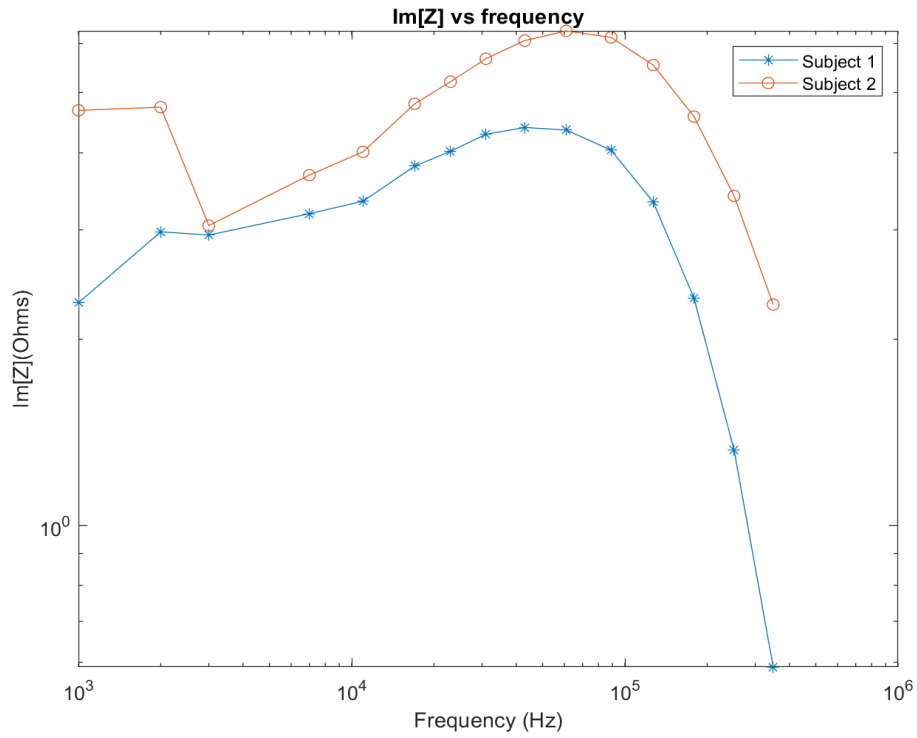


Figure 4.5: $Im[Z]$ vs frequency plot for subjects 1 and 2

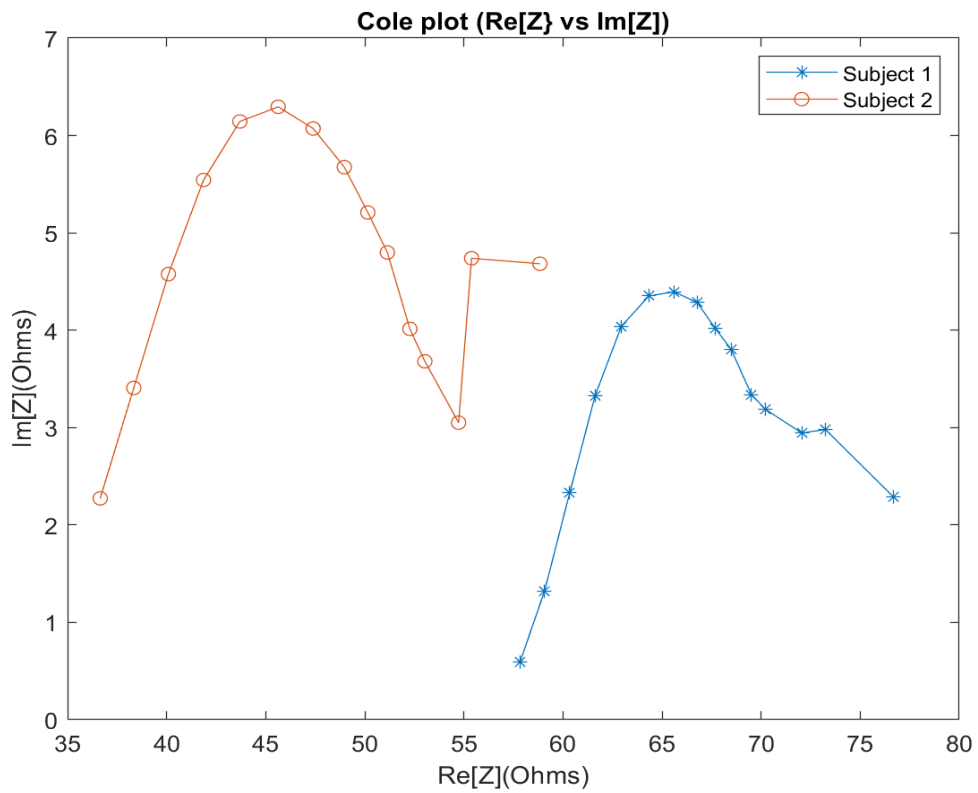


Figure 4.6: $Re[Z]$ vs $Im[Z]$ (Cole plot) for subjects 1 and 2

4.3 Discussion

The objective of the pilot experimentation on actual human forearm was to perform the impedance spectroscopy measurement in real-life situation and analyze the results in the context of those obtained from the simulation study. From Figure 4.7 it can be seen that the magnitudes of the impedance spectra differ by approximate values of 17 Ω to 21 Ω at low and high frequencies, respectively.

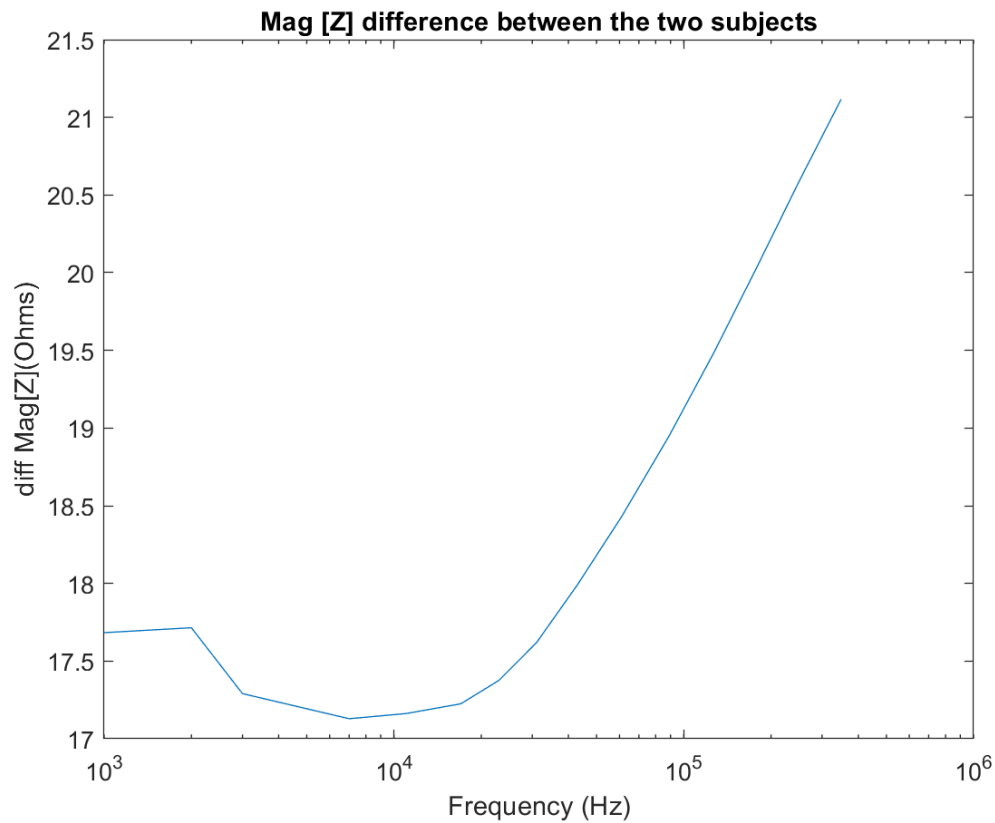


Figure 4.7: Difference in the impedance magnitudes between the two subjects

This can be accounted for due to the difference in the forearm sizes and dimensions. However, as was expected, the dispersion behavior was found to be the same for both subjects where the impedance spectra follow a Cole type behavior (Figure 4.6). Another observation that supports the similarity in both the subjects is the characteristic frequency (frequency at which maximum reactance is obtained) which can be seen to be approximately the same for both subjects, as seen in figure 4.5.

The reliability of the measurements was an important consideration and hence the procedure was repeated 3 times on each subject. The impedance spectra for 10 seconds were recorded and were found to be very similar with a deviation of as small as $\pm 1\%$. Moreover, as specified earlier, the overall spectrum was obtained as an average of 10000 spectra logged during a span of 10 seconds which established a good consistency of the measurements in relation to changing conditions with time.

4.3.1 Comparison with the simulation results

On comparing the experimental results (Figure 4.4, Figure 4.5 and Figure 4.6) with the simulation results (Figure 3.8, Figure 3.9 and Figure 3.10), it is clear that both the studies express a similar dispersion behavior of the tissues.

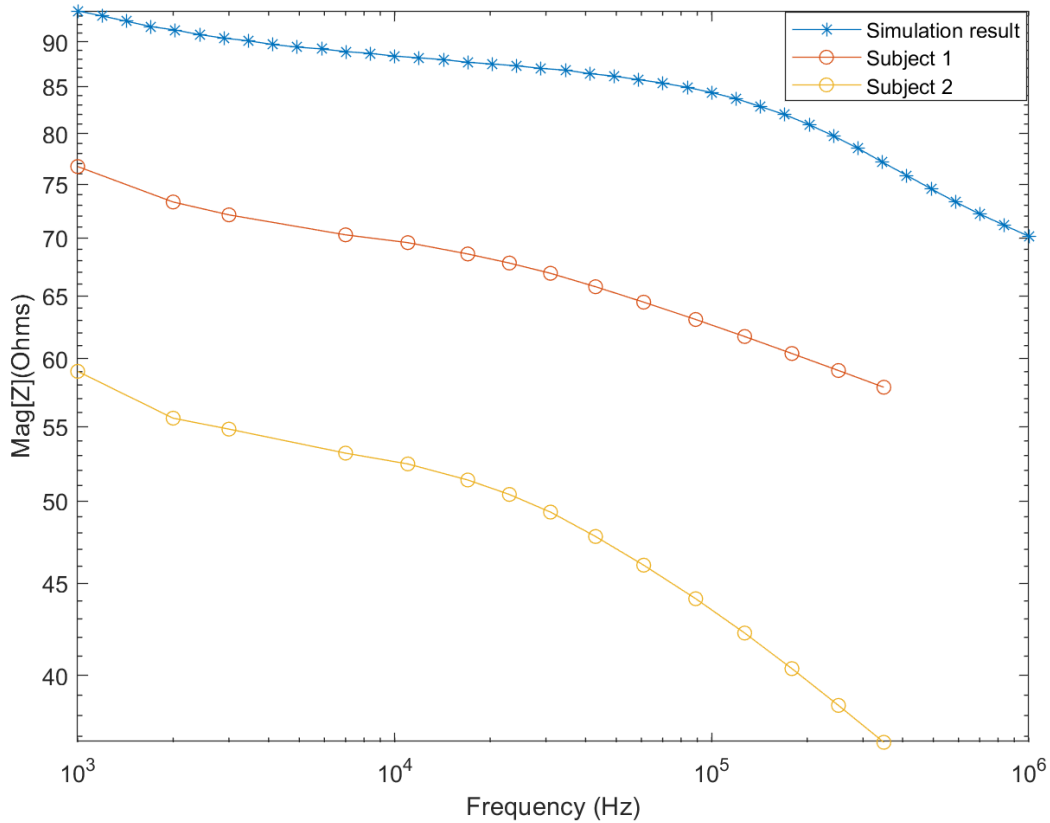


Figure 4.8: Comparison of the simulation results with the experimental results of subjects 1 and 2

However, a comparison of the results shows differences between the magnitudes of the spectra obtained in the three cases (simulation, subject 1 and 2) as well as the dispersion characteristic frequency (Figure 4.8). Different electrode interfaces and tissue domains in case of the simulation and actual measurements can explain the difference in impedance magnitudes, which have been tabulated in Table 4.1.

Table 4.1: Comparison between simulation and forearm measurements

	Simulation Analysis	Forearm measurements
Electrode Interface	No contribution of the electrode interface was considered in the simulations	The measurement device and the gel electrodes provided for an appropriate compensation for the electrode-skin interface.
Size of electrodes	The electrodes used were smaller in cross-sectional contact dimensions (2 mm diameter)	The electrodes used were commercially available surface gel electrodes (10 mm diameter)
Tissue layers	The dimensions of the fat and muscle tissue layers as modelled in the simulation geometry were relatively more uniform than an actual forearm. Also, skin layer was not considered.	The dimensions of the forearm tissue layers could have been different for each subject with different degree of non-uniformity.

The experimental results provide results which verify the behavior of the forearm tissues obtained from the simulation. The following chapter addresses the main objective of this research – modelling the overall results and isolating the parameters associated with individual tissue domains.

Chapter 5: Electrical modelling

Chapters 3 and 4 provided a basis to investigate the procedure involved in MF-BIA measurements. Chapter 3 focussed on a simulation perspective to quantify the electric field distribution within the modelled tissue layers – bone, fat, muscle and blood in terms of impedance spectrum within 1 kHz to 1 MHz. Chapter 4 followed up on the findings of the simulation analysis and identified a similar type of dispersion behavior for the forearm section on two subjects, which verified the approach and the measurement methodology. In this chapter, the main aim is to model the results obtained in the previous chapters and determine the response of individual tissue domains. Modelling the dielectric response of most biological materials can be generally performed through Debye or Cole theory. However, Debye relaxation cannot be used to model an accurate response of different tissues which interface with other tissues into an anatomical structure. Hence, this chapter presents a Cole modelling approach to model the results obtained from the simulation and the experimental measurements.

The chapter is divided into three sections – the first addresses the methods adopted for modelling, the second focusses on the modelling of simulation results and the third addresses the modelling of actual forearm measurements. The use of passive electrical circuit elements such as resistor and capacitor may be used to understand the response of tissues, however there is not enough literature to investigate their dielectric response over β dispersion frequency range. In this chapter, the sections focus on modelling the impedance measurements in terms of overall Cole parameters.

5.1 Modelling methodology

From Equation 1-13, we can write the Cole equation to define the impedance spectra as:

$$Z(\omega) = R_{\infty} + \frac{R_0 - R_{\infty}}{1 + (j\omega\tau)^k} \quad \text{Equation 5-1}$$

Where R_{∞} , R_0 , τ , and, $k(= 1 - \alpha)$ are the Cole parameters defining the overall impedance spectrum.

Equation 5-1 defines the impedance magnitude as a complex quantity and can be simplified by substituting the value of $(j)^k = \cos\left(k\frac{\pi}{2}\right) + j\sin\left(k\frac{\pi}{2}\right)$. The equation modifies to:

$$Z(\omega) = R_{\infty} + \frac{R_0 - R_{\infty}}{1 + \omega\tau^k \cos\left[k\frac{\pi}{2}\right] + j\omega\tau^k \sin\left[k\frac{\pi}{2}\right]} \quad \text{Equation 5-2}$$

The real and the imaginary parts of impedance Z can be obtained as:

$$Re(Z) = R_{\infty} + \frac{(R_0 - R_{\infty}) \left(1 + (\omega\tau)^k \cos \left[k \frac{\pi}{2}\right]\right)}{1 + 2(\omega\tau)^k \cos \left[k \frac{\pi}{2}\right] + (\omega\tau)^{2k}} \quad \text{Equation 5-3}$$

$$Img(Z) = -j \frac{(R_0 - R_{\infty})(\omega\tau)^k \sin \left[k \frac{\pi}{2}\right]}{1 + 2(\omega\tau)^k \cos \left[k \frac{\pi}{2}\right] + (\omega\tau)^{2k}} \quad \text{Equation 5-4}$$

Equation 5-3 and Equation 5-4 can be further combined to relate the Im(Z) directly in terms of Re(Z) so as to form an equation where Im (Z) is a function of Re(Z). To aid the understanding, Re (Z) can be symbolized as ‘R’ and Im (Z) can be symbolised as ‘X’. Equation 5-5 relates X and R:

$$4X + 2 \cot \left[\frac{k\pi}{2} \right] (R_0 - R_{\infty}) = \sqrt{2} \operatorname{cosec} \left[\frac{k\pi}{2} \right] * \sqrt{-4R^2 + 4RR_0 + R_0^2 + 4RR_{\infty} - 6R_0R_{\infty} + R_{\infty}^2 + \cos[k\pi](-2R + R_0 + R_{\infty})^2} \quad \text{Equation 5-5}$$

The methodology for curve fitting involved choosing a general dielectric Cole model with at-least four parameters (R_0 , R_{∞} , τ and k) that would define the dielectric relaxation spread in the frequency range of interest – 1 kHz to 1MHz. Moreover, a minimization cost function was implemented based on the sum of squared errors between the curve fit and simulation data as:

$$RMSE = \sqrt{\frac{\sum_{i=1}^N (R_{fit}^i - R_{sim}^i)^2}{N}} + \sqrt{\frac{\sum_{i=1}^N (X_{fit}^i - X_{sim}^i)^2}{N}}$$

where RMSE is the root mean squared error, R_{fit}^i and X_{fit}^i refer to the R and X curve fit data for i^{th} sample, R_{sim}^i and X_{sim}^i refer to the R and X simulation data for i^{th} sample and N is the number of samples. The modelling algorithms were mathematically represented using Matlab® 2019(a) platform. The modelling was performed in two stages:

- Single dispersion Cole model: for an overall identification of the tissue response
- Multi-dispersion Cole model: to address the dielectric relaxation of individual tissue layers.

5.2 Simulation modelling

This subsection addresses the modelling for the simulation data obtained in Chapter 3. One of the observations from the simulation results was that the Cole behavior was evident after a frequency of 10 kHz. Hence, the simulation data for modelling was considered within 10 kHz and 1 MHz.

5.2.1 Single dispersion Cole modelling

The single dispersion Cole modelling was performed to identify the overall dielectric dispersion of the collective tissue domains. Figure 5.1 (a) – (c) shows the comparison of the fitted model with the simulation data.

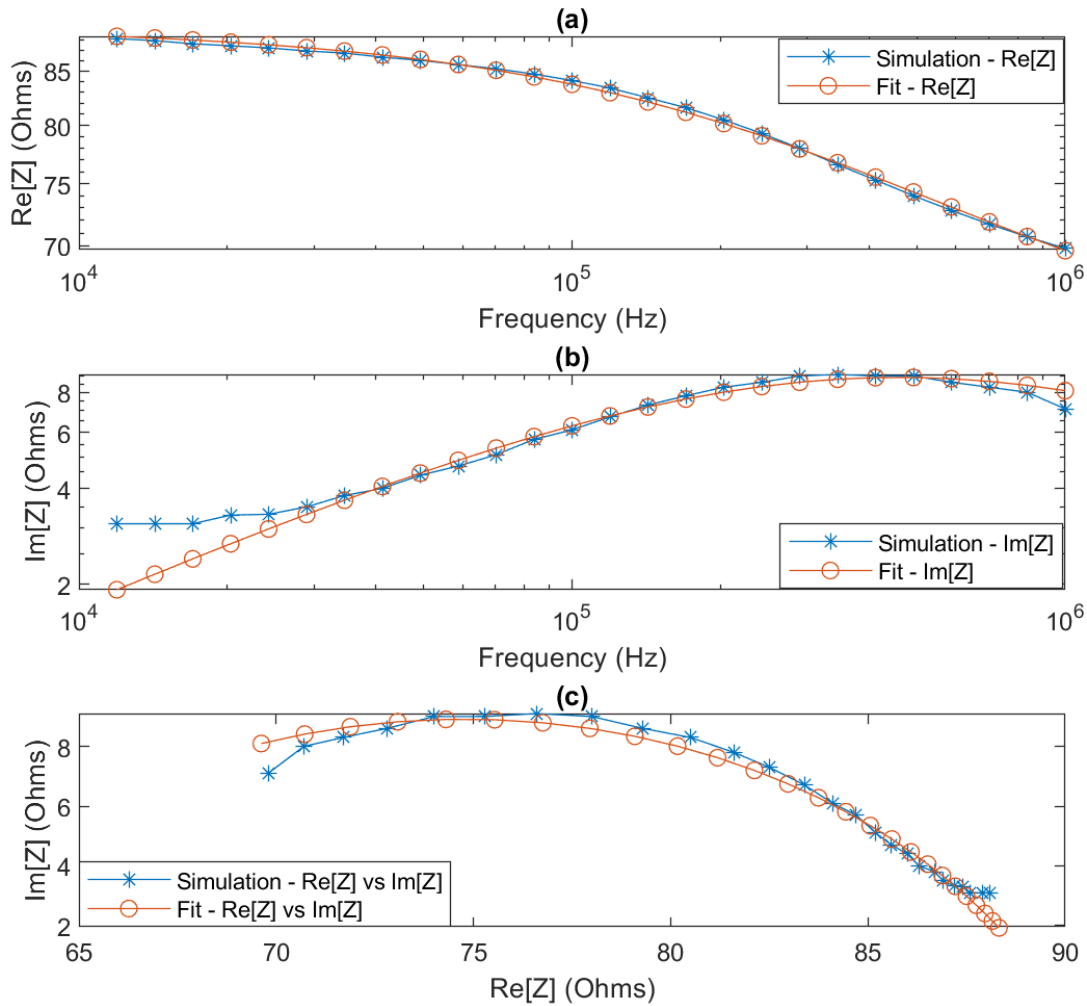


Figure 5.1: Comparison of the simulation measured data with single dispersion model fit for (a): $\text{Re}[Z]$, (b): $\text{Im}[Z]$, and (c) $\text{Re}[Z]$ vs $\text{Im}[Z]$ (Cole plot)

The estimated Cole parameters have been tabulated in Table 5.1 as:

Table 5.1: Cole parameters as estimated from the fit for simulation data

R_0	R_∞	k	τ
89.50	60.02	0.6923	3.45e-07

And the model describing the overall dielectric behavior can be written as:

$$Z(\omega) = 60.02 + \frac{29.48}{1+(j*\omega*3.45*10^{-7})^{0.6923}}$$

Equation 5-6

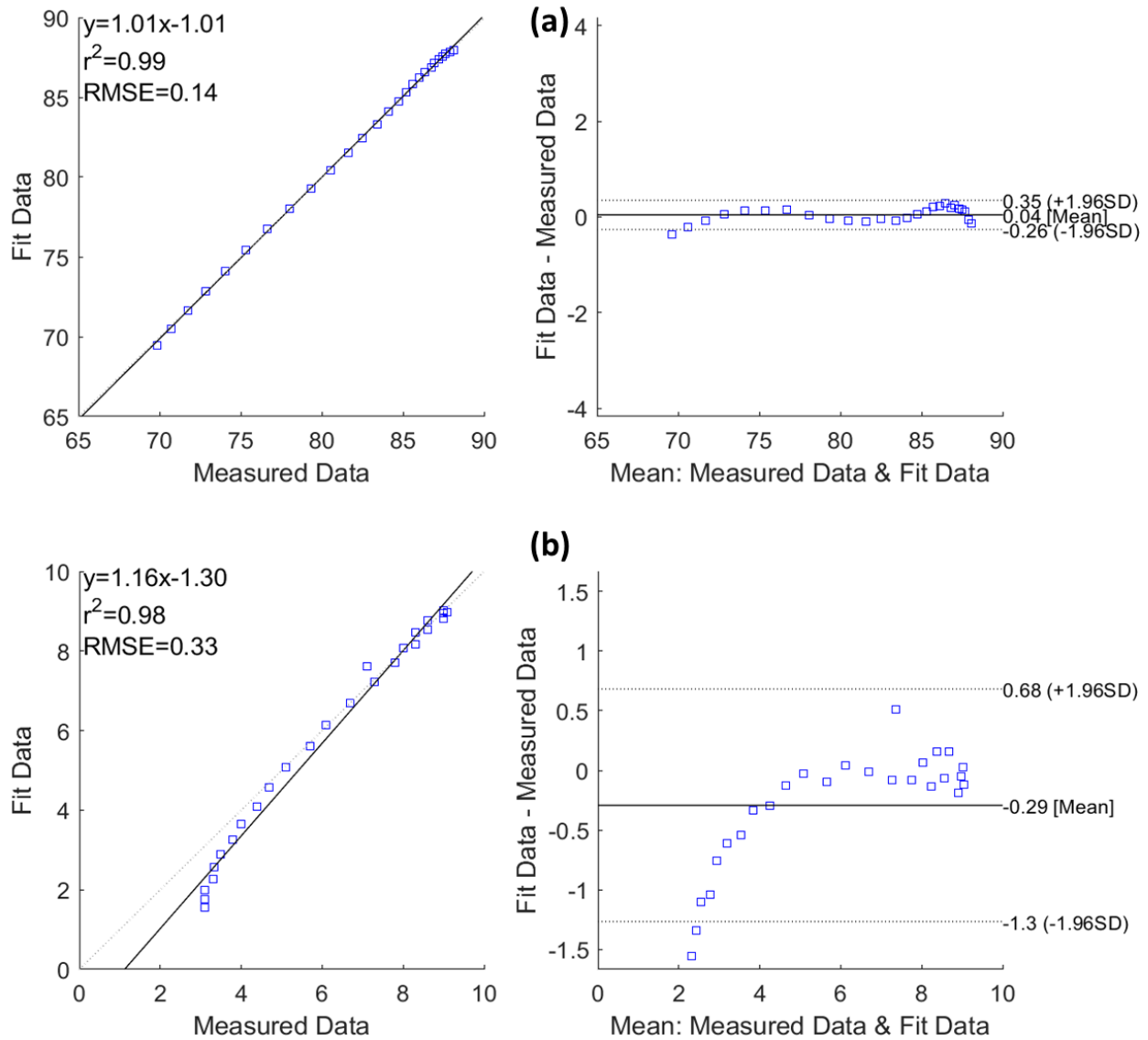


Figure 5.2: Correlation and Bland Altman plots for single dispersion fit (a). $Re[Z]$ and (b). $Im[Z]$

The performance of the fit was analysed using the Bland-Altman analysis (BAA). BAA is a measure of correlation between datasets and is done by specifying 95% limits of agreement as a measure of the similarity of two measurements, calculated as 95% confidence intervals (CI) ($\text{mean} \pm 1.96 \times \text{SD}$ (standard deviation)) of the difference between the datasets. The analysis is represented through plotting the difference between the two datasets against the mean of those datasets. Figure 5.2 (a) and (b) show the correlation plot (left) and the Bland Altman plot (right) for comparing the fit estimate with the measured data for $Re[Z]$ and $Im[Z]$, respectively. Also, the statistics on the plots mention Pearson’s coefficient of

correlation as r value squared to be 0.99 and 0.98 and RMSE of 0.14 and 0.33 for Re[Z] and Im[Z], respectively. From the BAA plot, it can be seen that the number of outliers is 1 for the Re[Z] and 2 for Im[Z] within the limits of SD. The outliers do affect the correlation of the datasets; however, the overall performance of the model fitting can be deemed to be good.

5.2.2 Multi-dispersion Cole modelling

Overall, the simulation model comprised of 4 tissue domains – bone, fat, muscle and blood. Bone tissue exhibits an almost constant conductivity of 0.02 S/m over the frequency range of interest. Hence, the contribution of the bone tissue domains was considered to be resistive. Each of the other three tissue domains were modelled using a multi-dispersion Cole model. The final model considered to represent the electrical response of the forearm tissue layers was:

$$Z(\omega) = R_{bone} + \frac{R_{0f}-R_{\infty f}}{1+(j\omega\tau_f)^{\alpha_f}} + \frac{R_{0m}-R_{\infty m}}{1+(j\omega\tau_m)^{\alpha_m}} + \frac{R_{0b}-R_{\infty b}}{1+(j\omega\tau_b)^{\alpha_b}} \quad \text{Equation 5-7}$$

In Equation 5-7, the first term represents the resistance of the bone tissues (collectively for radius and ulna) and the second, third and fourth terms describe the dispersion spectrum for fat, muscle and blood tissue layers, respectively. The simulation data was loaded into Matlab® and the spectrum within 10 kHz to 1 MHz was considered for Cole fitting, with the intention of extrapolating the obtained result to 1 kHz after attaining a good fit. The final fit compared to the simulation measurements can be seen in Figure 5.3 (a) – (c) for real part, imaginary part and real vs imaginary part of impedance, respectively.

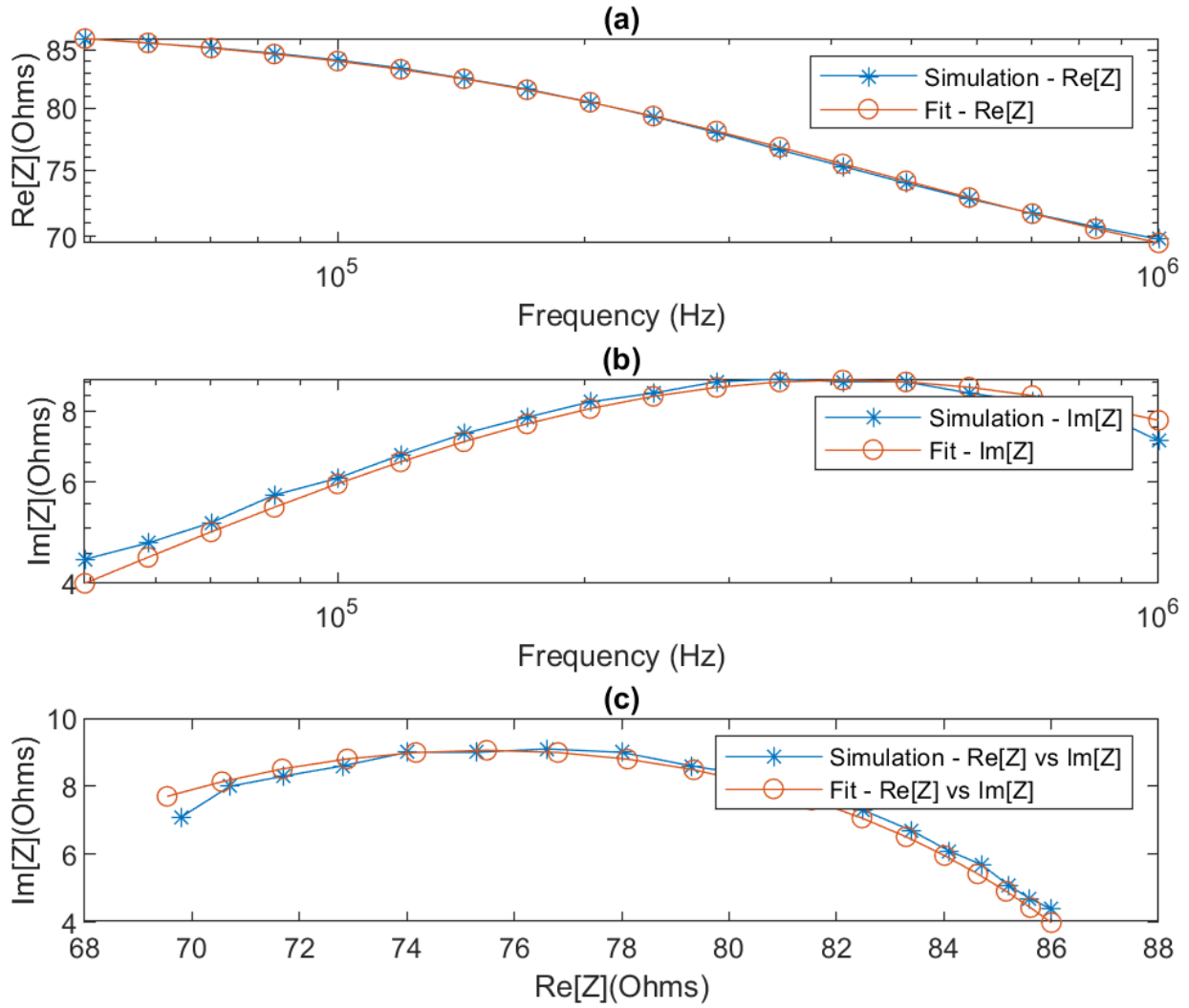


Figure 5.3: Comparison of measured data with multi-dispersion model fit data for simulation (a): $\text{Re}[Z]$, (b): $\text{Im}[Z]$, and (c) $\text{Re}[Z]$ vs $\text{Im}[Z]$ (Cole plot)

The Cole parameters, as identified in Equation 5-7, were estimated and are listed in Table 5.2

Table 5.2: Cole parameters as estimated from the multi-dispersion model fit for simulation

R_{bone}	R_{0f}	$R_{\infty f}$	α_f	τ_f	R_{0m}	$R_{\infty m}$	α_m	τ_m	R_{0b}	$R_{\infty b}$	α_b	τ_b
49.72	19.72	2.43	0.34	1.48E-09	21.44	0.98	0.83	4.08E-07	4.04	0.54	0.26	1.05E-04

Based on the above, the final model can be defined as in Equation 5-8.

$$Z(\omega) = 49.72 + \frac{17.29}{1+(j\omega*1.48e-9)^{0.34}} + \frac{20.46}{1+(j\omega*4.08e-7)^{0.83}} + \frac{3.5}{1+(j\omega*1.5e-4)^{0.26}} \quad \text{Equation 5-8}$$

Bland Altman analysis was used to analyse the performance of the fit and the results can be seen in Figure 5.4 (a) and (b) for $\text{Re}[Z]$ and $\text{Im}[Z]$, respectively.

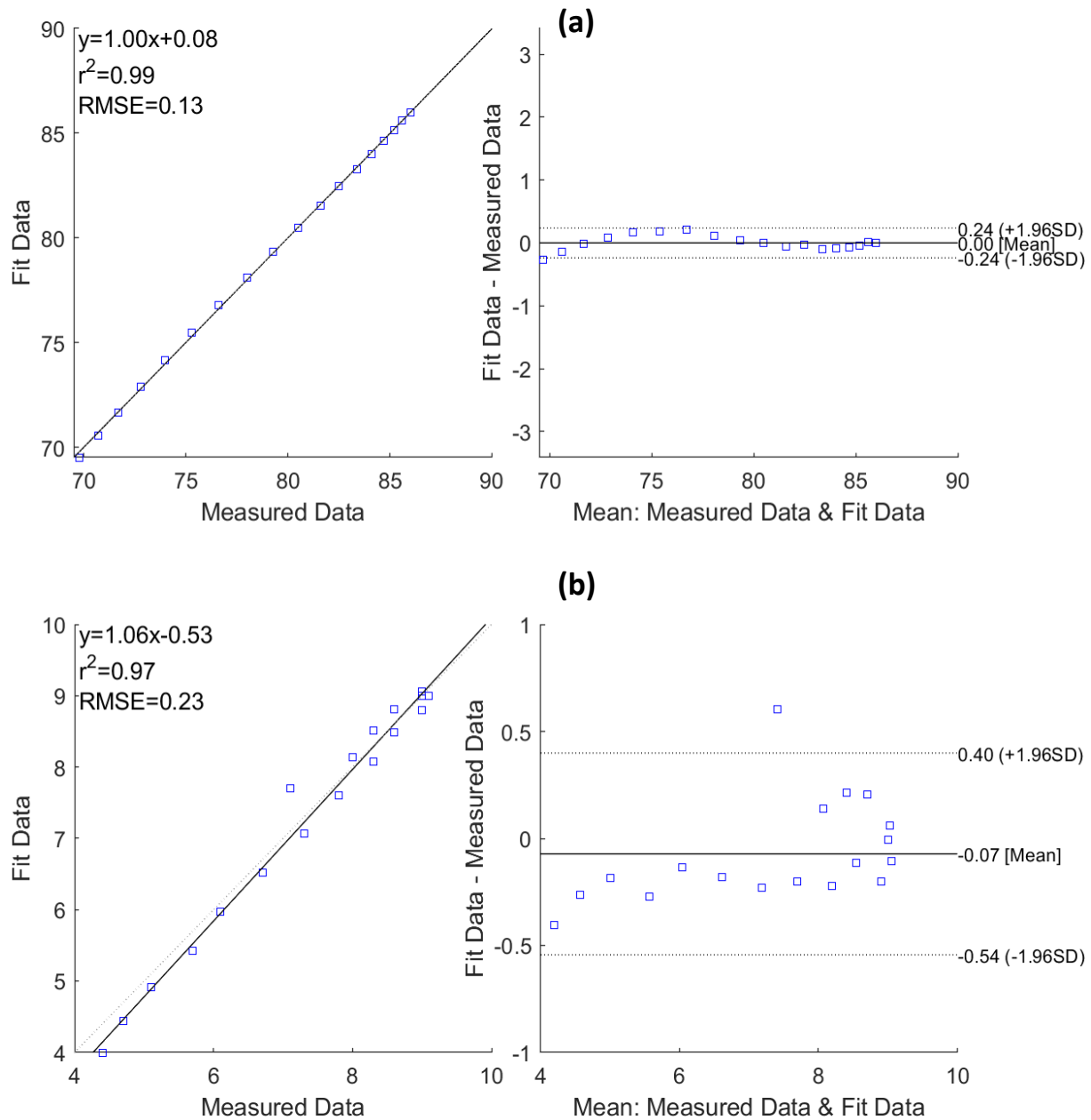


Figure 5.4: Correlation and Bland Altman plots for multi-dispersion fit (a). $\text{Re}[Z]$ and (b). $\text{Im}[Z]$

R-square values of 0.99 and 0.97 along with RMSE of 0.13 and 0.23 for $\text{Re}[Z]$ and $\text{Im}[Z]$ established the good quality of the fit. Based on the above model performance, the model was used to estimate the complete response of over the frequency range of 1 kHz to 1 MHz, as can be seen in Figure 5.5 (a) – (c).

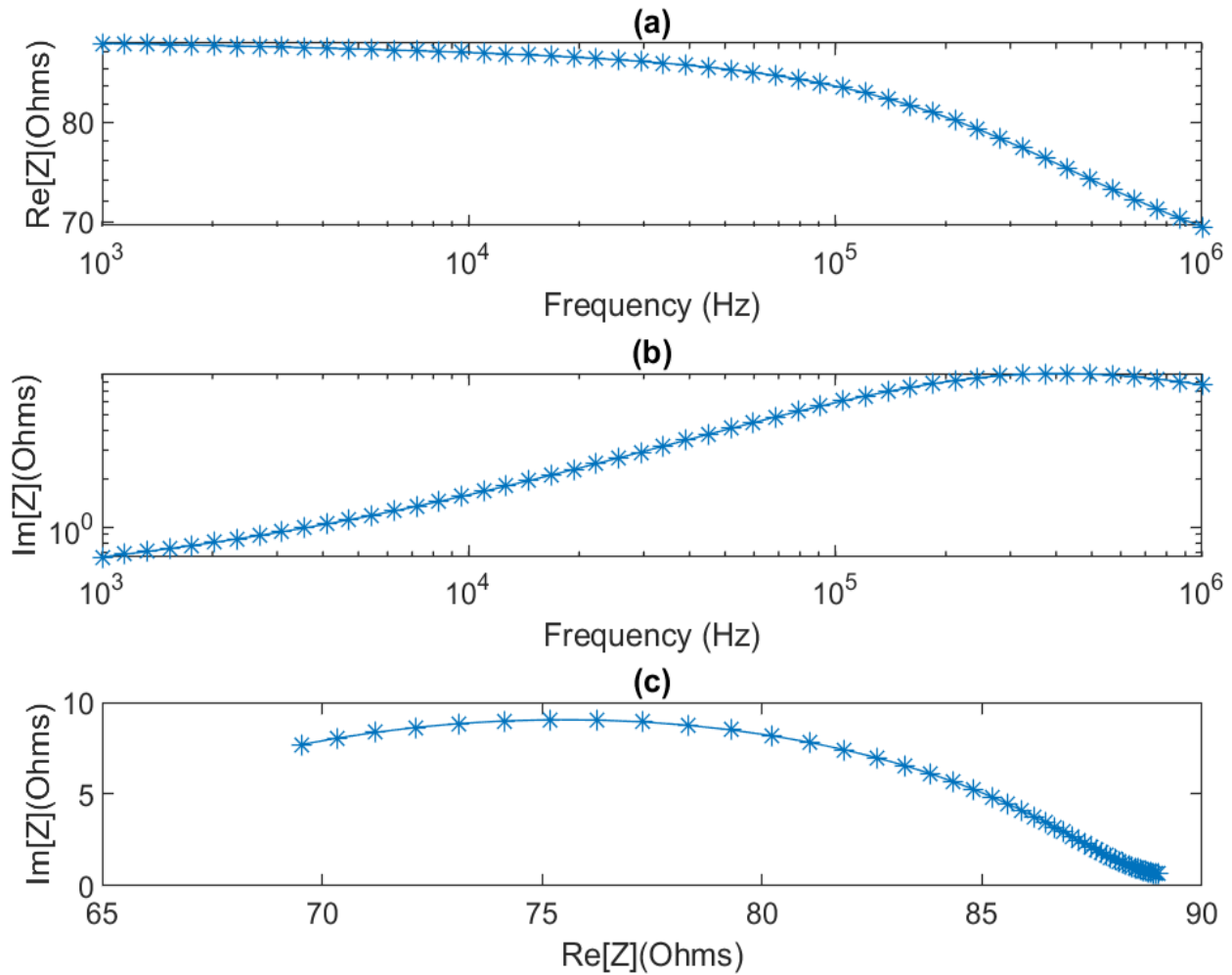


Figure 5.5: Complete response within 1 kHz – 1 MHz obtained from multi-dispersion model fit for simulation data (a): $\text{Re}[Z]$, (b): $\text{Im}[Z]$, and (c) $\text{Re}[Z]$ vs $\text{Im}[Z]$ (Cole plot)

5.3 Experimental modelling

This subsection addresses the electrical modelling for the experimentation on actual forearm on two subjects, as described in Chapter 4. As has been done in the last section, this section will also focus on modelling an overall Cole model followed by a multi-dispersion Cole model for the experimental data from two subjects.

5.3.1 Single dispersion Cole modelling

Figure 5.6 (a) – (c) show the result of a single dispersion Cole model fit to the experimental data for both the subjects.

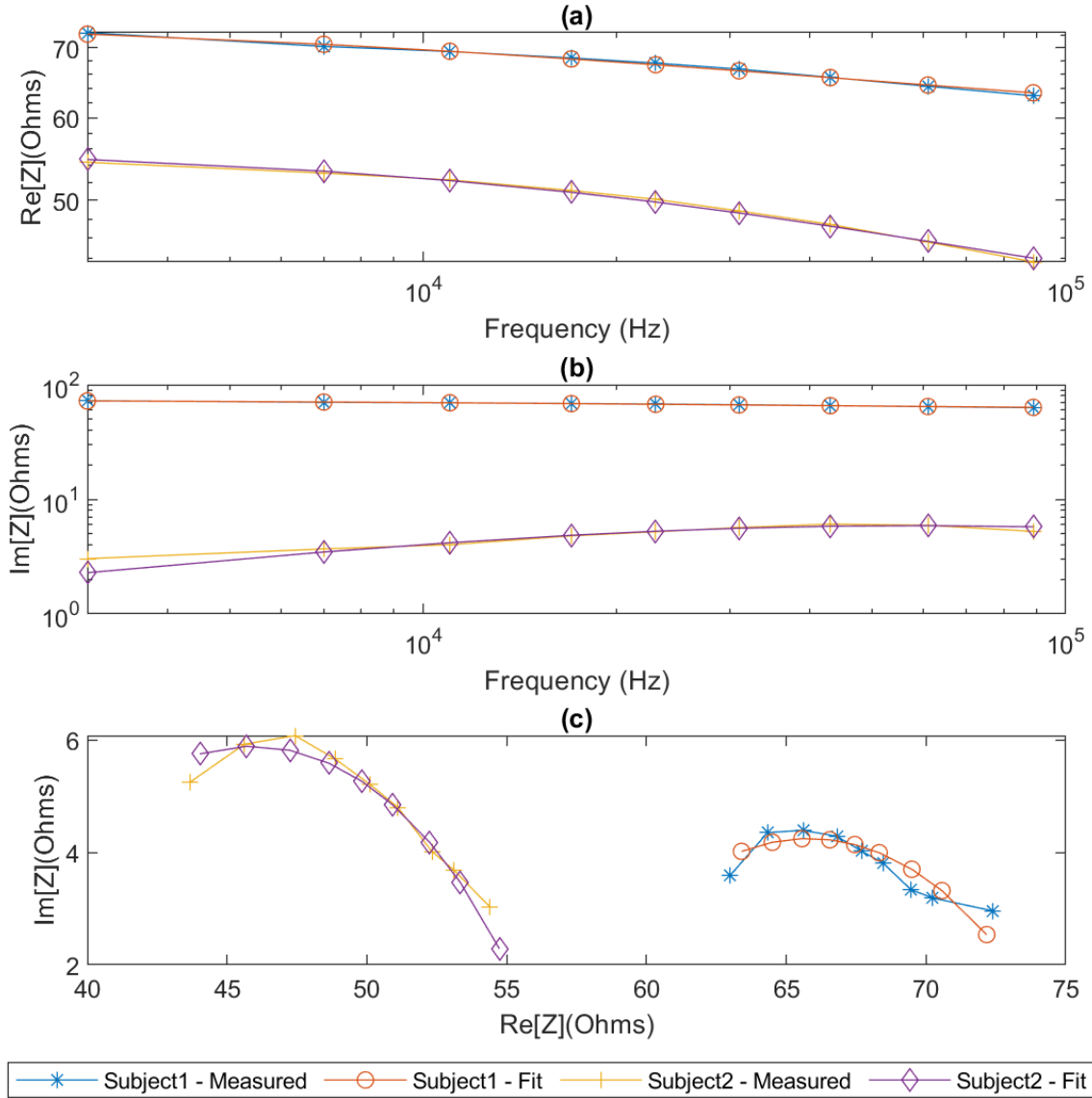


Figure 5.6: Comparison of the experimental measured data with single-dispersion model fit for Subject 1 and 2, (a): $Re[Z]$, (b): $Im[Z]$, and (c) $Re[Z]$ vs $Im[Z]$ (Cole plot)

The Cole parameters for each subject have been tabulated in Table 5.3.

Table 5.3: Cole parameters as estimated from the fit for experimental data for Subject 1 and 2

	R_0	R_∞	k	τ
Subject 1	75.29	56.32	0.54	4.00E-06
Subject 2	56.59	35.18	0.64	2.73E-06

Equation 5-9 and Equation 5-10 describe the overall Cole model for the two subjects, respectively, based on the above parameters.

$$Z_{subject1}(\omega) = 56.32 + \frac{18.97}{1+(j*\omega*4.004*10^{-6})^{0.54}} \quad \text{Equation 5-9}$$

$$Z_{subject2}(\omega) = 35.18 + \frac{21.41}{1+(j*\omega*2.73*10^{-6})^{0.64}}$$

Equation 5-10

The performance analysis for $\text{Re}[Z]$ and $\text{Im}[Z]$ have been represented as Bland Altman plots in Figure 5.7 and Figure 5.8 for subject 1 and 2, respectively.

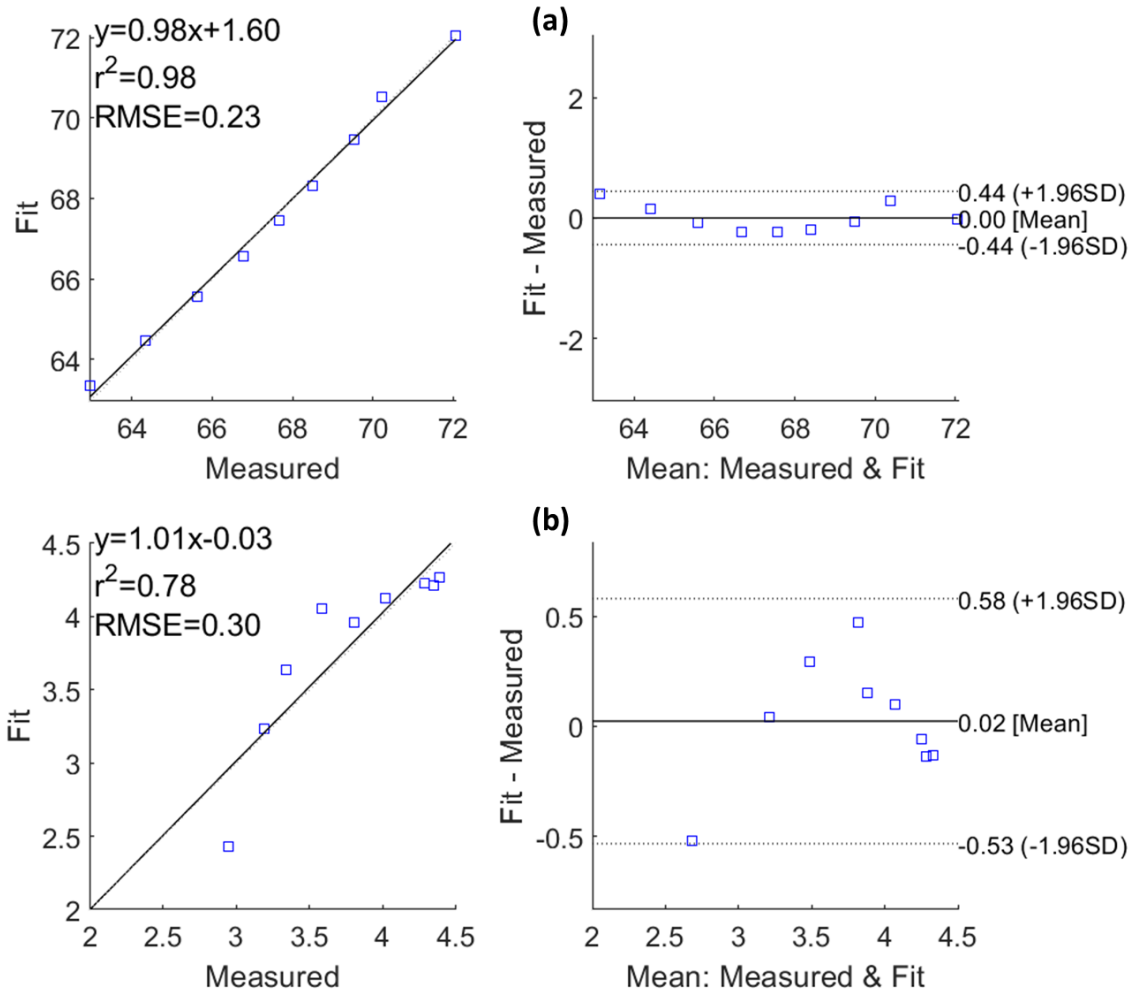


Figure 5.7: Correlation and Bland Altman plots for (a). $\text{Re}[Z]$ and (b). $\text{Im}[Z]$ for subject 1

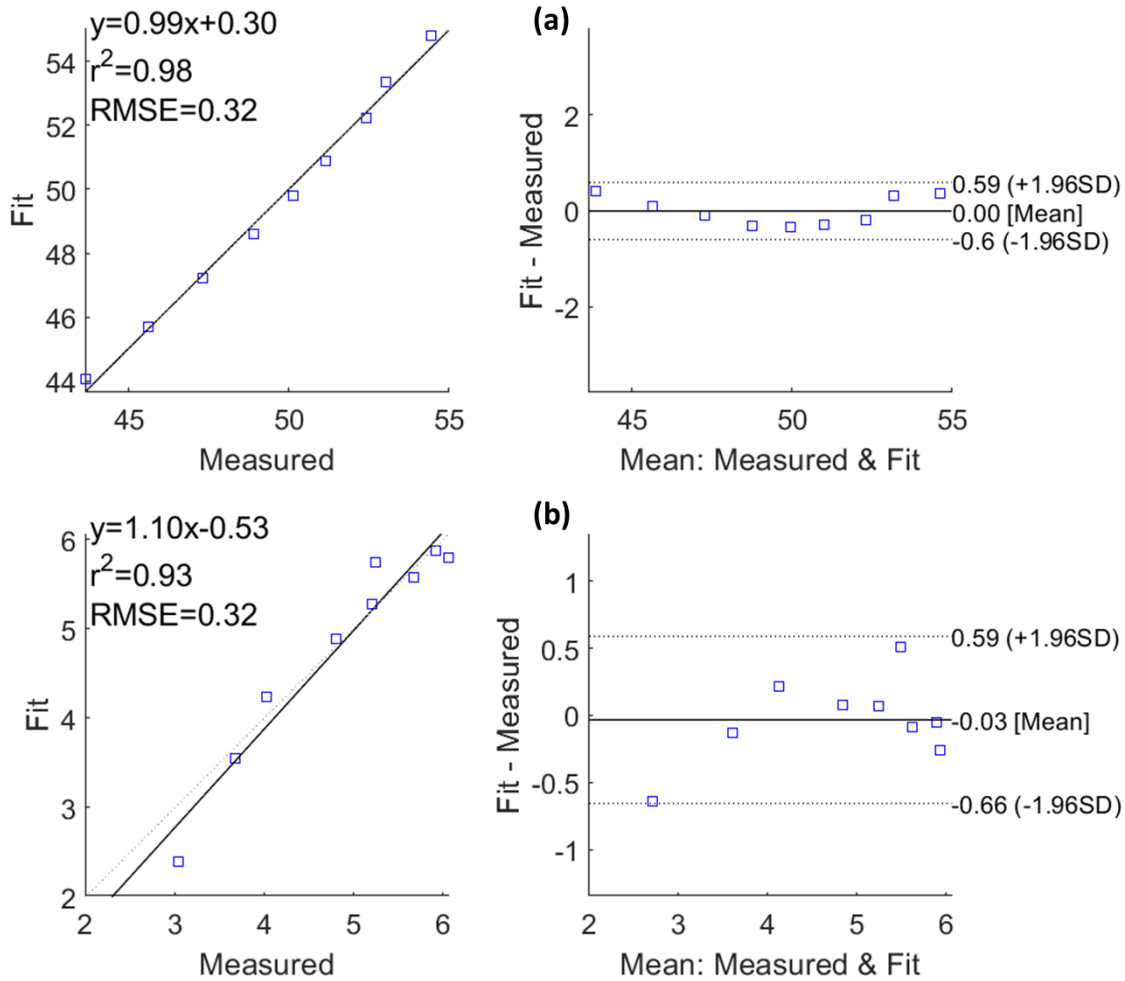


Figure 5.8: Correlation and Bland Altman plots for (a). $Re[Z]$ and (b). $Im[Z]$ for subject 2

The above results show an above par performance for a single dispersion Cole fitting to both the subjects. For each subject, the BAA shows the average performance with r squared values for the real part around 0.98 and imaginary part as 0.78 and 0.93 for subject 1 and 2, respectively. This shows a greater deviation in the reactive impedance spectra for both the subjects where a good fit performance was not achieved. However, the real parts showed an excellent correlation with scope for improvements in the Cole parameters.

Furthermore, the model fit (obtained for measured data between 1 kHz – 349 kHz from Quadra® device) was used to estimate the single-dispersion response over our frequency range of interest: 1 kHz – 1 MHz. The impedance spectra for both the subjects can be seen in Figure 5.9 (a) – (c) for $Re[Z]$, $Im[Z]$ and $Re[Z]$ vs $Im[Z]$, respectively.

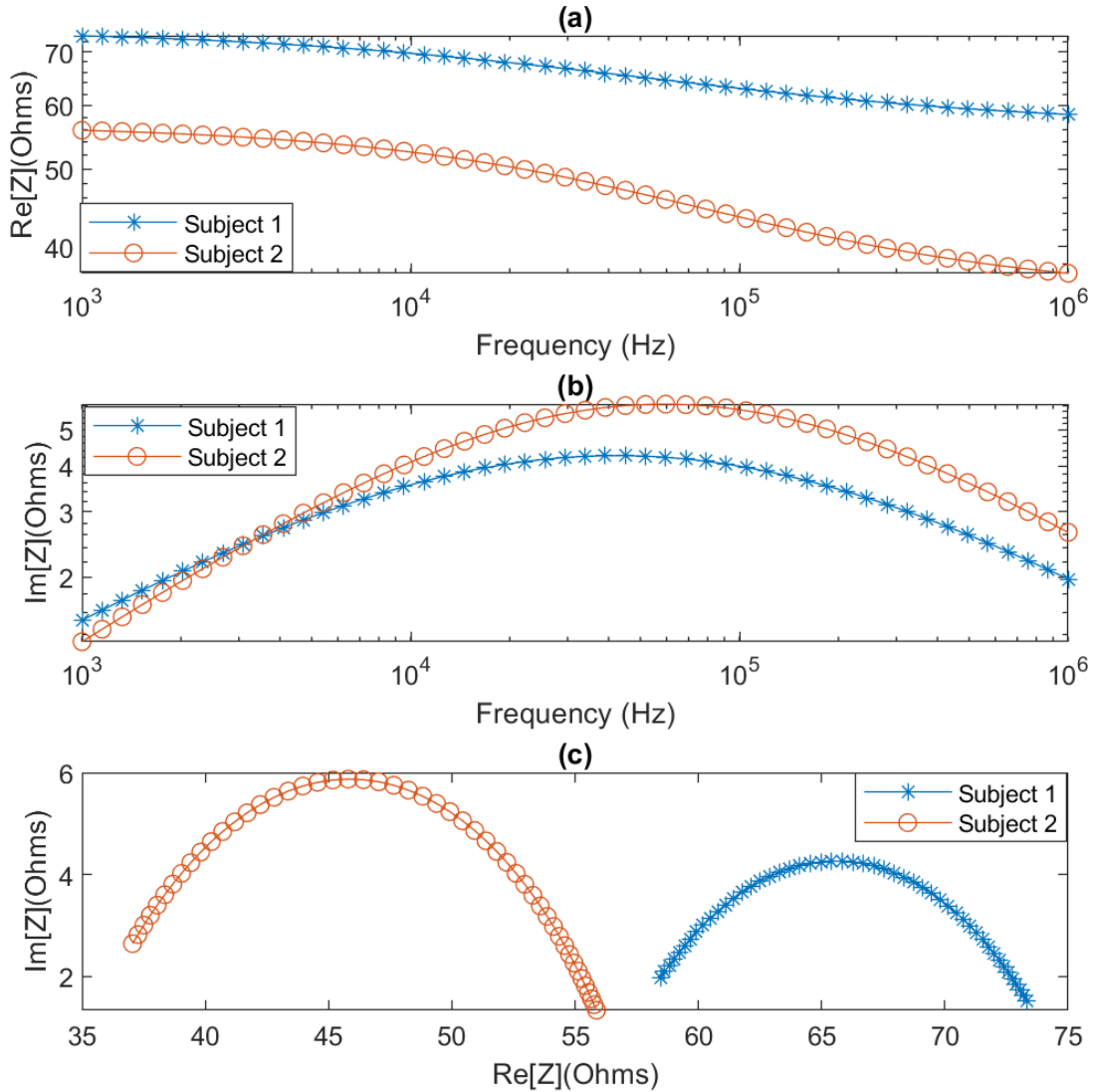


Figure 5.9: Complete response within 1 kHz – 1 MHz obtained from single dispersion model fit for subjects 1 and 2
 (a): $Re[Z]$, (b): $Im[Z]$, and (c) $Re[Z]$ vs $Im[Z]$ (Cole plot)

5.3.2 Multi-dispersion Cole modelling

To model the experimental observations of both subjects in a multi-dispersion Cole model, it was assumed that the effect of skin was countered by using gel electrodes. For the remainder of the tissues, Equation 5-7 was used to represent all four tissue domains. Following up on that, the model fitting results can be seen in Figure 5.10 (a) – (c) for both subjects.

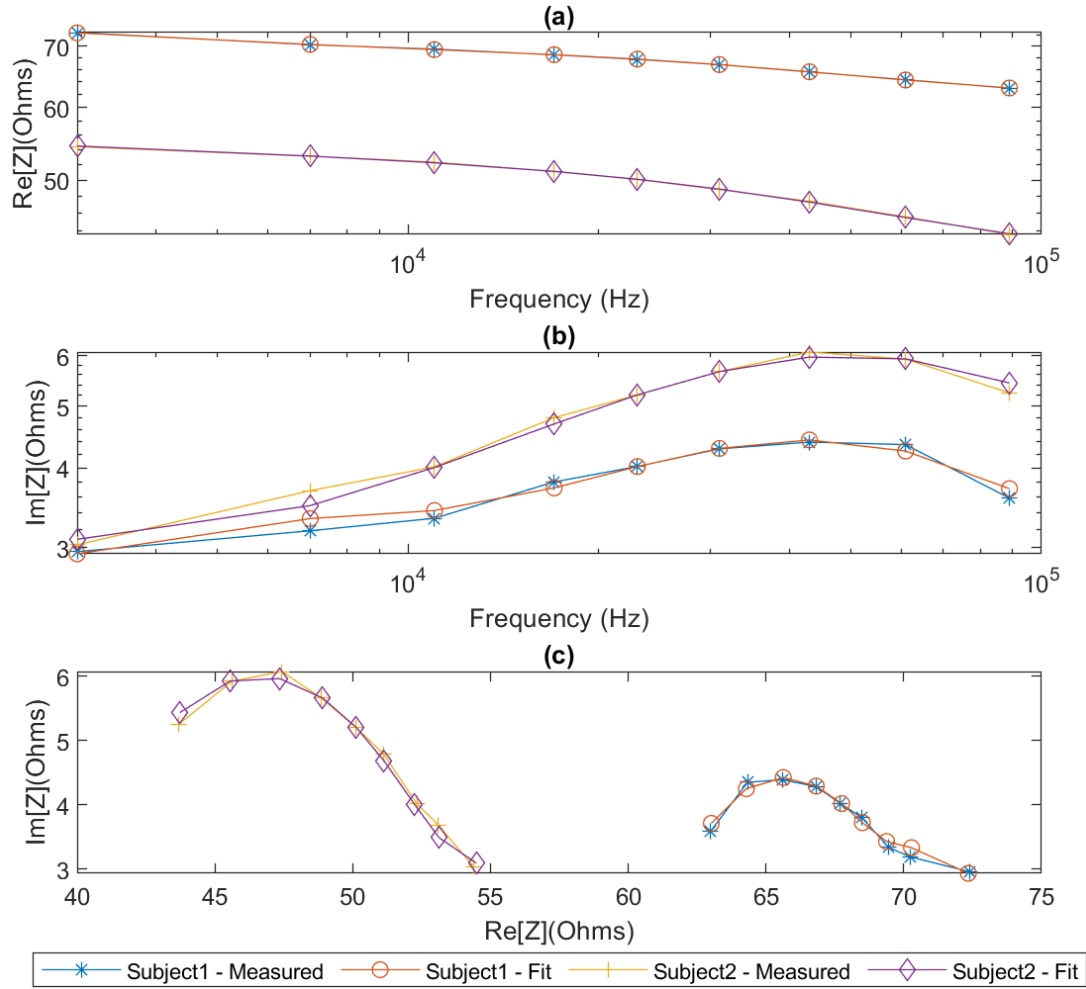


Figure 5.10: Comparison of the experimental measured data with multi-dispersion model fit for Subject 1 and 2, (a): $Re[Z]$, (b): $Im[Z]$, and (c) $Re[Z]$ vs $Im[Z]$ (Cole plot)

The estimated Cole parameters for each subject have been tabulated in Table 5.4.

Table 5.4: Cole parameters as estimated from the multi-dispersion model fit for subject 1 and 2

	R_{bone}	R_{0f}	$R_{\infty f}$	α_f	τ_f	R_{0m}	$R_{\infty m}$	α_m	τ_m	R_{0b}	$R_{\infty b}$	α_b	τ_b
Subject 1	57.98	25.51	16.09	0.65	7.29E-05	24.50	15.82	0.67	6.91E-05	3.54	0.62	0.62	1.63E-04
Subject 2	38.83	25.59	12.30	0.72	2.32E-04	26.80	14.59	0.88	3.91E-05	2.86	0.53	0.66	6.28E-04

Equation 5-11 and Equation 5-12 describe the overall Cole model for both subjects, based on the above parameters.

$$Z_{subject1}(\omega) = 57.98 + \frac{9.42}{1+(j\omega*7.29e-5)^{0.65}} + \frac{8.68}{1+(j\omega*6.91e-5)^{0.67}} + \frac{2.92}{1+(j\omega*1.63e-4)^{0.62}} \quad \text{Equation 5-11}$$

$$Z_{subject2}(\omega) = 38.83 + \frac{13.29}{1+(j\omega*2.32e-4)^{0.72}} + \frac{12.21}{1+(j\omega*3.91e-5)^{0.88}} + \frac{2.33}{1+(j\omega*6.28e-4)^{0.66}} \quad \text{Equation 5-12}$$

Figure 5.11 and Figure 5.12 show the Bland Altman analysis for each subject to analyse the model fit for $\text{Re}[Z]$ and $\text{Im}[Z]$.

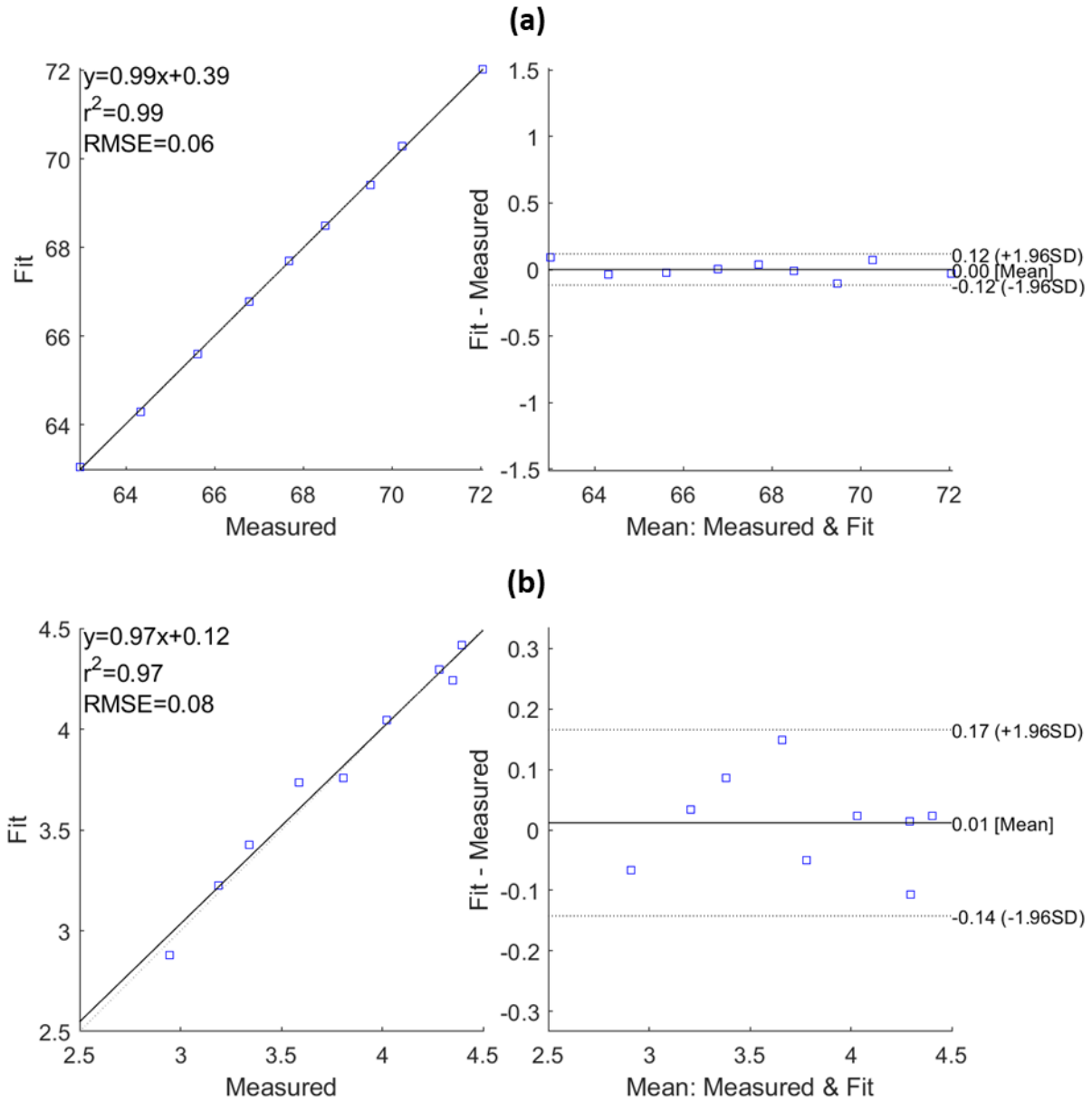


Figure 5.11: Correlation and Bland Altman plots for multi-dispersion fit (a). $\text{Re}[Z]$ and (b). $\text{Im}[Z]$ for subject 1

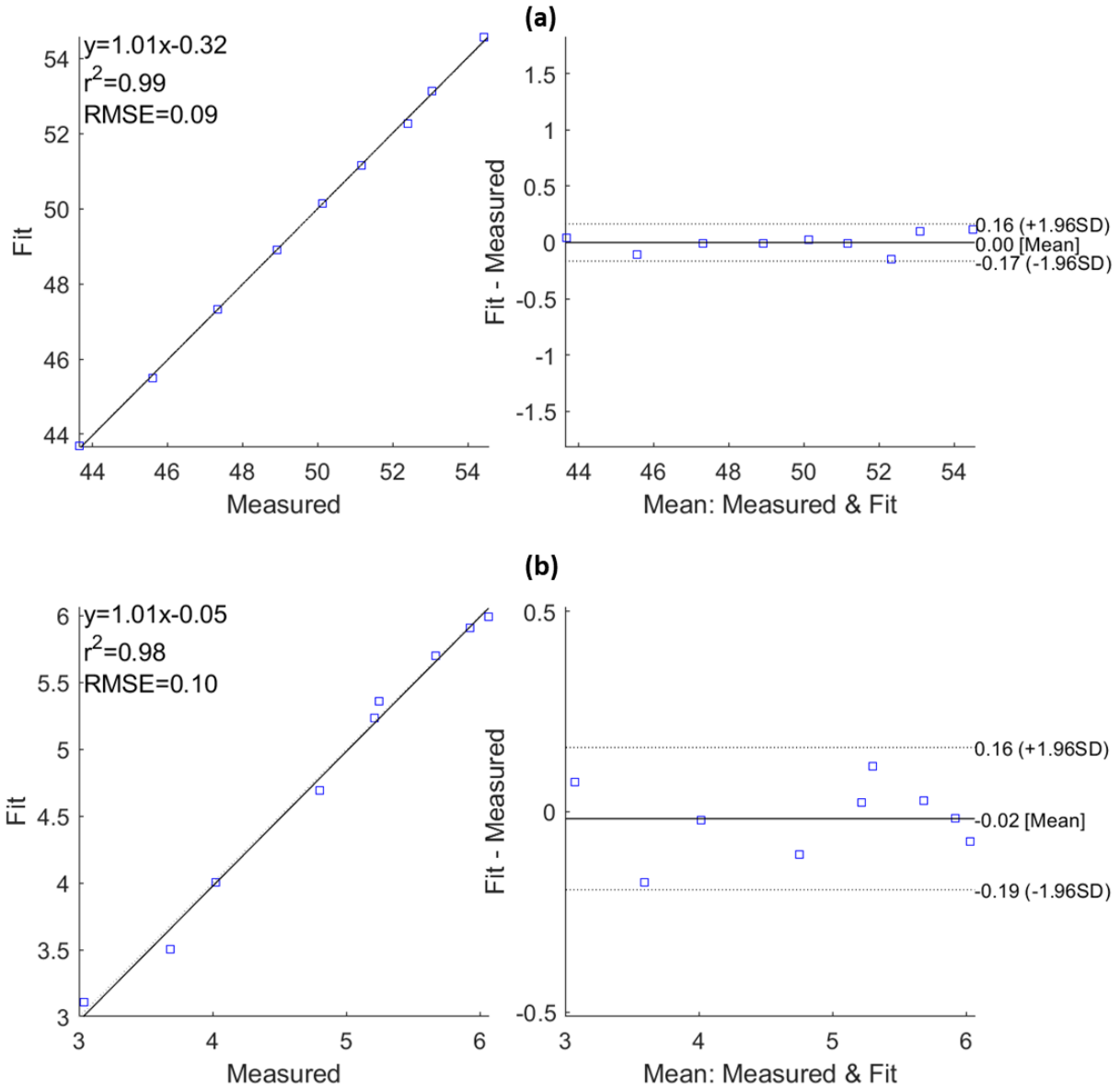


Figure 5.12: Correlation and Bland Altman plots for multi-dispersion fit (a). $Re[Z]$ and (b). $Im[Z]$ for subject 2

The BAA plots for both subjects show an improved fit performance from the single dispersion fit, with RMSEs within 0.1 for $Re[Z]$ and $Im[Z]$. R squared values obtained for both $Re[Z]$ and $Im[Z]$ are close to 0.99, showing an excellent correlation of the model fit to the measured data.

Finally, the overall response of the forearm tissue geometry, between 1 kHz – 1 MHz, for subject 1 and 2 have been shown in Figure 5.13 (a) – (c).

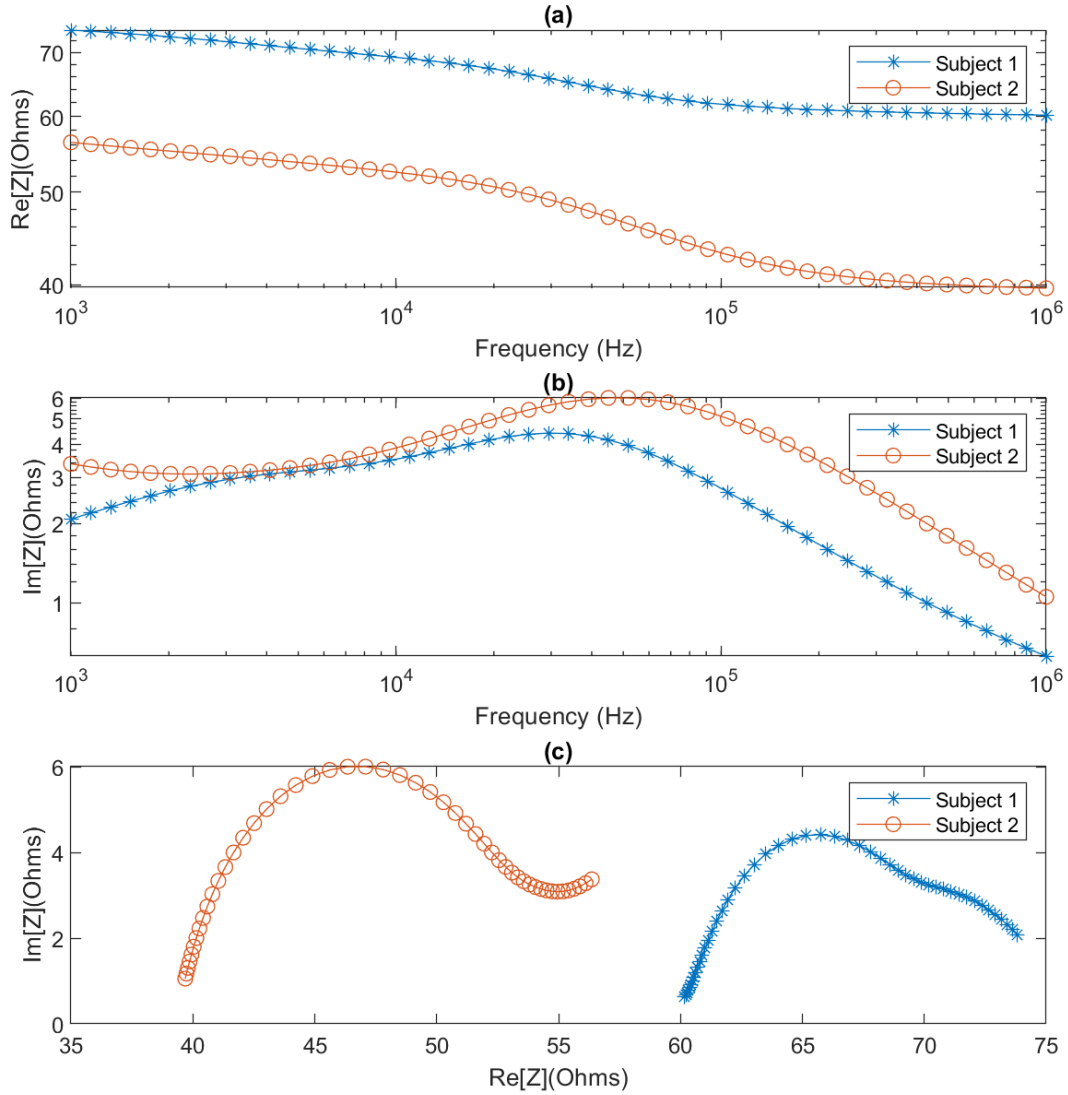


Figure 5.13: Complete response within 1kHz – 1MHz obtained from multi-dispersion model fit for subjects 1 and 2
 (a): $Re[Z]$, (b): $Im[Z]$, and (c) $Re[Z]$ vs $Im[Z]$ (Cole plot)

5.4 Discussion

In Section 2.7, we identified the following research question:

Can we isolate the response of individual tissues from an overall BIA measurement?

The objectives of this research revolved around resolving this research question. The primary objective of this study, and of this chapter, was to model the MF BIA response from the simulation analysis (Chapter 3) and pilot experimentation (Chapter 4) to estimate the impedance contribution from each tissue layer. To achieve this objective, a two-stage methodology was adopted. Initially, the overall BIA response was modelled as a collective, single dispersion Cole model which would verify the collective behavior of the

tissues. Following from that, the measurements were modelled through a multi-dispersion Cole relation, where each dispersion addressed a specific tissue domain. The aim was to attain a good quality fit which will give an idea about not only the resistance contribution of each tissue, but also the other Cole dispersion parameters.

5.4.1 Simulation modelling

The simulation data was analysed in Chapter 3 and it was observed that a Cole type response was exhibited between 10 kHz to 1 MHz. The data was modelled initially to a single dispersion Cole equation with a good quality of fit obtained. The fit data for both the real and imaginary parts of impedance were found to be in excellent correlation with their simulation measurement counterparts, with r-squared values of 0.99 and 0.98, respectively. The single dispersion modelling was followed by the multi-dispersion modelling, giving the r squared values of 0.99 and 0.97 for $\text{Re}[Z]$ and $\text{Im}[Z]$, respectively. The improved performance of the multi-dispersion modelling was indicated as the RMSE reduced from 0.14 to 0.13 and 0.33 to 0.23 from single-dispersion model fit to multi-dispersion model fit for $\text{Re}[Z]$ and $\text{Im}[Z]$, respectively. On achieving and verifying a good quality fit, the models for both single and multi-dispersion stages were used to estimate the response over the desired frequency range of interest: 1 kHz – 1 MHz.

5.4.2 Experimental modelling

Following the modelling methodology from the simulation analysis, both stages of modelling were repeated on the experimental results obtained from subject 1 and 2, between 1 kHz – 349 kHz. The quality of fit obtained from the single dispersion modelling for both the subjects was good for the real part of impedance, with r squared values of 0.98, but not as good for the imaginary part, with r-squared values of 0.78 and 0.93 for subject 1 and 2, respectively. However, this improved significantly with the multi-dispersion Cole modelling for both subjects, where the r squared values for real part of impedance changed slightly to 0.99 and imaginary part of impedance changed to 0.97 and 0.98 for subject 1 and 2, respectively. This indicated that the multi-dispersion Cole model is more appropriate to be used to model the dielectric properties of tissues, measured collectively. Every tissue domain experiences a different dispersion phenomenon and hence may not be accurately modelled using a single Cole dispersion model. Moreover, a multi-dispersion model describes the Cole parameters of each tissue, hence isolating the behavior of every tissue domain from the overall MFBIA measurements.

Chapter 6: Conclusion and Future Work

This work focussed on investigating the dielectric properties of human forearm tissues to understand the properties and impedance contribution of each tissue domain in MFBIAs applications. The study focussed on the following aspects:

- Simulating a human forearm model with four layers – bone, fat, muscle and blood, with the aim of understanding the distribution of electric field within these tissue domains within the frequency range of 1 kHz and 1 MHz.
- Experimentally conducting MFBIAs measurements on human forearm section to analyse the actual response of the tissues and verify the type of dispersion phenomenon exhibited by them.
- Parametrically modelling the simulation and experimental results to isolate the impedance of each tissue domain from the overall measurements.

The research gaps and the objectives of this study were identified after an extensive literature review of BIA systems and applications, electrical properties of tissues and electrical modelling approaches.

6.1 Simulation study

Chapter 3 focussed on addressing the simulation perspective to understanding the dielectric behavior of human forearm tissue domains and the distribution of electric field within them. The simulation study was carried out through quantifying the electrical response of modelled tissue layers (bone, fat, muscle and radial artery) using an electromagnetic finite element analysis in Ansys® HFSS. The frequency range of interest was chosen within 1 kHz – 1 MHz (within β dispersion). One of the limitations of the setup was that it neglected any dynamic changes (like blood flow) and inhomogeneity in the tissue domains. Also, skin tissue layer was not considered, however its effects can be assumed to be negated by using wet electrodes during actual measurements. The tissues were considered as layered, homogenous dielectric domains with frequency dependent properties in terms of bulk conductivity and relative permittivity. Some of the conclusions from the study can be listed as:

1. An electromagnetic simulation perspective for modelling the dielectric properties of forearm tissues was established and the results verified a Cole type behavior of the tissues within 10 kHz and 1 MHz.

2. The resistive effects were found to be quite dominant at lower range of frequencies. For the frequencies below 10 kHz, the model was found to not exhibit Cole type behavior, suggesting an overlap between the α and β dispersion regions corresponding to the material properties compiled in Gabriel's database.

6.2 Experimentation on human forearm

Chapter 4 focussed on carrying out the actual MFBIA measurements on human forearm section. The aim of the experimentation was to perform the BIA on actual forearm tissues and be able to calculate the impedance dispersion spectra of each tissue layer from the measured results. For this pilot experimentation, two subjects were chosen to perform the BIA analysis using a commercial device (Quadra® EIS). The length of the forearm section as well as the electrode separation was chosen to be the same as simulation. The frequency range of measurement was limited to 349 kHz which was the maximum frequency offered by the device. The conclusions from the experimental study were:

1. The results verified a Cole type response of the forearm tissue layers for both the subjects within the measured frequency range.
2. The magnitude of the impedance spectra for both the subjects were found to be different but showing a similar dispersion behavior. Moreover, the impedance spectra magnitude was different for both the subjects and the simulation, probably due to tissue homogeneity and linear considerations in the simulation study.

6.3 Electrical modelling

In Chapter 5, the simulation and the experimental MFBIA measurements were parametrically modelled to isolate the impedance response of each tissue layer – bone, fat, muscle and blood. The objective was to estimate the individual response of each tissue layer from the overall MFBIA measurements – the primary objective of this study. Two-staged modelling was performed for both the simulation and experimental measurements – first modelling the results in a single dispersion Cole model, and second in a multi-dispersion Cole model where each dispersion corresponds to a specific tissue domain. Matlab® was used for modelling the results and the fit performance was quantified through Bland Altman analysis. Conclusions from the electrical modelling can be summarised as:

1. A single dispersion Cole model was found to represent the overall behavior of the simulation results to a good degree. However, it did not perform as well for modelling the experimental results on subject 1 and 2, especially the imaginary parts of impedance.
2. The multi-dispersion Cole model was found to perform very well in representing overall response of the tissues and estimating the response of each tissue domain as a separate dispersion medium. Equation 5-11 and Equation 5-12 define the obtained Cole parameters associated with different tissue domains.

6.4 Future Work

In summary, this research investigated the simulation and experimental approaches to MFBI analysis and succeeded in proposing single and multi-dispersion Cole modelling to estimate the response of each of the considered tissue layers. However, the work had some limitations, which can be addressed through the following future directions:

- The simulation analysis assumed a layered, lumped tissue modelling approach assuming a homogenous and isotropic distribution of tissue dielectric properties. Future work may direct towards a more distributed tissue model in trying to mimic the actual tissue interaction in the forearm as closely as possible. This can be done through considering blood perfusion in muscle tissue and/or other arteries and capillary structures involved in the tissue section under test.
- The work can be used as a basis to isolate the response of blood flow from the overall measurements. In present work, the combined impedance of all the tissue domains has been modelled through estimating their respective dispersion spectra. Blood flow will primarily reflect as periodic changes over time and can be calculated following a similar approach.
- Experimental study was performed as a pilot investigation on two subjects. However, a more extensive validation under varying physiological conditions will be required for directing this outcome towards a practical system.

The human tissues are complex structures with varying levels of inhomogeneity and anisotropy. This work has aimed to put forward an electrical modelling approach to identify the response of each tissue domain. The results obtained are promising and indicate the potential of using MFBI in investigating tissue behavior. Further analysis and improvements can help place this methodology at the centre of existing BIA techniques and help standardise its current applications. Future work may include considerations of different electrode geometries to optimise the electric field sensitivity and including the effect of skin.

References

- [1] S. Grimnes and O. G. Martinsen, *Bioimpedance and Bioelectricity Basics*. Academic Press, 2014.
- [2] E. Atzler and G. Lehmann, *Anatomie und physiologie der arbeit*, vol. 1. C. Marhold, 1930.
- [3] J. Nyboer, S. Bango, A. Barnett, and R. H. Halsey, “Radiocardiograms: Electrical impedance changes of the heart in relation to electrocardiograms and heart sounds,” *J Clin Invest*, vol. 19, p. 963, 1940.
- [4] R. P. Patterson, “Fundamentals of impedance cardiography,” *IEEE Eng. Med. Biol. Mag.*, vol. 8, no. 1, pp. 35–38, Mar. 1989, doi: 10.1109/51.32403.
- [5] R. Y. T. Sung, P. Lau, C. W. Yu, P. K. W. Lam, and E. A. S. Nelson, “Measurement of body fat using leg to leg bioimpedance,” *Arch. Dis. Child.*, vol. 85, no. 3, pp. 263–267, 2001.
- [6] H. D. McCarthy, T. J. Cole, T. Fry, S. A. Jebb, and A. M. Prentice, “Body fat reference curves for children,” *Int. J. Obes.*, vol. 30, no. 4, pp. 598–602, 2006.
- [7] M. Lintsi, H. Kaarma, and I. Kull, “Comparison of hand-to-hand bioimpedance and anthropometry equations versus dual-energy X-ray absorptiometry for the assessment of body fat percentage in 17–18-year-old conscripts,” *Clin. Physiol. Funct. Imaging*, vol. 24, no. 2, pp. 85–90, 2004.
- [8] S. A. Jebb, M. Siervo, P. R. Murgatroyd, S. Evans, G. Frühbeck, and A. M. Prentice, “Validity of the leg-to-leg bioimpedance to estimate changes in body fat during weight loss and regain in overweight women: a comparison with multi-compartment models,” *Int. J. Obes.*, vol. 31, no. 5, pp. 756–762, 2007.
- [9] F. R. Faria *et al.*, “Body Fat Equations and Electrical Bioimpedance Values in Prediction of Cardiovascular Risk Factors in Eutrophic and Overweight Adolescents,” *Int. J. Endocrinol.*, vol. 2013, p. e501638, 2013, doi: 10.1155/2013/501638.
- [10] D. B. Geselowitz, “An application of electrocardiographic lead theory to impedance plethysmography,” *Biomed. Eng. IEEE Trans. On*, no. 1, pp. 38–41, 1971.
- [11] H. G. Puurtinen, J. Hyttinen, P. Kauppinen, N. Takano, P. Laarne, and J. Malmivuo, “Application of lead field theory and computerized thorax modeling for the ECG inverse problem,” in *2001 Conference Proceedings of the 23rd Annual International Conference of the IEEE Engineering in Medicine and Biology Society*, 2001, vol. 1, pp. 363–366 vol.1, doi: 10.1109/IEMBS.2001.1018935.
- [12] P. K. Kauppinen, J. A. Hyttinen, T. Kööbi, and J. Malmivuo, “Lead field theoretical approach in bioimpedance measurements: towards more controlled measurement sensitivity,” *Ann. N. Y. Acad. Sci.*, vol. 873, pp. 135–142, Apr. 1999, doi: 10.1111/j.1749-6632.1999.tb09460.x.
- [13] J. Malmivuo and R. Plonsey, *Bioelectromagnetism: principles and applications of bioelectric and biomagnetic fields*. New York: Oxford University Press, 1995.
- [14] J. Hohl and S. Rush, “The complete heart-lead relationship in the einthoven triangle,” *Bull. Math. Biophys.*, vol. 30, no. 4, pp. 615–623, Dec. 1968, doi: 10.1007/BF02476678.
- [15] D. A. Brody, B. D. Erb, and W. E. Romans, “The approximate determination of lead vectors and the Burger triangle in normal human subjects,” *Am. Heart J.*, vol. 51, no. 2, pp. 211–220, Feb. 1956, doi: 10.1016/0002-8703(56)90082-5.
- [16] *The London, Edinburgh and Dublin Philosophical Magazine and Journal of Science*. Taylor & Francis, 1862.
- [17] P. Debye, “Zur Theorie der anomalen Dispersion im Gebiete der langwelligen elektrischen Strahlung,” *Ber Dt Phys Ges*, vol. 15, pp. 777–793, 1913.
- [18] K. W. Wagner, “Erklärung der dielektrischen Nachwirkungsvorgänge auf Grund Maxwellscher Vorstellungen,” *Arch. Für Elektrotechnik*, vol. 2, no. 9, pp. 371–387, doi: 10.1007/BF01657322.
- [19] R. W. Sillars, “The properties of a dielectric containing semiconducting particles of various shapes,” *J. Inst. Electr. Eng.*, vol. 80, no. 484, pp. 378–394, Apr. 1937, doi: 10.1049/jjee-1.1937.0058.

- [20] L. K. H. Van Beek, "The Maxwell-Wagner-Sillars effect, describing apparent dielectric loss in inhomogeneous media," *Physica*, vol. 26, no. 1, pp. 66–68, 1960.
- [21] D. Miklavčič, N. Pavšelj, and F. X. Hart, "Electric Properties of Tissues," in *Wiley Encyclopedia of Biomedical Engineering*, John Wiley & Sons, Inc., 2006.
- [22] K. S. Cole, "Permeability and impermeability of cell membranes for ions," in *Cold Spring Harbor Symposia on Quantitative Biology*, 1940, vol. 8, pp. 110–122.
- [23] K. S. Cole and R. H. Cole, "Dispersion and absorption in dielectrics I. Alternating current characteristics," *J. Chem. Phys.*, vol. 9, no. 4, pp. 341–351, 1941.
- [24] A. Sherwood(Chair), M. T. Allen, J. Fahrenberg, R. M. Kelsey, W. R. Lovallo, and L. J. P. van Doornen, "Methodological Guidelines for Impedance Cardiography," *Psychophysiology*, vol. 27, no. 1, pp. 1–23, Jan. 1990, doi: 10.1111/j.1469-8986.1990.tb02171.x.
- [25] A. Adler, R. Amyot, R. Guardo, J. H. T. Bates, and Y. Berthiaume, "Monitoring changes in lung air and liquid volumes with electrical impedance tomography," *J. Appl. Physiol.*, vol. 83, no. 5, pp. 1762–1767, 1997.
- [26] R. V. Luepker, J. R. Michael, and J. R. Warbasse, "Transthoracic electrical impedance: quantitative evaluation of a non-invasive measure of thoracic fluid volume," *Am. Heart J.*, vol. 85, no. 1, pp. 83–93, 1973.
- [27] J. Hatlestad, B. Moon, J. W. Hartley, and J. E. Stahmann, *Calibration of impedance monitoring of respiratory volumes using thoracic DC impedance*. Google Patents, 2009.
- [28] F. G. Spinale, H. D. Reines, M. C. Cook, and F. A. Crawford, "Noninvasive estimation of extravascular lung water using bioimpedance," *J. Surg. Res.*, vol. 47, no. 6, pp. 535–540, 1989.
- [29] M. Pomerantz, F. Delgado, and B. Eiseman, "Clinical evaluation of transthoracic electrical impedance as a guide to intrathoracic fluid volumes.," *Ann. Surg.*, vol. 171, no. 5, p. 686, 1970.
- [30] H. Heijboer, H. R. Buller, A. Lensing, A. Turpie, L. P. Colly, and J. W. ten Cate, "A comparison of real-time compression ultrasonography with impedance plethysmography for the diagnosis of deep-vein thrombosis in symptomatic outpatients," *N. Engl. J. Med.*, vol. 329, no. 19, pp. 1365–1369, 1993.
- [31] R. D. Hull *et al.*, "Diagnostic efficacy of impedance plethysmography for clinically suspected deep-vein thrombosis," *Ann Intern Med*, vol. 102, no. 2, p. 28, 1985.
- [32] P. S. Wells *et al.*, "Value of assessment of pretest probability of deep-vein thrombosis in clinical management," *The Lancet*, vol. 350, no. 9094, pp. 1795–1798, 1997.
- [33] R. D. Allison, E. L. Holmes, and J. Nyboer, "Volumetric dynamics of respiration as measured by electrical impedance plethysmography," *J. Appl. Physiol.*, vol. 19, no. 1, pp. 166–173, Jan. 1964.
- [34] E. C. Hoffer, C. K. Meador, and D. C. Simpson, "Correlation of whole-body impedance with total body water volume.," *J. Appl. Physiol.*, vol. 27, no. 4, pp. 531–534, 1969.
- [35] P. S. Kurtin, A. C. Shapiro, H. Tomita, and D. Raizman, "Volume Status and Body Composition of Chronic Dialysis Patients: Utility of Bioelectric Impedance Plethysmography," *Am. J. Nephrol.*, vol. 10, no. 5, pp. 363–367, 1990, doi: 10.1159/000168151.
- [36] B. M. Eyüboğlu, "Electrical Impedance Plethysmography," in *Wiley Encyclopedia of Biomedical Engineering*, John Wiley & Sons, Inc., 2006.
- [37] V. Cherepenin *et al.*, "A 3D electrical impedance tomography (EIT) system for breast cancer detection," *Physiol. Meas.*, vol. 22, no. 1, p. 9, 2001.
- [38] Y. Zou and Z. Guo, "A review of electrical impedance techniques for breast cancer detection," *Med. Eng. Phys.*, vol. 25, no. 2, pp. 79–90, 2003.
- [39] M. H. Choi, T.-J. Kao, D. Isaacson, G. J. Saulnier, and J. C. Newell, "A reconstruction algorithm for breast cancer imaging with electrical impedance tomography in mammography geometry," *IEEE Trans. Biomed. Eng.*, vol. 54, no. 4, pp. 700–710, 2007.
- [40] B. H. Brown, "Medical impedance tomography and process impedance tomography: a brief review," *Meas. Sci. Technol.*, vol. 12, no. 8, p. 991, 2001.
- [41] B. H. Brown, "Electrical impedance tomography (EIT): a review," *J. Med. Eng. Technol.*, vol. 27, no. 3, pp. 97–108, 2003.

- [42] D. Holder, "Biomedical applications of electrical impedance tomography," *Physiol. Meas.*, vol. 23, no. 1, 2002.
- [43] T. Dowrick, C. Blochet, and D. Holder, "In vivo bioimpedance measurement of healthy and ischaemic rat brain: implications for stroke imaging using electrical impedance tomography," *Physiol. Meas.*, vol. 36, no. 6, p. 1273, 2015.
- [44] T. A. T. Hughes, P. Liu, H. Griffiths, B. W. Lawrie, and C. M. Wiles, "Simultaneous electrical impedance tomography and videofluoroscopy in the assessment of swallowing," *Physiol. Meas.*, vol. 17, no. 2, p. 109, 1996.
- [45] H. P. Schwan, "Electrical properties of tissue and cell suspensions.," *Adv. Biol. Med. Phys.*, vol. 5, p. 147, 1957.
- [46] J. R. Matthie, "Bioimpedance measurements of human body composition: critical analysis and outlook," 2008.
- [47] A. D. Lorenzo, A. Andreoli, J. Matthie, and P. Withers, "Predicting body cell mass with bioimpedance by using theoretical methods: a technological review," *J. Appl. Physiol.*, vol. 82, no. 5, pp. 1542–1558, May 1997.
- [48] S. Rush and D. A. Driscoll, "EEG electrode sensitivity—an application of reciprocity," *Biomed. Eng. IEEE Trans. On*, no. 1, pp. 15–22, 1969.
- [49] D. C. Barber, B. H. Brown, and I. L. Freeston, "Imaging spatial distributions of resistivity using applied potential tomography—APT," in *Information Processing in Medical Imaging*, 1984, pp. 446–462.
- [50] L. A. Geddes and C. Sadler, "The specific resistance of blood at body temperature," *Med. Biol. Eng.*, vol. 11, no. 3, pp. 336–339, 1973.
- [51] S. Rush, J. A. Abildskov, and R. McFee, "Resistivity of body tissues at low frequencies," *Circ. Res.*, vol. 12, no. 1, pp. 40–50, 1963.
- [52] B. R. Epstein and K. R. Foster, "Anisotropy in the dielectric properties of skeletal muscle," *Med. Biol. Eng. Comput.*, vol. 21, no. 1, pp. 51–55, 1983.
- [53] H. P. SCHWAN and C. F. KAY, "Specific resistance of body tissues," *Circ. Res.*, vol. 4, no. 6, pp. 664–670, 1956.
- [54] L. A. Geddes and L. E. Baker, "The specific resistance of biological material—a compendium of data for the biomedical engineer and physiologist," *Med. Biol. Eng.*, vol. 5, no. 3, pp. 271–293, 1967.
- [55] S. Saha and P. A. Williams, "Electric and dielectric properties of wet human cortical bone as a function of frequency," *Biomed. Eng. IEEE Trans. On*, vol. 39, no. 12, pp. 1298–1304, 1992.
- [56] C. Gabriel, S. Gabriel, and E. Corthout, "The dielectric properties of biological tissues: I. Literature survey," *Phys. Med. Biol.*, vol. 41, no. 11, p. 2231, 1996.
- [57] S. Gabriel, R. W. Lau, and C. Gabriel, "The dielectric properties of biological tissues: II. Measurements in the frequency range 10 Hz to 20 GHz," *Phys. Med. Biol.*, vol. 41, no. 11, pp. 2251–2269, Nov. 1996, doi: 10.1088/0031-9155/41/11/002.
- [58] S. Gabriel, R. W. Lau, and C. Gabriel, "The dielectric properties of biological tissues: III. Parametric models for the dielectric spectrum of tissues," *Phys. Med. Biol.*, vol. 41, no. 11, p. 2271, 1996, doi: 10.1088/0031-9155/41/11/003.
- [59] C. Gabriel, "Compilation of the Dielectric Properties of Body Tissues at RF and Microwave Frequencies.," DTIC Document, 1996.
- [60] S. Grimnes and Ø. G. Martinsen, "Bioimpedance," in *Wiley Encyclopedia of Biomedical Engineering*, John Wiley & Sons, Inc., 2006.
- [61] H. Fricke, "XXXIII. The theory of electrolytic polarization," *Lond. Edinb. Dublin Philos. Mag. J. Sci.*, vol. 14, no. 90, pp. 310–318, 1932.
- [62] W. G. Kubicek, *Minnesota impedance cardiograph model 303*. Univ. of Minnesota press, Minneapolis, 1968.
- [63] S. N. Mohapatra, *Non-invasive cardiovascular monitoring by electrical impedance technique*. Pitman Medical, 1981.

- [64] R. Pethig, "Dielectric properties of biological materials: Biophysical and medical applications," *Electr. Insul. IEEE Trans. On*, no. 5, pp. 453–474, 1984.
- [65] P. Bertemes Filho, "Tissue Characterisation Using an Impedance Spectroscopy Probe," 2002.
- [66] W. Mitchell and R. Sundararajan, "Electric Field Distribution in Biological Tissues for Various Electrode Configurations-A FEMLAB Study," *COMSOL Multiphysics Boston Mass USA*, 2005.
- [67] L.-Y. Shyu, C.-Y. Chiang, C.-P. Liu, and W.-C. Hu, "Portable impedance cardiography system for real-time noninvasive cardiac output measurement," *J. Med. Biol. Eng.*, vol. 20, no. 4, pp. 193–202, 2000.
- [68] M. Jaffrin, H. Morel, and Y. Lavielle, "Body composition measurements in limbs using eight-electrodes bioimpedance," in *13th International Conference on Electrical Bioimpedance and the 8th Conference on Electrical Impedance Tomography*, 2007, pp. 771–774.
- [69] T. Nakamura, Y. Yamamoto, T. Yamamoto, and H. Tsuji, "Fundamental characteristics of human limb electrical impedance for biodynamic analysis," *Med. Biol. Eng. Comput.*, vol. 30, no. 5, pp. 465–472, 1992.
- [70] S. C. Kim, K. C. Nam, D. W. Kim, C. Y. Ryu, Y. H. Kim, and J. C. Kim, "Optimum electrode configuration for detection of arm movement using bio-impedance," *Med. Biol. Eng. Comput.*, vol. 41, no. 2, pp. 141–145, Mar. 2003, doi: 10.1007/BF02344881.
- [71] F. G. Hirsch *et al.*, "THE ELECTRICAL CONDUCTIVITY OF BLOOD I. RELATIONSHIP TO ERYTHROCYTE CONCENTRATION," *Blood*, vol. 5, no. 11, pp. 1017–1035, 1950.
- [72] S. Graff, A. B. Voorhees, and A. H. Blakemore, "Electrical resistance of whole blood," *Science*, vol. 106, no. 2742, pp. 68–69, 1947.
- [73] R. L. Rosenthal and C. W. Tobias, "Measurement of the electric resistance of human blood; use in coagulation studies and cell volume determinations," *J Lab Clin Med*, vol. 33, pp. 1110–1122, 1948.
- [74] S. N. Mohapatra and D. W. Hill, "The changes in blood resistivity with haematocrit and temperature," *Eur. J. Intensive Care Med.*, vol. 1, no. 4, pp. 153–162, 1975.
- [75] H. Fricke, "A mathematical treatment of the electric conductivity and capacity of disperse systems I. The electric conductivity of a suspension of homogeneous spheroids," *Phys. Rev.*, vol. 24, no. 5, p. 575, 1924.
- [76] S. N. Mohapatra, "Impedance cardiography," *Encycl. Med. Devices Instrum.*, pp. 1622–1632, 1988.
- [77] L. L. Hause, F. A. Gayon, and M. E. Aleksza, "Impedance measurements during simulated blood flow," in *Engineering in Medicine and Biology Society, 1989. Images of the Twenty-First Century., Proceedings of the Annual International Conference of the IEEE Engineering in*, 1989, p. 1232 vols.4-, doi: 10.1109/IEMBS.1989.96169.
- [78] E. Sigman, A. Kolin, L. Katz, and K. Jochim, "Effect of motion on the electrical conductivity of the blood," *Am. J. Physiol. Content*, vol. 118, no. 4, pp. 708–719, 1937.
- [79] W. G. Kubicek, R. P. Patterson, and D. A. Witsoe, "Impedance Cardiography as a Noninvasive Method of Monitoring Cardiac Function and Other Parameters of the Cardiovascular System*," *Ann. N. Y. Acad. Sci.*, vol. 170, no. 2, pp. 724–732, Jul. 1970, doi: 10.1111/j.1749-6632.1970.tb17735.x.
- [80] H. Griffiths and A. Ahmed, "A dual-frequency applied potential tomography technique: computer simulations," *Clin. Phys. Physiol. Meas.*, vol. 8, no. 4A, p. 103, 1987.
- [81] A. Lozano, J. Rosell, and R. Pallas-Areny, "Two-frequency impedance plethysmograph: real and imaginary parts," *Med. Biol. Eng. Comput.*, vol. 28, no. 1, pp. 38–42, 1990.
- [82] P. M. Record, R. Gadd, and F. Vinther, "Multifrequency electrical impedance tomography," *Clin. Phys. Physiol. Meas.*, vol. 13, no. A, p. 67, 1992.
- [83] A. R. Waterworth, P. Milnes, R. H. Smallwood, and B. H. Brown, "Cole equation modelling to measurements made using an impulse driven transfer impedance system," *Physiol. Meas.*, vol. 21, no. 1, p. 137, 2000.
- [84] M. E. Valentinuzzi, "Bioelectrical impedance techniques in medicine. Part I: Bioimpedance measurement. First section: general concepts.," *Crit. Rev. Biomed. Eng.*, vol. 24, no. 4–6, pp. 223–255, 1995.

- [85] B. H. Brown, P. V. Lawford, R. H. Smallwood, D. R. Hose, and D. C. Barber, *Medical Physics and Biomedical Engineering*. 1999. Institute of Physics Publishing, London.
- [86] “IEC 60601,” *Wikipedia, the free encyclopedia*. 16-Oct-2015.
- [87] C. W. Denyer, F. J. Lidgley, Q. S. Zhu, and C. N. McLeod, “High output impedance voltage controlled current source for bio-impedance instrumentation,” in *Proceedings of the 15th Annual International Conference of the IEEE Engineering in Medicine and Biology Society, 1993*, 1993, pp. 1026–1027, doi: 10.1109/IEMBS.1993.978988.
- [88] C. W. Denyer, F. J. Lidgley, Q. S. Zhu, and C. N. McLeod, “A high output impedance current source,” *Physiol. Meas.*, vol. 15, no. 2A, p. A79, 1994.
- [89] C. W. Denyer, F. J. Lidgley, C. N. McLeod, and Q. S. Zhu, “Current source calibration simplifies high-accuracy current source measurement,” *Innov. Technol. En Biol. Médecine*, vol. 15, pp. 47–55, 1994.
- [90] B. Blad, K. Lindstrom, L. Bertenstam, B. R. Persson, and N.-G. Holmer, “A current injecting device for electrical impedance tomography,” *Physiol. Meas.*, vol. 15, no. 2A, p. A69, 1994.
- [91] J. Li, C. Joppek, and U. Faust, “An isolated wideband current source used in multifrequency electrical impedance tomography,” *Innov. Technol. En Biol. Médecine*, vol. 15, pp. 62–68, 1994.
- [92] L. Lu and B. H. Brown, “The electrode and electronic interface in an EIT spectroscopy system,” *Innov. Technol. En Biol. Médecine*, vol. 15, pp. 97–103, 1994.
- [93] J. Jossinet, G. Tourtel, and R. Jarry, “Performance and operation of a set of wide band current generators for eit,” *Innov. Technol. En Biol. Médecine*, vol. 15, pp. 40–46, 1994.
- [94] G. Cusick, D. S. Holder, A. Birkett, and K. Boone, “A system for impedance imaging epilepsy in ambulatory human subjects,” *Innov. Technol. En Biol. Médecine*, vol. 15, pp. 33–39, 1994.
- [95] J. Jossinet, C. Tourtel, and R. Jarry, “Active current electrodes for in vivo electrical impedance tomography,” *Physiol. Meas.*, vol. 15, no. 2A, p. A83, 1994.
- [96] O. Casas, J. Rosell, R. Bragós, A. Lozano, and P. J. Riu, “A parallel broadband real-time system for electrical impedance tomography,” *Physiol. Meas.*, vol. 17, no. 4A, p. A1, 1996.
- [97] R. Bragos, J. Rosell, and P. Riu, “A wide-band AC-coupled current source for electrical impedance tomography,” *Physiol. Meas.*, vol. 15, no. 2A, p. A91, 1994.
- [98] P. J. Riu, J. Rosell, A. Lozano, and R. Pallàs-Areny, “A broadband system for multifrequency static imaging in electrical impedance tomography,” *Clin. Phys. Physiol. Meas.*, vol. 13, no. A, p. 61, 1992.
- [99] J. C. Márquez Ruiz, “Sensor-Based Garments that Enable the Use of Bioimpedance Technology: Towards Personalized Healthcare Monitoring,” 2013.
- [100] J.-J. Wang, W.-C. Hu, T. Kao, C.-P. Liu, and S.-K. Lin, “Development of forearm impedance plethysmography for the minimally invasive monitoring of cardiac pumping function.,” *J. Biomed. Sci. Eng.*, vol. 4, no. 2, 2011.
- [101] B. E. Hurwitz, L.-Y. Shyu, C.-C. Lu, S. P. Reddy, N. Schneiderman, and J. H. Nagel, “Signal fidelity requirements for deriving impedance cardiographic measures of cardiac function over a broad heart rate range,” *Biol. Psychol.*, vol. 36, no. 1–2, pp. 3–21, Aug. 1993, doi: 10.1016/0301-0511(93)90076-K.
- [102] S. Havriliak and S. Negami, “A complex plane representation of dielectric and mechanical relaxation processes in some polymers,” *Polymer*, vol. 8, pp. 161–210, Jan. 1967, doi: 10.1016/0032-3861(67)90021-3.
- [103] D. W. Davidson and R. H. Cole, “Dielectric relaxation in glycerine,” *J. Chem. Phys.*, vol. 18, no. 10, pp. 1417–1417, 1950.
- [104] F. Kremer and A. Schönhals, *Broadband Dielectric Spectroscopy*. Springer Science & Business Media, 2002.
- [105] R. Kohlrausch, “Theorie des elektrischen Rückstandes in der Leidener Flasche,” *Ann. Phys.*, vol. 167, no. 2, pp. 179–214, 1854.
- [106] R. Bandyopadhyay *et al.*, “Evolution of particle-scale dynamics in an aging clay suspension,” *Phys. Rev. Lett.*, vol. 93, no. 22, p. 228302, 2004.

- [107] Y.-H. Hwang, J.-A. Seo, H.-J. Kwon, and H. K. Kim, "Relaxation Dynamics of Sugar Glasses," *Rep Inst. Fluid Sci.*, vol. 19, pp. 27–34, 2007.
- [108] G. Medrano, A. Ubl, N. Zimmermann, T. Gries, and S. Leonhardt, "Skin electrode impedance of textile electrodes for bioimpedance spectroscopy," in *13th International Conference on Electrical Bioimpedance and the 8th Conference on Electrical Impedance Tomography*, 2007, pp. 260–263.
- [109] F. Zhu and N. W. Levin, "An electrical resistivity model of segmental body composition using bioimpedance analysis," in *Proceedings of the 25th Annual International Conference of the IEEE Engineering in Medicine and Biology Society*, 2003, 2003, vol. 3, pp. 2679–2682 Vol.3, doi: 10.1109/IEMBS.2003.1280468.
- [110] G. N. Jager, N. Westerhof, and A. Noordergraaf, "Oscillatory Flow Impedance in Electrical Analog of Arterial System: Representation of Sleeve Effect and Non-Newtonian Properties of Blood," *Circ. Res.*, vol. 16, no. 2, pp. 121–133, Feb. 1965, doi: 10.1161/01.RES.16.2.121.
- [111] U. M. Moissl *et al.*, "Body fluid volume determination via body composition spectroscopy in health and disease," *Physiol. Meas.*, vol. 27, no. 9, p. 921, 2006.
- [112] H. Keren, D. Burkhoff, and P. Squara, "Evaluation of a noninvasive continuous cardiac output monitoring system based on thoracic bioreactance," *Am. J. Physiol. - Heart Circ. Physiol.*, vol. 293, no. 1, pp. H583–H589, Jul. 2007, doi: 10.1152/ajpheart.00195.2007.
- [113] B. Benomar, A. Ouattara, P. Estagnasie, A. Brusset, and P. Squara, "Fluid responsiveness predicted by noninvasive bioreactance-based passive leg raise test," *Intensive Care Med.*, vol. 36, no. 11, pp. 1875–1881, 2010.
- [114] Y. Ballesterio *et al.*, "Measurement of cardiac output in children by bioreactance," *Pediatr. Cardiol.*, vol. 32, no. 4, pp. 469–472, 2011.
- [115] I. C. Henry, D. P. Bernstein, and M. J. Banet, "Stroke volume obtained from the brachial artery using transbrachial electrical bioimpedance velocimetry," in *2012 Annual International Conference of the IEEE Engineering in Medicine and Biology Society (EMBC)*, 2012, pp. 142–145, doi: 10.1109/EMBC.2012.6345891.
- [116] "ANSYS HFSS: High Frequency Electromagnetic Field Simulation." [Online]. Available: <http://www.ansys.com/products/electronics/ansys-hfss>. [Accessed: 13-Feb-2017].
- [117] V. Mooser *et al.*, "Non-invasive measurement of internal diameter of peripheral arteries during the cardiac cycle," *J. Hypertens.*, vol. 6, no. 4, Dec. 1988.
- [118] S. Trazzi, S. Omboni, C. Santucci, G. Parati, and G. Mancina, "Variability in arterial diameter and compliance: compliance modulation reserve," *J. Hypertens.*, Aug. 1992.
- [119] "Compact and Fast Impedance Spectroscopy Platform - Quadra," *Eliko*. [Online]. Available: <https://www.eliko.ee/products/quadra-impedance-spectroscopy/>. [Accessed: 24-Jul-2018].